Tuning the Structure, Reactivity and Magnetic Communication of Nitride-Bridged Uranium Complexes with the Ancillary Ligands

Chad T. Palumbo, Luciano Barluzzi, Rosario Scopelliti, Ivica Zivkovic, Alberto Fabrizio, Clemence Corminboeuf, and Marinella Mazzanti *

Insititut des Sciences et Ingénierie Chimiques, Ecole Polytechnique Fédérale de Lausanne (EPFL), 1015 Lausanne, Switzerland

Electronic Supplementary Information (ESI)

Table of Contents

Materials and Methods

General Considerations. The syntheses and manipulations described below were conducted under argon with rigorous exclusion of air and water using an MBraun glovebox equipped with a purifier unit along with vacuum and Schlenk line techniques. Anhydrous solvents were purchased from Aldrich and further distilled from K/benzophenone (THF, DME, toluene, hexane). Depleted uranium turnings were purchased from IBILABS, Florida (USA). Potassium metal was purchased from Sigma Aldrich and was washed with hexane and scraped to provide fresh surfaces before use. Deuterated solvents for NMR spectroscopy were purchased from Cortecnet. NBu_4N_3 was purchased from Sigma Aldrich and used as received. $[U(N(SiMe_3)_2)_3]$,[1] $[Cs\{((^tBuO)_3SiO)_3U\}_2(\mu\text{-}N)]$,[2] **[Cs]-1**, $[Na(DME)_3][((Me_3Si)_2N)_2U(\mu_2\text{-}\kappa^1\text{-}N\text{-}N(SiMe_3)(SiMe_2\text{-}\kappa^1\text{-}C\text{-}CH_2)(\mu_2\text{-}N)U(N(SiMe_3)_2)_3]$,[3] **3**, $[U(OSi(O^tBu)_3)_2(\mu\text{-}OSi(O^tBu)_3)]_2$,[4] and $AgBPh_4$[5] were prepared as previously described. Carbon monoxide (N47 Bt-S 10/200) was purchased from Carbagas and stored over activated 3 Å molecular sieves. CO_2 (99.9999% purity) and H_2 (99.9999% purity) were purchased from Carbagas. ^{13}CO (93.13% ^{13}C), $^{13}CO_2$ (93.13% ^{13}C), and D_2 (99.8% D) were purchased from Cortecnet and transferred to a flask containing activated 3 Å molecular sieves prior to use. Elemental analyses were performed under nitrogen with a ThermoScientific Flash 2000 Organic Elemental Analyzer. NMR experiments were carried out using NMR tubes adapted with J. Young valves. ^1H and ^{13}C spectra were recorded using Avance 400 MHz (^{13}C 125 MHz) or Avance III-HD 600 MHz (^{13}C 151 MHz) NMR spectrometers and chemical shifts are referenced internally to residual proteo-solvent references. IR spectra were recorded with a Perkin Elmer 1600 Series FTIR spectrometer flushed with N_2. The UV-Vis-NIR spectra were recorded with a Perkin Elmer

Lambda 750 instrument. The spectra were recorded at 25°C in 1 mm cells adapted with J. Young valves as 6.5-10 mM THF solution of complexes **[NBu$_4$]-1**, **2**, and **5.**

Caution: Depleted uranium (primary isotope ^{238}U) is a weak α-emitter (4.197 MeV) with a half-life of 4.47 x 10^9 years. Manipulations and reactions should be carried out in monitored fume hoods or in an inert glovebox in a radiation laboratory equipped with α- and β-counting equipment.

Magnetic Measurements. Magnetic measurements were performed using a QuantumDesign MPMS-5T superconducting quantum interferencedevice (SQUID) magnetometer in a temperature range 2–300 K. The crushed crystalline samples were enclosed in an evacuated and flame-sealed quartz capsule and placed inside a plastic straw. Samples were restrained in an eicosane or deuterated cyclohexane (C_6D_{12}) matrix to prevent sample torquing during measurements. Diamagnetic corrections were applied to the data using Pascal's constants.[6]

[NBu$_4$][{((*t*BuO)$_3$SiO)$_3$U}$_2$(μ-N)], [NBu$_4$]-1. In an argon-filled glovebox, NBu_4N_3 (22.3mg, 0.078 mmol) dissolved in thf (3 mL) was added to a stirred solution of $[U(OSi(O^tBu)_3)_3]_2$ (160.9 mg, 0.0782 mmol) in thf (1.5 mL) at −40°C. After 3 d, the reaction is complete and the resultant pink-brown solution was filtered using a 0.2 μm porosity filter frit and the volatiles of the filtrate were removed under vacuum. The pink-brown oily residue was triturated with hexane and the resultant solid was dissolved in toluene (1.5 mL). Addition of hexane (0.2 mL) and storage at −40 °C overnight in the glovebox freezer produced single pink-brown crystals of [NBu$_4$][{((*t*BuO)$_3$SiO)$_3$U}$_2$(μ-N)], **[NBu$_4$]-1**, characterizable by X-ray crystallography (126.8 mg, 70%). ^{1}H NMR (400 MHz, thf-d_8, 298 K): δ 3.20 (t, NC*H*$_2$CH$_2$CH$_2$CH$_3$,

8H), 1.63 (m, $NCH_2CH_2CH_2CH_3$, 8H), 1.35 (m, $NCH_2CH_2CH_2CH_3$, 8H), 0.94 (t, $NCH_2CH_2CH_2CH_3$, 12H), −0.31 (s, $OCCH_3$, 162H) ppm. ^{1}H NMR (400 MHz, toluene-d_8, 298 K): δ 1.67 (m, $NCH_2CH_2CH_2CH_3$, 8H), −0.33 (s, $OCCH_3$, 162H), −1.14 (t, $CH_2CH_2CH_2CH_3$, 8H), −1.30 (m, $NCH_2CH_2CH_2CH_3$, 12H), −2.04 (m, $NCH_2CH_2CH_2CH_3$, 8H) ppm. Anal. Calcd for $C_{88}H_{198}N_2O_{24}Si_6U_2$: C, 45.69; H, 8.63; N, 1.21. Found: C, 45.86; H, 8.66; N, 1.36. When the reaction is carried out at room temperature, **[NBu$_4$]-1**, unreacted starting material and unidentified species are formed.

[NBu$_4$][{((Me$_3$Si)$_2$N)$_3$U}$_2$(μ-N)], 2. In an argon-filled glovebox, toluene was poured onto a solid mixture of [U(N(SiMe$_3$)$_2$)$_3$] (75.8 mg, 0.105 mmol) and NBu_4N_3 (15.0 mg, .053 mmol). A stir bar was added, and the dark purple slurry was stirred at −40 °C. After 1 h, the solids of the resultant brown slurry were left to settle, and the light orange solution was decanted. The solids were washed with toluene (2 x 1 mL) and hexane (1 mL) and dried under vacuum which gave tan colored solids of analytically pure [NBu$_4$][{((Me$_3$Si)$_2$N)$_3$U}$_2$(μ-N)], **2**, (49.0 mg, 58%). Single crystals suitable for X-ray diffraction were grown from toluene-d_8 in a J-Young NMR tube while studying the low temperature synthesis of **2**. ^{1}H NMR (400 MHz, thf-d_8, −60 °C): δ 116.2 (br s, ffhw = 1100 Hz, SiMe_3), 18.0 (br s, ffhw = 800 Hz, SiMe_3), 3.06 (br m, ffhw = 25 Hz, $NCH_2CH_2CH_2CH_3$, 8H), 1.42 (br m, ffhw = 25 Hz, $NCH_2CH_2CH_2CH_3$, 8H), 1.05 (br m, ffhw = 25 Hz, $NCH_2CH_2CH_2CH_3$, 8H), 0.67 (br m, ffhw = 14 Hz $NCH_2CH_2CH_2CH_3$, 12H), −14.0 (br s, ffhw = 36 Hz, SiMe_3), −31.9 (br s, ffhw = 770 Hz SiMe_3), −36.1 (br s, ffhw = 36 Hz, SiMe_3), −59.8 (br s, ffhw = 400 Hz, SiMe_3) ppm. At room temperature, only the $[NBu_4]^+$ proton signals are apparent. Anal. Calcd for $C_{52}H_{144}N_8Si_{12}U_2$: C, 36.85; H, 8.56; N, 6.61. Found: C, 36.89; H, 8.56; N, 6.53. *Note: It is important that toluene is poured onto the solid reagents. Attempts to add a toluene solution of NBu_4N_3 to [U(N(SiMe$_3$)$_2$)$_3$] in toluene gave **2** in very low*

yield along with unreacted [U(N(SiMe$_3$)$_2$)$_3$]. Complex **2** persists in solution for several days but shows resonances due to decomposition within hours.

[{((Me$_3$Si)$_2$N)$_3$U}$_2$(μ-N)], 4. In an argon-filled glovebox, a slurry of $AgBPh_4$ (5.1 mg, 12 μmol) in Et_2O (1 mL) was added to a stirred brown solution of [NBu_4][{((Me$_3$Si)$_2$N)$_3$U}$_2$(μ-N)] (20.0 mg, 11.8 μmol) in Et_2O (1 mL). After stirring for 2.5 h in the dark, the volatiles were removed under vacuum and the residue was extracted with hexane (2 mL). The resultant brown slurry was filtered, and the volatiles were removed from the filtrate under vacuum to afford [{(Me$_3$Si)$_2$N)$_3$U}$_2$(μ-N)] as a brown microcrystalline solid (10.2 mg, 60%). Dark brown needles suitable for characterization by X-ray crystallography were obtained by cooling a concentrated toluene solution to −40 °C. ^{1}H NMR (400 MHz, thf-d_8, −60 °C): δ 28.0 (br s, ffhw = 400 Hz, Si*Me*$_3$), 6.75 (br s, ffhw = 460 Hz, Si*Me*$_3$), −3.52 (br s, ffhw = 60 Hz, Si*Me*$_3$), −8.35 (br s, ffhw = 325 Hz, Si*Me*$_3$), −10.0 (br s, ffhw = 60 Hz, Si*Me*$_3$), −17.8 (br s, ffhw = 200 Hz Si*Me*$_3$) ppm. ^{1}H NMR (400 MHz, toluene-d_8, −60 °C): δ 28.5 (br s, ffhw = 400 MHz, Si*Me*$_3$), 7.11 (br s, analysis of ffhw complicated by toluene-d_8 resonances, Si*Me*$_3$), −3.46 (br s, ffhw = 20 Hz, Si*Me*$_3$), −8.42 (br s, ffhw = 300 Hz, Si*Me*$_3$), −9.95 (br s, ffhw = 20 Hz, Si*Me*$_3$), −18.0 (br s, ffhw, 180 Hz, Si*Me*$_3$) ppm. Anal. Calcd for $C_{36}H_{108}N_7Si_{12}U_2$: C, 29.77; H, 7.50; N, 6.75. Found: C, 26.83; H, 6.21; N, 6.04. The low value is consistent with the formula $C_{36}H_{108.07}N_{7.00}$ and suggests incomplete combustion. Satisfactory elementary analyses could not be obtained despite multiple attempts. Similar results were obtained when using [Cp_2Fe][BPh_4]as the oxidizing agent.

[Na(dme)$_3$][((Me$_3$Si)$_2$N)$_3$U(μ-N)U(N(SiMe$_3$)$_2$)(OSi(O^{t}Bu)$_3$)], 5. In an argon-filled glovebox, a solution of HOSi(O^{t}Bu)$_3$ (10.0 mg, 38.0 μmol) in Et_2O (2 mL) was added to a stirred brown solution of [Na(dme)$_3$][((Me$_3$Si)$_2$N)$_2$U(μ-N)(μ-κ^2:C,N- $CH_2SiMe_2NSiMe_3$)U(N(SiMe$_3$)$_2$)$_2$],

3, (60.0 mg, 38.0 μmol) in Et_2O (2 mL) at −40 °C. After 3 h at room temperature, the volatiles of the resultant red-brown solution were removed under vacuum. Hexane (4 mL) was added to the pink solid and to the resultant pink slurry was added 1,2-dimethoxyethane (1 drop, excess). The solids were filtered and washed with hexane (2 x 2 mL) yielding $[Na(dme)_3][((Me_3Si)_2N)_3U(\mu\text{-}N)U(N(SiMe_3)_2)_2(OSi(O^tBu)_3)]$, **5**, as a pink microcrystalline solid (48.7 mg, 70%). Single-crystals of $[Na(dme)_3][((Me_3Si)_2N)_3U(\mu\text{-}N)U(N(SiMe_3)_2)_2(OSi(O^tBu)_3)]$ characterizable by X-ray diffraction were grown by diffusion of hexane into an Et_2O solution of $[Na(dme)_3][((Me_3Si)_2N)_3U(\mu\text{-}N)U(N(SiMe_3)_2)_2(OSi(O^tBu)_3)]$. ^{1}H NMR (400 MHz, thf-d_8, 23 °C): δ 1.08 (br s, $SiMe_3$, 36H) −0.02 (br s, SiMe_3, 54H), −5.40 (br s, OC(CH_3)$_3$, 27H) ppm. The resonances of **5** are broadened into the baseline at low temperatures. Anal. Cald for $C_{54}H_{147}N_6NaO_{10}Si_{11}U_2$: C, 35.08; H, 8.01; N, 4.55. Found: C, 34.58; H, 8.02; N, 4.48.

Thermal Stability of [NBu_4]-2. In an argon-filled glovebox, thf-d_8 (0.5 mL) was added to **[NBu_4]-2** (5.5 mg, 3.2 μmol) in a J-Young NMR tube. The tube was stored in the glovebox at room temperature and analyzed by ^{1}H NMR spectroscopy at −60 °C (at low temperature the spectrum is better resolved). After 6 d, the **[NBu_4]-2** was still present in solution but only as a minor component, Figures S13 and S14. The ^{1}H NMR spectrum shows that at least two products are formed, namely $HN(SiMe_3)_2$ and the $[NBu_4]^+$ analogue of the previously reported bis(cyclometalate) complex $[((Me_3Si)_2N)U(\kappa^2\text{-}CH_2SiMe_2NSiMe_3)_2]^-$.[7] ^{1}H NMR (400 MHz, thf-d_8, 23 °C): 39.1 (s, SiMe_3, 18H), 31.6 (s, SiMe_2CH_2, 6H), −6.15 (s, SiMe_2CH_2, 6H), −36.7 (s, SiMe_3, 18H), −283.0 (s, $SiMe_2CH_2$, 1H) −294.1 (s, $SiMe_2CH_2$, 1H) ppm.

Thermolysis of [NBu_4]-2. In an argon-filled glovebox, thf-d_8 (0.6 mL) was added to **[NBu_4]-2** (9.0 mg, 5.9 μmol) into a J-Young NMR tube. The resultant brown solution was brought out of the glovebox and placed in an oil bath heated at 66 °C for 4 h. No color change was observed. The solution was then removed from the oil bath for analysis by ^{1}H NMR

spectroscopy. The ^{1}H NMR spectrum indicates that at least 3 products were produced, as shown in Figure S15. $HN(SiMe_3)_2$ is produced along with the anion, $[((Me_3Si)_2)_2U(\mu\text{-}N)(\mu\text{-}\kappa^2\text{-}C,N\text{-}CH_2SiMe_2NSiMe_3)U(N(SiMe_3)_2)_2]^-$, presumably as **[NBu$_4$]-3**. ^{1}H NMR (400 MHz, thf-d_8, 23 °C): δ 6.40 (br s, NSiMe_3, 36H), 5.51 (s, Me_3SiNSiMe$_2$CH$_2$, 9H), 2.08 (dd, J_{HH} = 10 Hz, NCH_2CH$_2$CH$_2$CH$_3$, 8H), 0.62 (m, NCH$_2$CH_2CH$_2$CH$_3$, 8H), 0.43 (m, NCH$_2$CH$_2$CH_2CH$_3$, 8H), 0.24 (t, NCH$_2$CH$_2$CH$_2$CH_3, 12H), −5.51 (br s, NSiMe_3, 36H), −53.5 (s, SiMe_2CH$_2$, 6H), −283.0 (s, SiMe$_2$CH_2, 1H), −294.1 (s, SiMe$_2$CH_2, 1H) ppm. The previously reported $[Na(dme)_3][((Me_3Si)_2)_2U(\mu\text{-}N)(\mu\text{-}\kappa^2\text{-}C,N\text{-}CH_2SiMe_2NSiMe_3)U(N(SiMe_3)_2)_2]$, **3**, was characterized by ^{1}H NMR spectroscopy in thf-d_8 for comparison.[3] ^{1}H NMR (400 MHz, thf-d_8, 23 °C): δ 6.30 (br s, NSiMe_3, 36H), 5.50 (s, Me_3SiNSiMe$_2$CH$_2$, 9H), 3.43 (s, CH$_3$OCH_2CH_2OCH$_3$, 12H), 3.27 (s, CH_3OCH$_2$CH$_2$OCH_3, 18H), −5.51 (br s, NSiMe_3, 36H), −53.5 (s, SiMe_2CH$_2$, 6H) ppm, the methylene resonances were not observed. The bis(cyclometalate) complex $[NBu_4][((Me_3Si)_2N)U(\kappa^2\text{-}CH_2SiMe_2NSiMe_3)_2]$ was also observed.[7] The ^{1}H NMR resonances of complex **2** were not observed at -60°C indicating complete consumption. The mixture was brought back into the glovebox and the volatiles were removed under vacuum.

General procedure for the reactions of complexes 1-5 with CO and ^{13}CO. In an argon-filled glovebox, 10-15 mg of a nitride complex **1-5** was dissolved in thf-d_8 or toluene-d_8 (0.6 mL) and transferred to a NMR tube equipped with a J-Young valve. The tube was brought out of the glovebox, attached to a Schlenk line, and degassed by three freeze-pump-thaw cycles. To the solution, CO or ^{13}CO (1 atm or 1-2 equiv) was added and the mixture was analyzed by ^{1}H and ^{13}C NMR spectroscopies. Attempts to isolate the reaction products were not successful. The solutions were then brought back into the glovebox, the volatiles were removed. After removal of the volatiles, the residue was taken out of the glovebox and

hydrolyzed with 0.6 mL of pD = 12 D_2O and the hydrolysis products were analyzed by ^{13}C NMR spectroscopy.

General Procedure for CO_2 and $^{13}CO_2$ Reactions. In an argon-filled glovebox, 10-15 mg of a nitride complex **1-5** was dissolved in thf-d_8 or toluene-d_8 (0.6 mL) in an NMR tube equipped with a J-Young valve. The tube was brought out of the glovebox, attached to a Schlenk line, and degassed by three freeze-pump-thaw cycles. To the frozen solution, CO_2 or $^{13}CO_2$ (1 atm or 1-2 equiv condensed) was added. When stoichiometric amounts were used, the amount of CO_2 was measured with a recently calibrated pressure gauge and condensed onto the frozen solution. The mixtures were thawed and then analyzed by ^1H and ^{13}C NMR spectroscopies. Attempts to isolate the reaction products were not successful. After removal of the volatiles, the residues were taken out of the glovebox and hydrolyzed with 0.6 mL of a pD = 12 D_2O and the deuterolysis products were analyzed by ^{13}C NMR spectroscopy.

General Procedure for H_2 and D_2 Reactions. In an argon-filled glovebox, 10-15 mg of a nitride complex **1-5** was dissolved in thf-d_8 or toluene-d_8 (0.6 mL) in an NMR tube equipped with a J-Young valve. The tube was brought out of the glovebox, attached to a Schlenk line, and degassed by three freeze-pump-thaw cycles. To the solution, H_2 or D_2 (1 atm) were added and the mixture was analyzed by ^1H NMR spectroscopy. For the unreactive $N(SiMe_3)_2$ complexes, the solutions were monitored for several days, and for complex **3**, even heated overnight. Despite these efforts, reactivity was observed only for the all-siloxide complexes which gave imide-hydride products.

Reaction of 3 with CO and isolation of $[[((Me_3Si)_2N)_2U(\mu\text{-}O)]_3$, 6, and $[((Me_3Si)_2N)_2U(\mu\text{-}O)U(\mu\text{-}\kappa^2\text{-}O,N\text{-}OC(=C)SiMe_2NSiMe_3)U(N(SiMe_3)_2)_2]$, 7. In an argon-filled glovebox, a Schlenk flask was charged with $[Na(dme)_3][\{((Me_3Si)_2N)_2U(\mu\text{-}N)(\mu\text{-}\kappa^2\text{-}C,N\text{-}CH_2SiMe_2NSiMe_3)U(N(SiMe_3)_2)_2]$, **3**, (100 mg, 0.063 mmol) and 4 mL of thf. The brown

solution was brought out of the glovebox, attached to a Schlenk line, and degassed by three freeze-pump-thaw cycles. To the thawed solution was added CO (1 atm, excess) which caused a slow color change from brown to yellow. After stirring overnight, the volatiles were removed from the resultant yellow solution. The flask was brought back into the glovebox and the yellow-brown residue was extracted into hexane (4 mL) and concentrated (1 mL). One drop of dme was added and the mixture was stored at −40 °C in the glovebox freezer producing a mixture of crystals. Single crystals of the trimetallic U^{4+} oxo, $[((Me_3Si)_2N)_3U(O)]_3$, **6**, and of the CO insertion product, $[((Me_3Si)_2N)_2U(\mu\text{-}O)U(\mu\text{-}\kappa^2\text{-}O,N\text{-}OC(=C)SiMe_2NSiMe_3)U(N(SiMe_3)_2)_2]$, **7**, were characterized by X-ray crystallography.

Reaction of $[NBu_4]$-1 with CO_2 and isolation of $[NBu_4][\{((^tBuO)_3SiO)_3U\}_2(\mu\text{-}NC_2O_4)]$, 8. In an argon-filled glovebox, toluene-d_8 (0.6 mL) was added to a vial containing **$[NBu_4]$-1**. The resultant pink-brown solution was pipetted into an NMR tube equipped with a J-Young valve. The tube was brought out of the glovebox, attached to a Schlenk line, and degassed by three freeze-pump-thaw cycles. To the frozen solution was added 2 equiv of CO_2 and upon thawing, the pink brown solution changed color to light blue. Addition of hexane (0.1 mL) and storage at −40 °C overnight in the glovebox freezer produced light-blue crystals of $[NBu_4][\{((^tBuO)_3SiO)_3U\}_2(\mu\text{-}NC_2O_4)]$, **8**, characterizable by X-ray crystallography. The previously reported $[U(OSi(O^tBu)_3)_4]$[8] complex is also produced in the reaction and cocrystallizes with **8** rendering impossible elemental analysis determination for complex **8**.

Reaction of $[NBu_4]$-1 with H_2 and isolation of $[NBu_4][\{((^tBuO)_3SiO)_3U\}_2(\mu\text{-}NH)(\mu\text{-}H)]$, 9. In an argon-filled glovebox, toluene (1 mL) was added to **$[NBu_4]$-1** (55.8 mg, 0.024 mmol, 1 equiv) in a reaction tube equipped with a J-Young valve. The tube was brought out of the glovebox, attached to a Schlenk line, and degassed by three freeze-pump-thaw cycles. To the frozen solution H_2 (1 atm) was added and upon thawing, the pink brown solution changed color to

yellow-green. Concentration of the resultant solution until 0.2 mL, addition of hexane (0.2 mL), and storage at −40 °C overnight in the glovebox freezer produced single yellow-green crystals of $[NBu_4][\{((^tBuO)_3SiO)_3U\}_2(\mu\text{-}NH)(\mu\text{-}H)]$, **9**, characterizable by X-ray crystallography (35.4 mg, 63.4%). ^{1}H NMR (400 MHz, toluene-d_8, 298 K): δ 720 (s, 1H, NH or H), 189 (s, 1H, NH or H), 0.42 (m, 2H, CH_2), 0.27 (m, 3H, CH_3), −0.41 (m, 2H, CH_2), −0.73 (s, 162H, CH_3) ppm. Anal. Calcd for $C_{88}H_{200}N_2O_{24}Si_6U_2 \cdot (\text{toluene})_{0.25}$: C, 46.10; H, 8.71; N, 1.20. Found: C, 46.08; H, 9.08; N, 1.43. Complex **9** is stable in solution in the absence of H_2 in the headspace and in the solid state under vacuum.

NMR Spectra

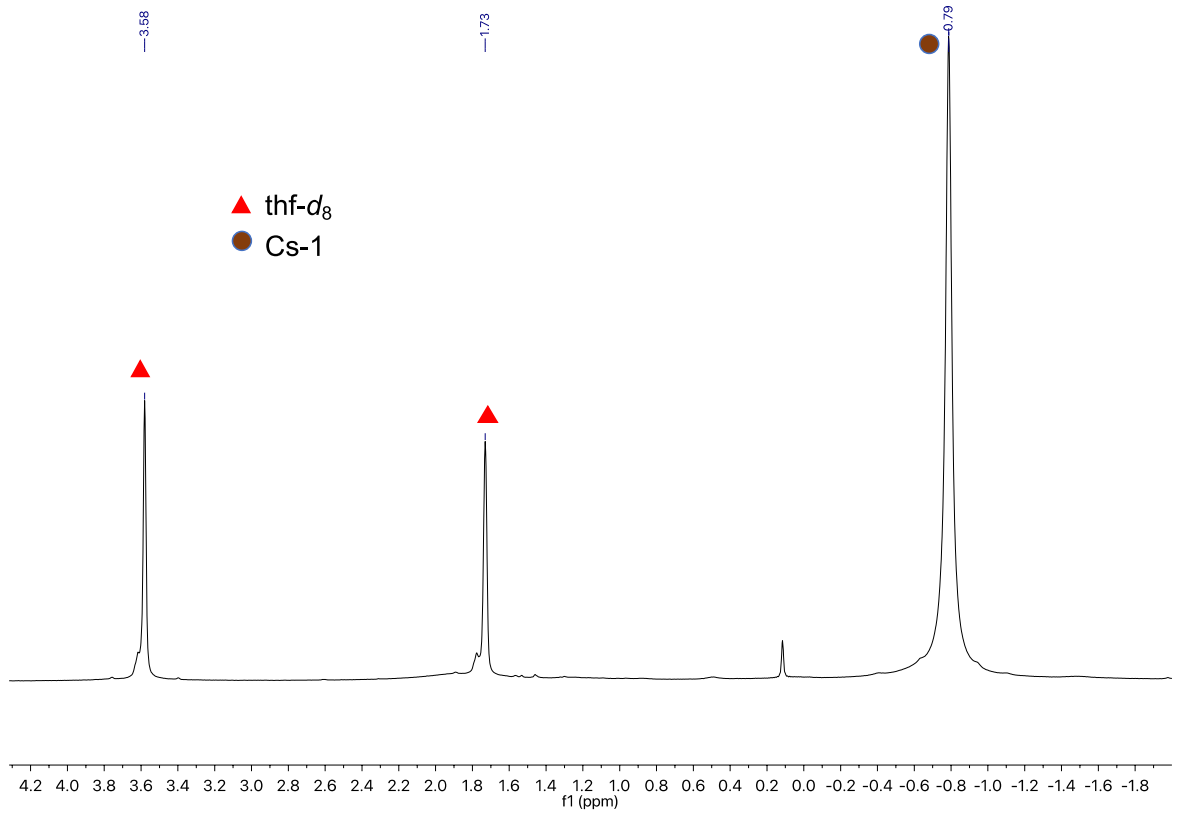

Figure S1. ^{1}H NMR spectrum (400 MHz, 23 °C) of [Cs{((ᵗBuO)$_3$SiO)$_3$U}$_2$(μ-N)], **[Cs]-1**, in thf-d_8.

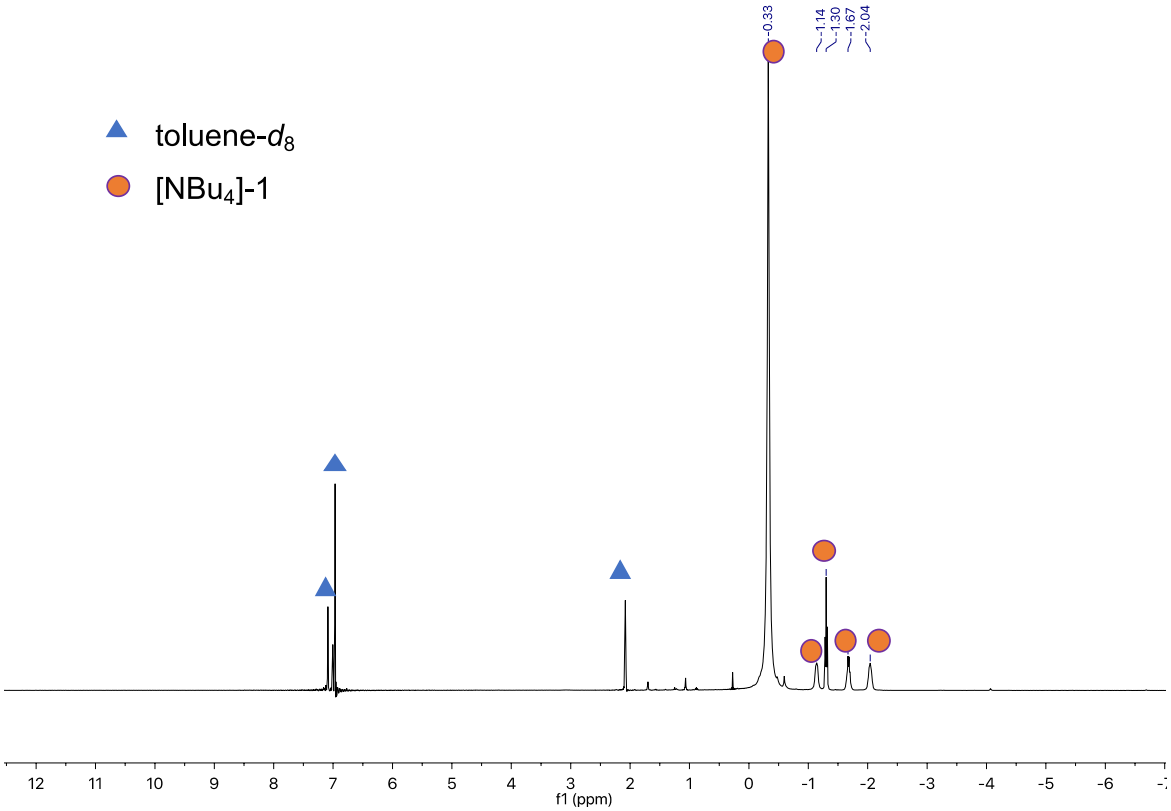

Figure S2. ^{1}H NMR spectrum (400 MHz, 23 °C) of [NBu$_4$][((^{t}BuO)$_3$SiO)$_3$U}$_2$(μ-N)], **[NBu$_4$]-1**, in toluene-d_8.

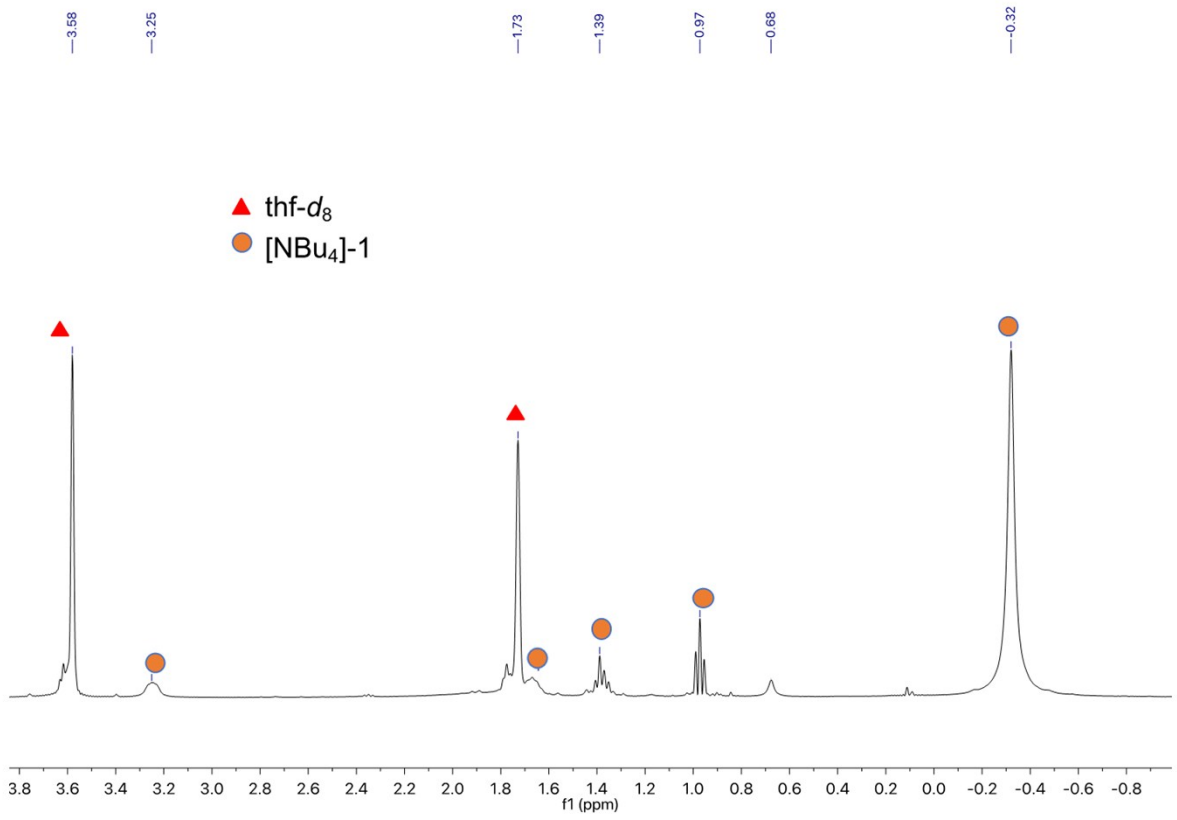

Figure S3. ^{1}H NMR spectrum (400 MHz, 23 °C) of [NBu$_4$][((^{t}BuO)$_3$SiO)$_3$U}$_2$(μ-N)], **[NBu$_4$]-1**, in thf-d_8

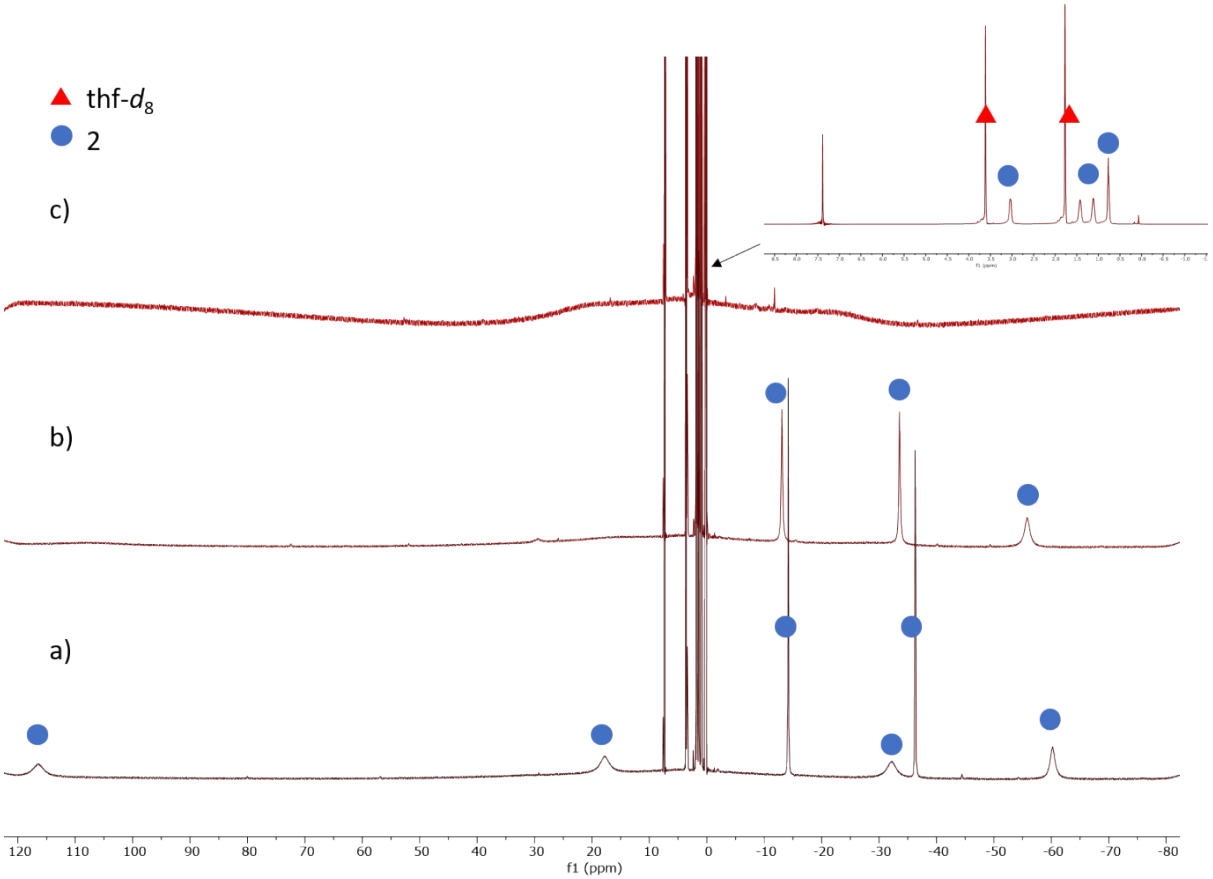

Figure S4. ^{1}H NMR spectrum (400 MHz) of $[NBu_4][((Me_3Si)_2N)_3U\}_2(\mu\text{-}N)]$, **2**, in thf-$d_8$ at (a) −60 °C, (b) −40 °C, and (c) 23 °C. The upper-right image shows the resonances for NBu_4^+.

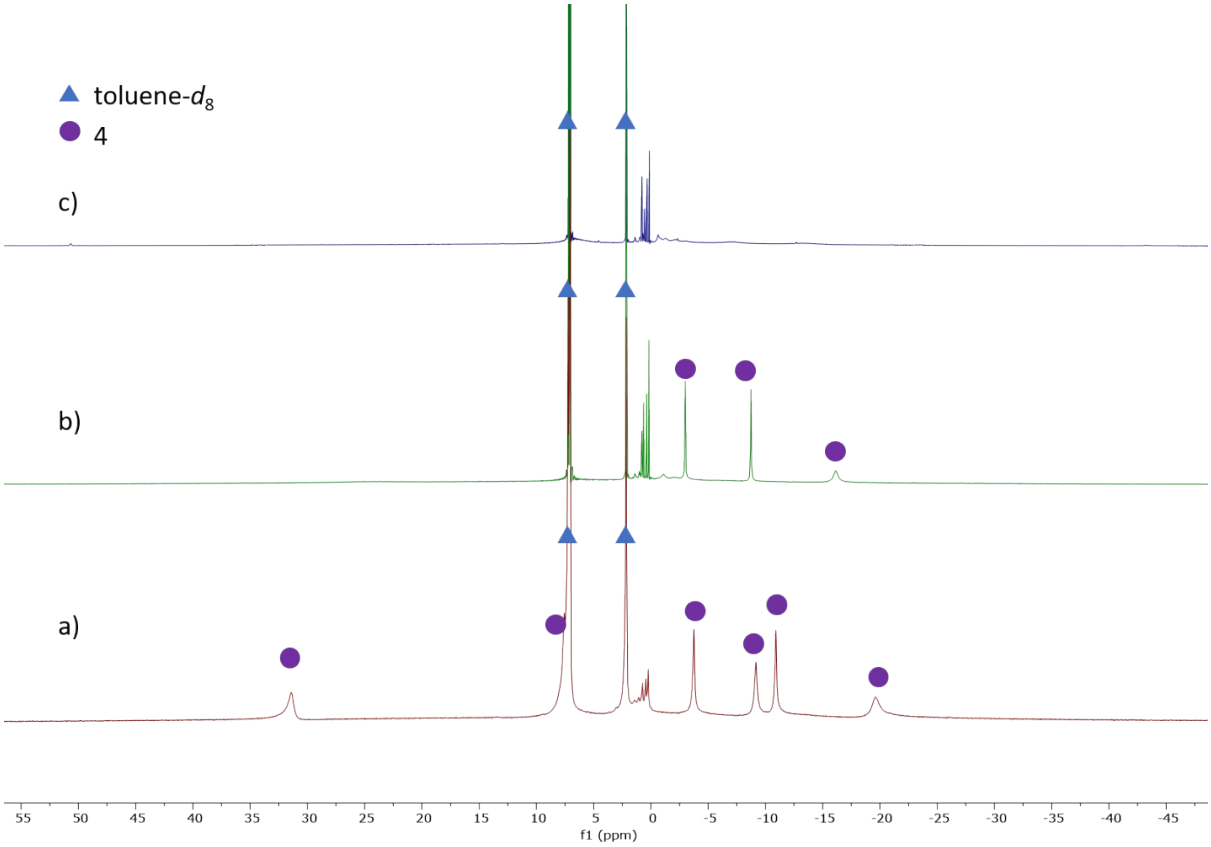

Figure S5. ^{1}H NMR spectrum (400 MHz) of $[((Me_3Si)_2N)_3U\}_2(\mu\text{-}N)]$, **4**, in toluene-$d_8$ at (a) −60 °C, (b) −40 °C, and (c) 23 °C.

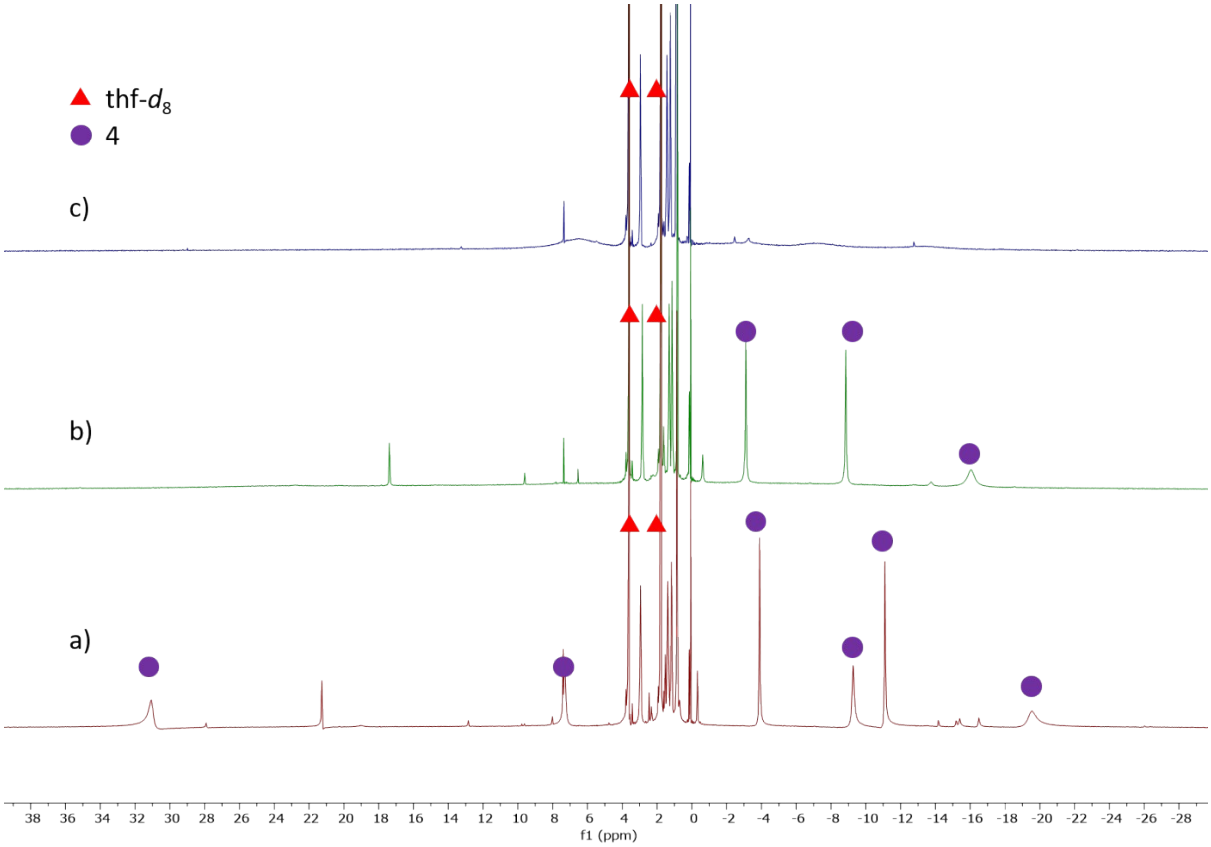

Figure S6. ^{1}H NMR spectrum (400 MHz) of $[((Me_3Si)_2N)_3U\}_2(\mu\text{-}N)]$, **4**, in thf-$d_8$ at (a) −60 °C, (b) −40 °C, and (c) 23 °C. The spectrum was generated from the reaction mixture of **2** and AgI.

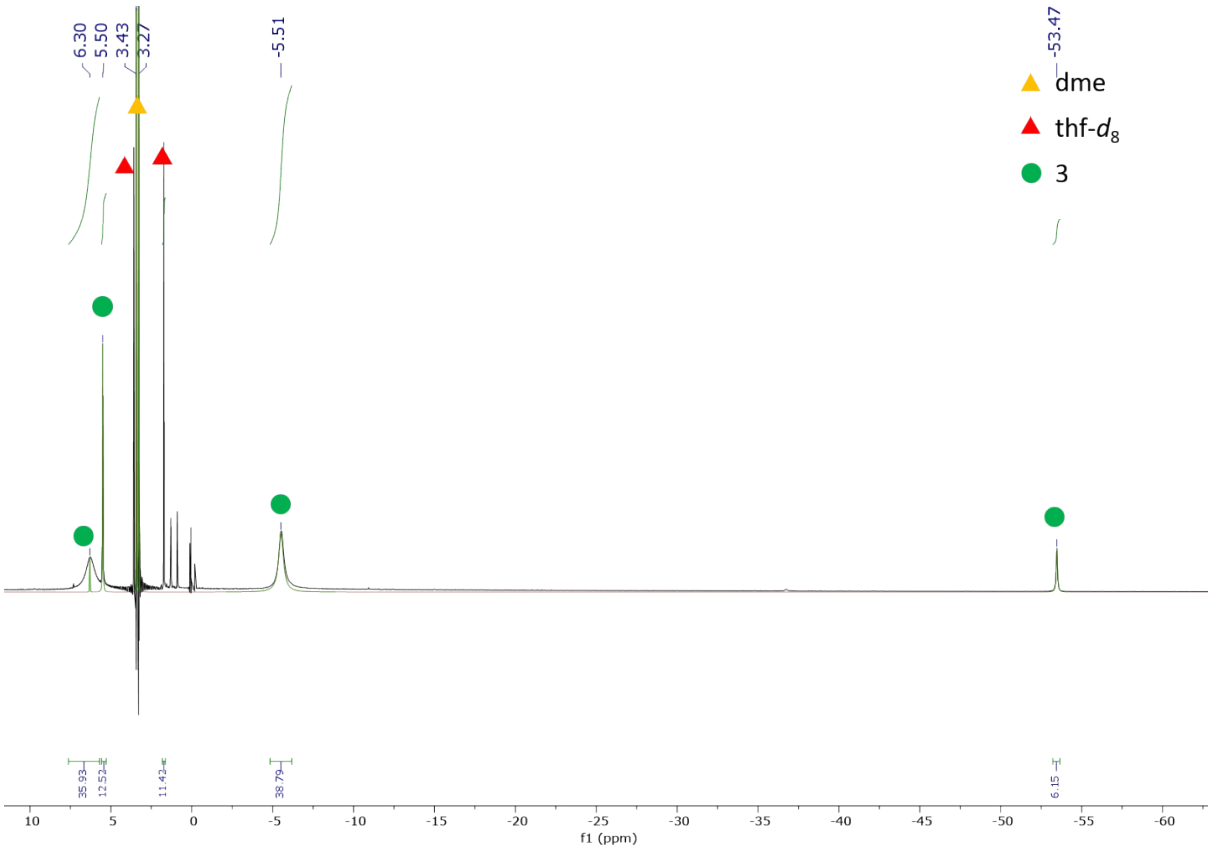

Figure S7. ^{1}H NMR spectrum (400 MHz, 23 °C) of [Na(dme)$_3$][((Me$_3$Si)$_2$)$_2$U(μ-N)(μ-κ^2-C,N-CH$_2$SiMe$_2$NSiMe$_3$)U(N(SiMe$_3$)$_2$)$_2$],[3] **3**, in thf-d_8.

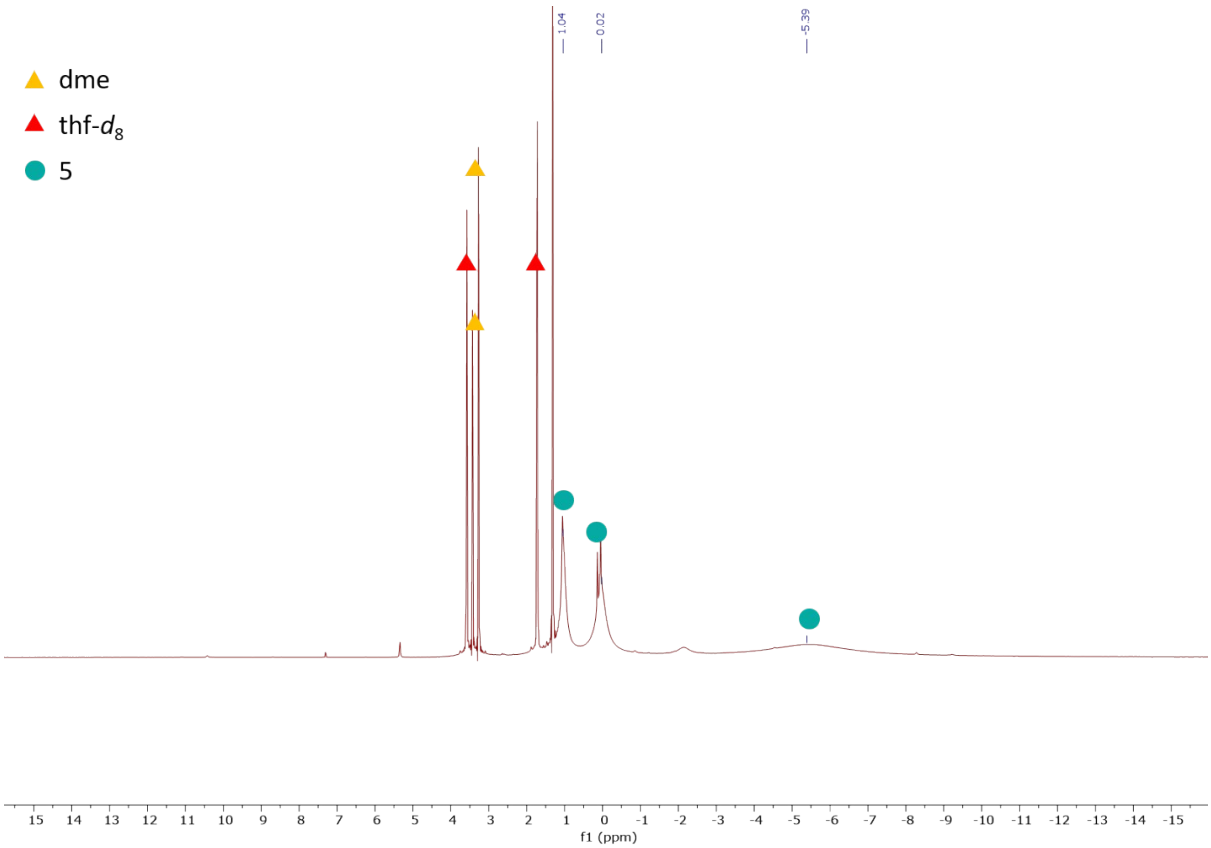

Figure S8. ^{1}H NMR spectrum (400 MHz, 23 °C) of [Na(dme)$_3$][((Me$_3$Si)$_2$N)$_3$U(μ-N)U(N(SiMe$_3$)$_2$)(OSi(O^{t}Bu)$_3$)], **5**, in thf-d_8.

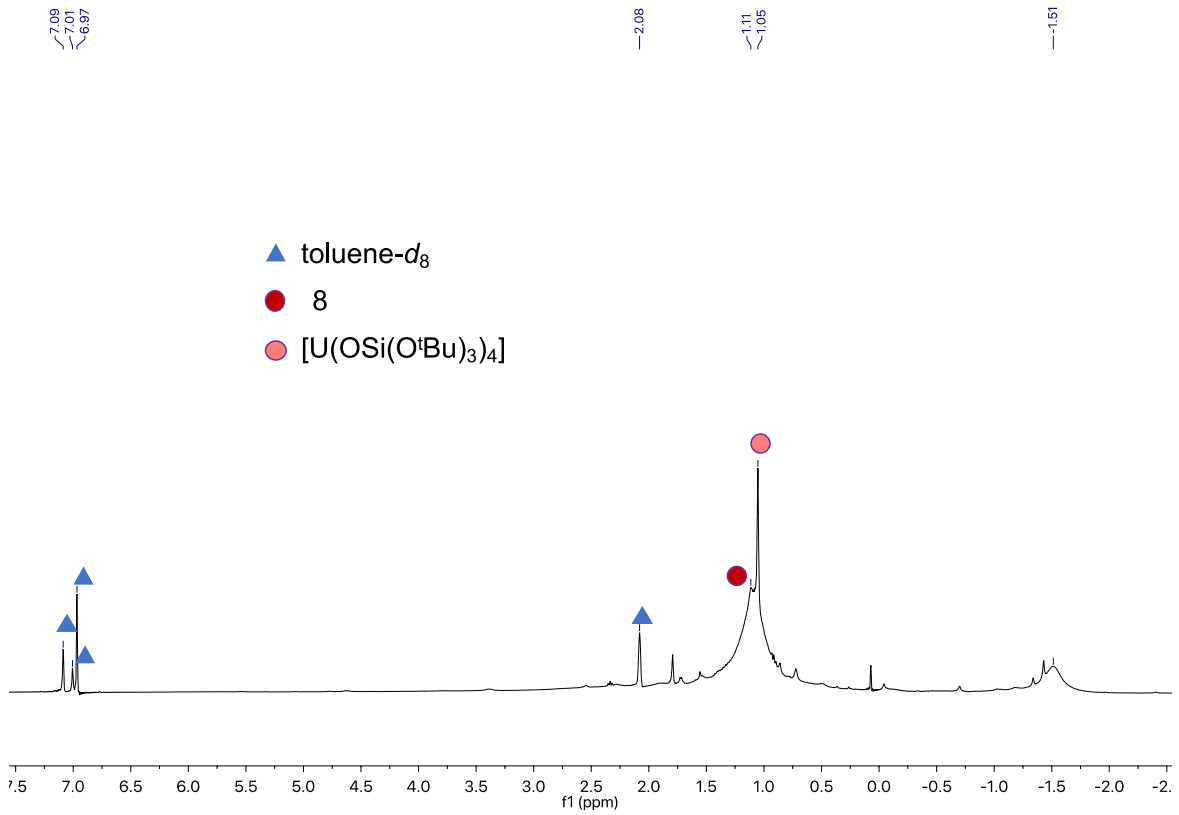

Figure S9. ^{1}H NMR spectrum (400 MHz, 23 °C, toluene-d_8) of the reaction mixture of **[NBu$_4$]-1** and CO_2.

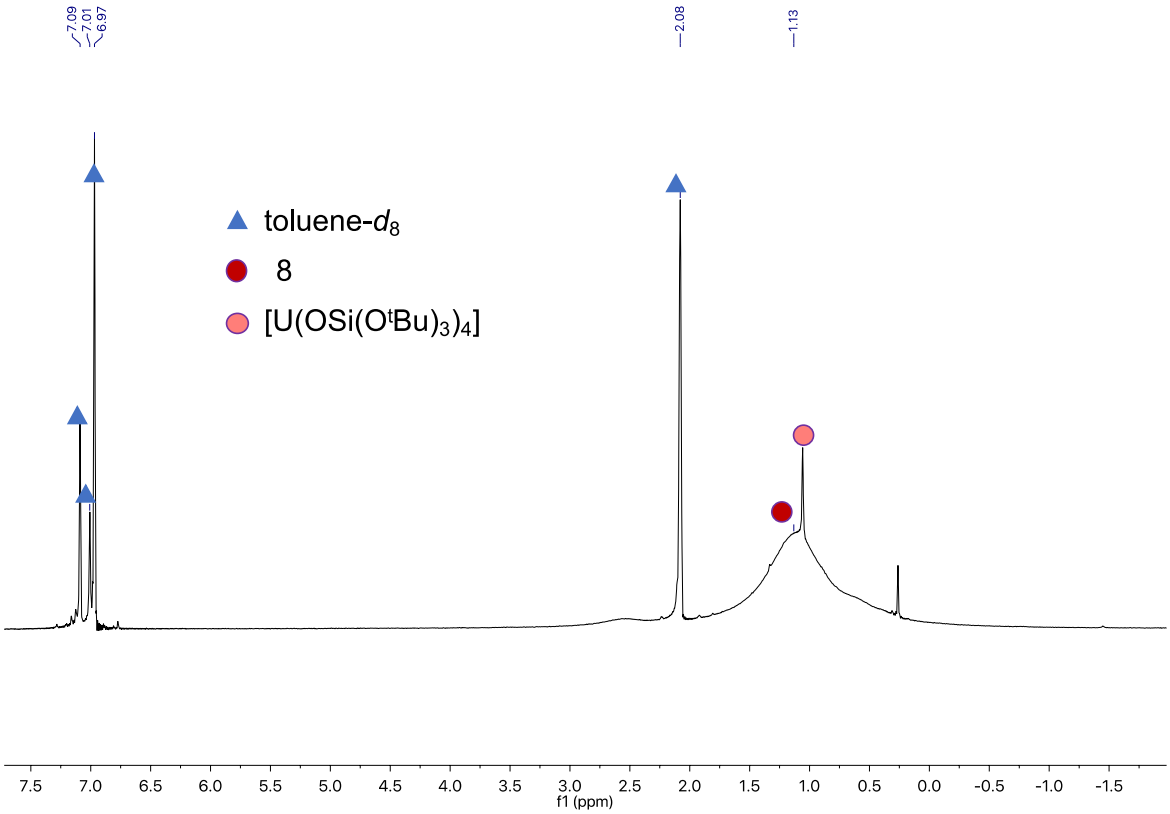

Figure S10. ^{1}H NMR Spectrum of (400 MHz, 23 °C, toluene-d_8) of [NBu$_4$][{((^{t}BuO)$_3$SiO)$_3$U}$_2$(μ-NC$_2$O$_4$)], **8**; isolated crystals always contain traces of the [U(OSi(O^{t}Bu)$_3$)$_4$][8] by product.

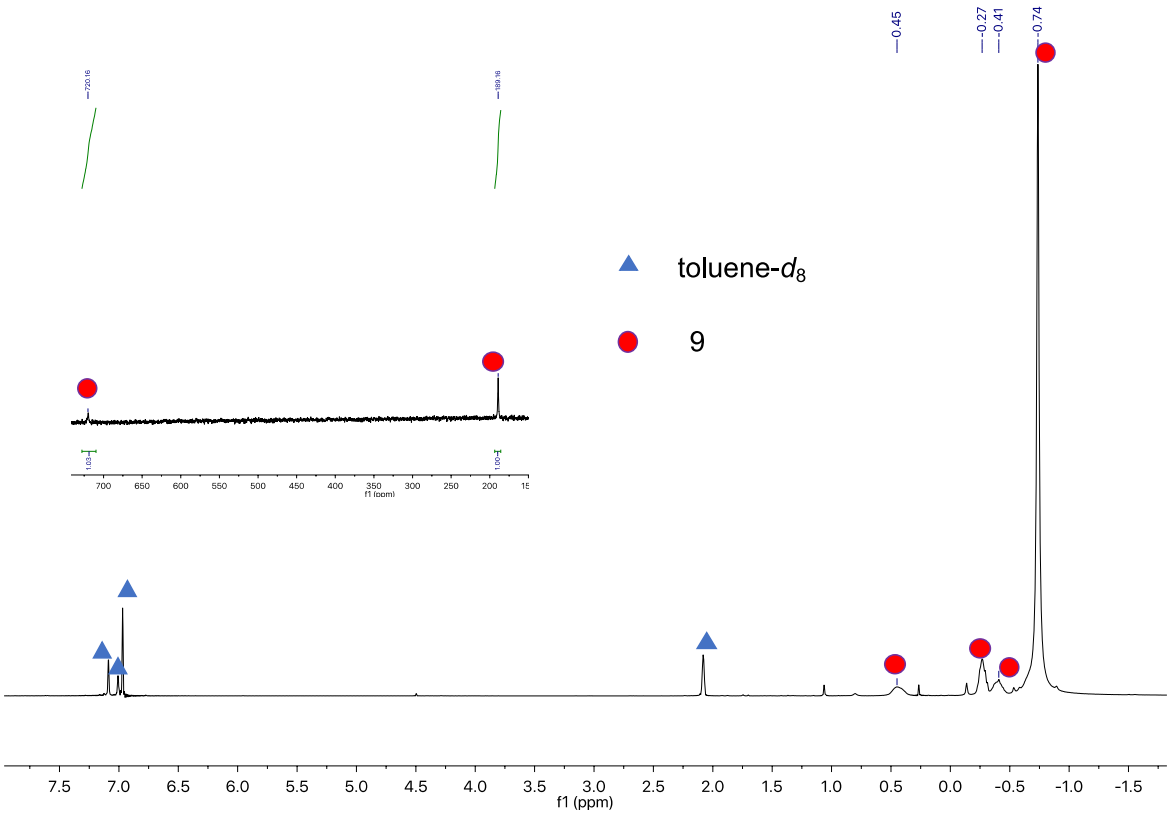

Figure S11. ^{1}H NMR Spectrum of (400 MHz, 23 °C, toluene-d_8) of $[NBu_4][\{((^tBuO)_3SiO)_3U\}_2(\mu\text{-}NH)(\mu\text{-}H)]$, **9**. The upper-left image shows the resonances for NH and H protons.

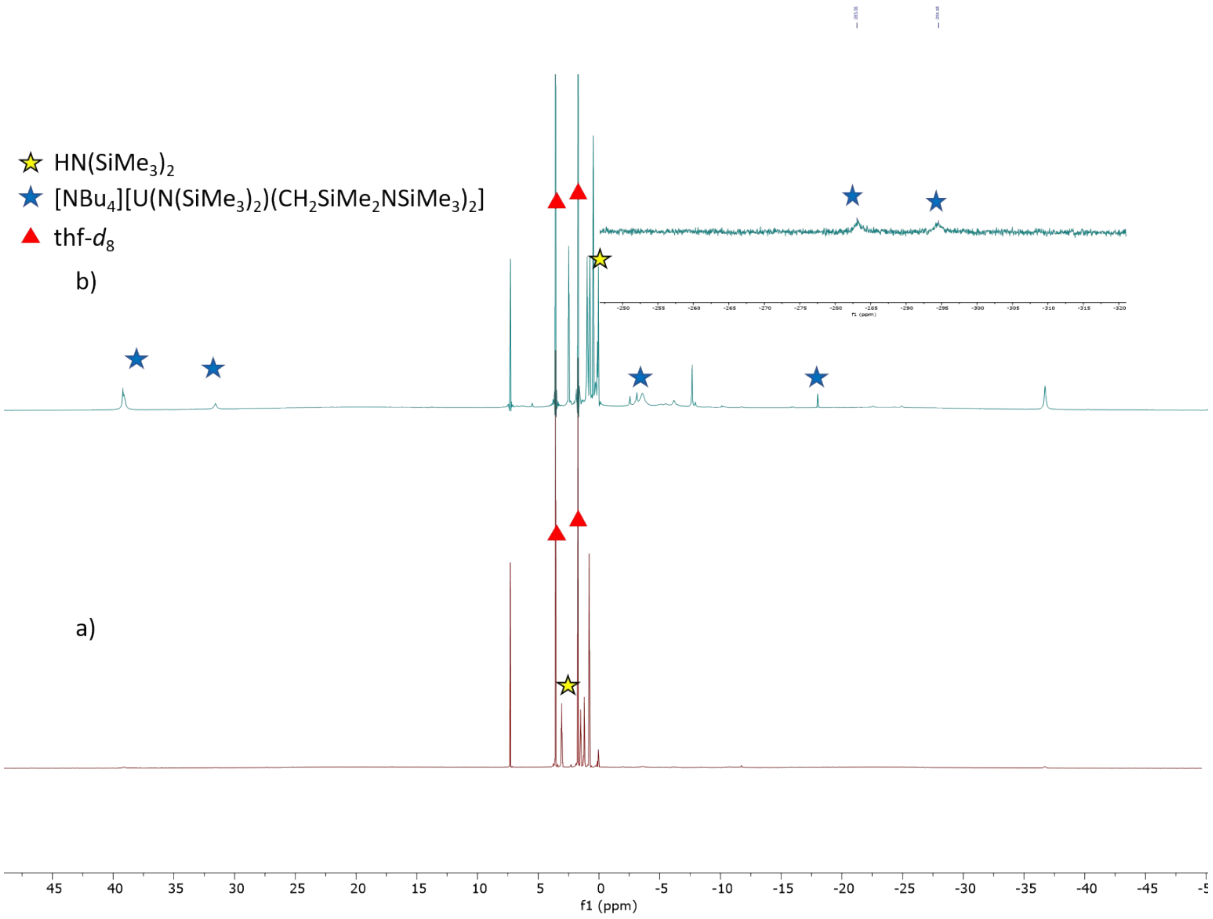

Figure S12. ^{1}H NMR spectra (400 MHz, 23 °C) showing the room temperature decomposition of **2** in thf-d_8 after (a) 10 min and (b) 24 h.

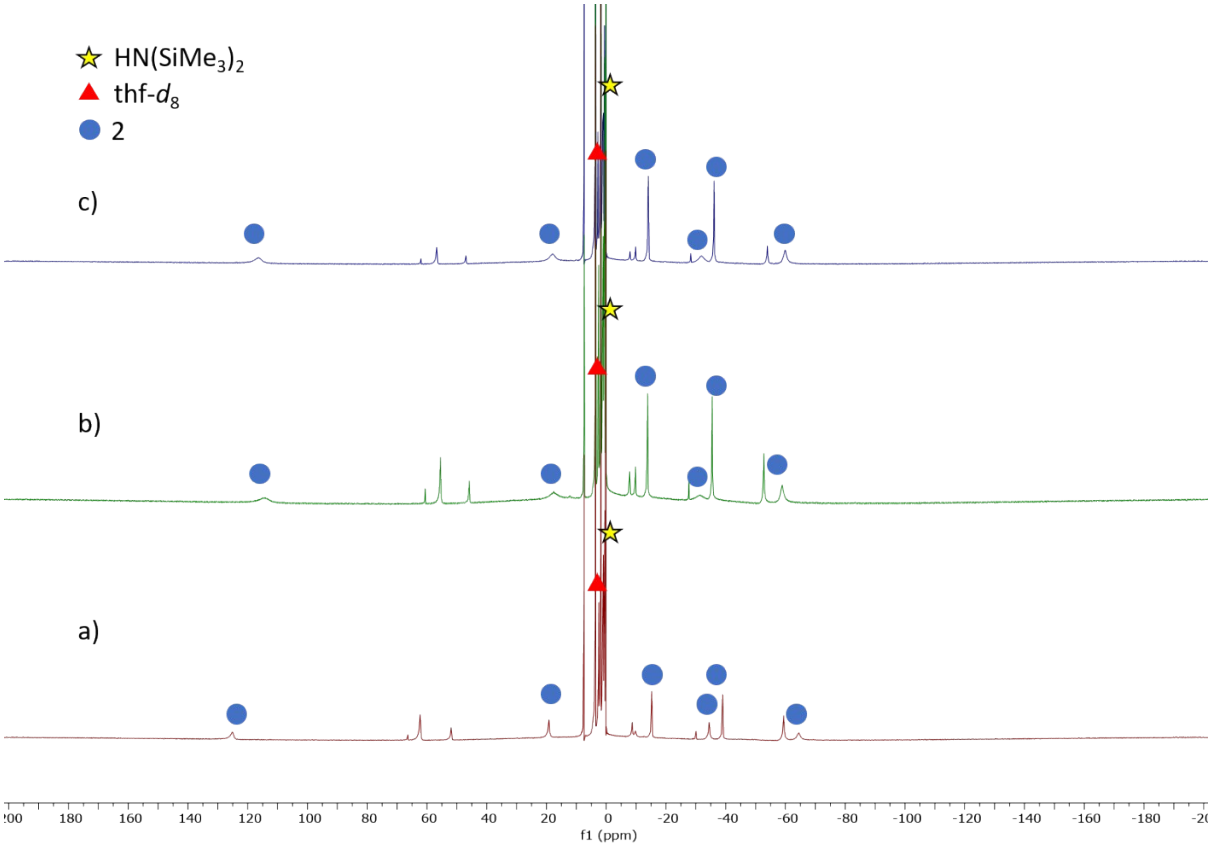

Figure S13. ^{1}H NMR spectra (400 MHz) showing the room temperature decomposition of **2** in thf-d_8 at (a) −60 °C, after 2 d; (b) −60 °C, after 4 d; (c) −80 °C, after 6 d.

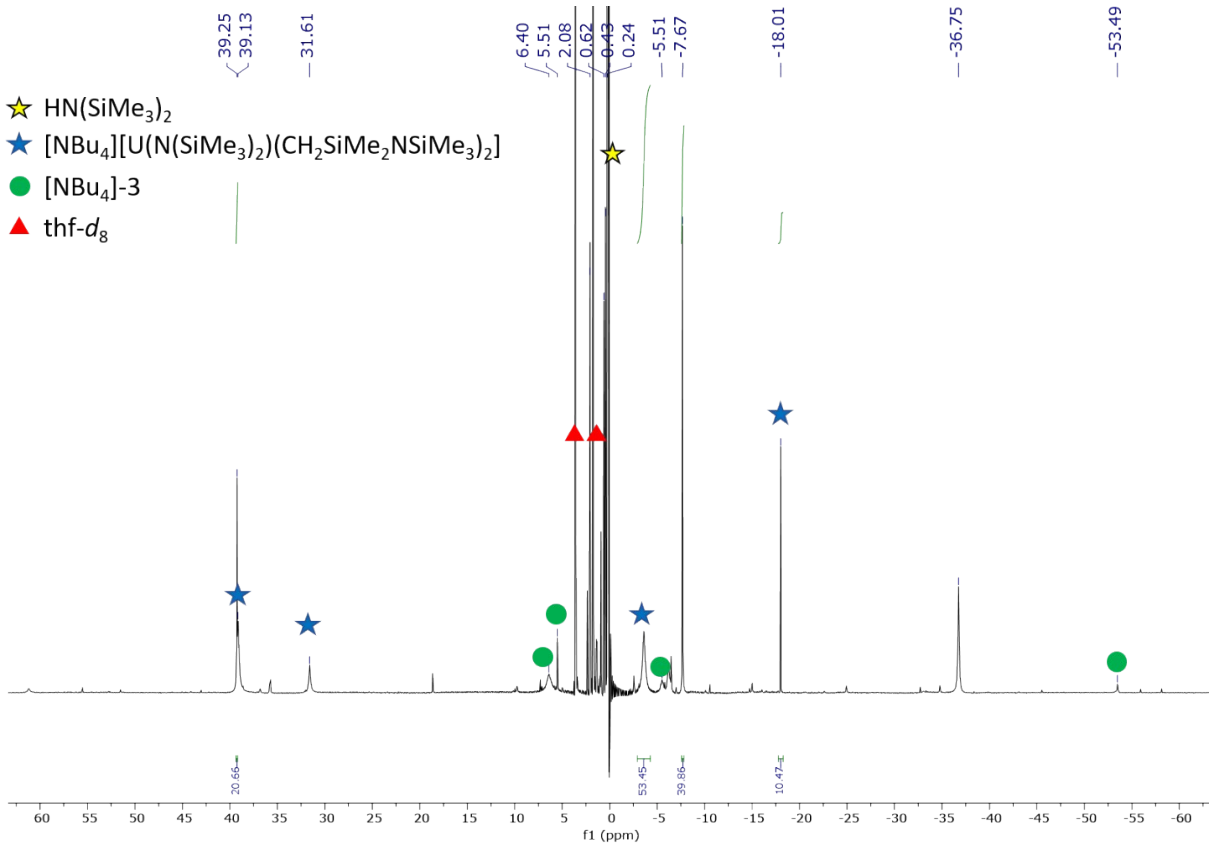

Figure S14. ^{1}H NMR spectra (400 MHz, 23 °C, thf-d_8) after heating **2** at 66 °C for 2 h in thf-d_8.

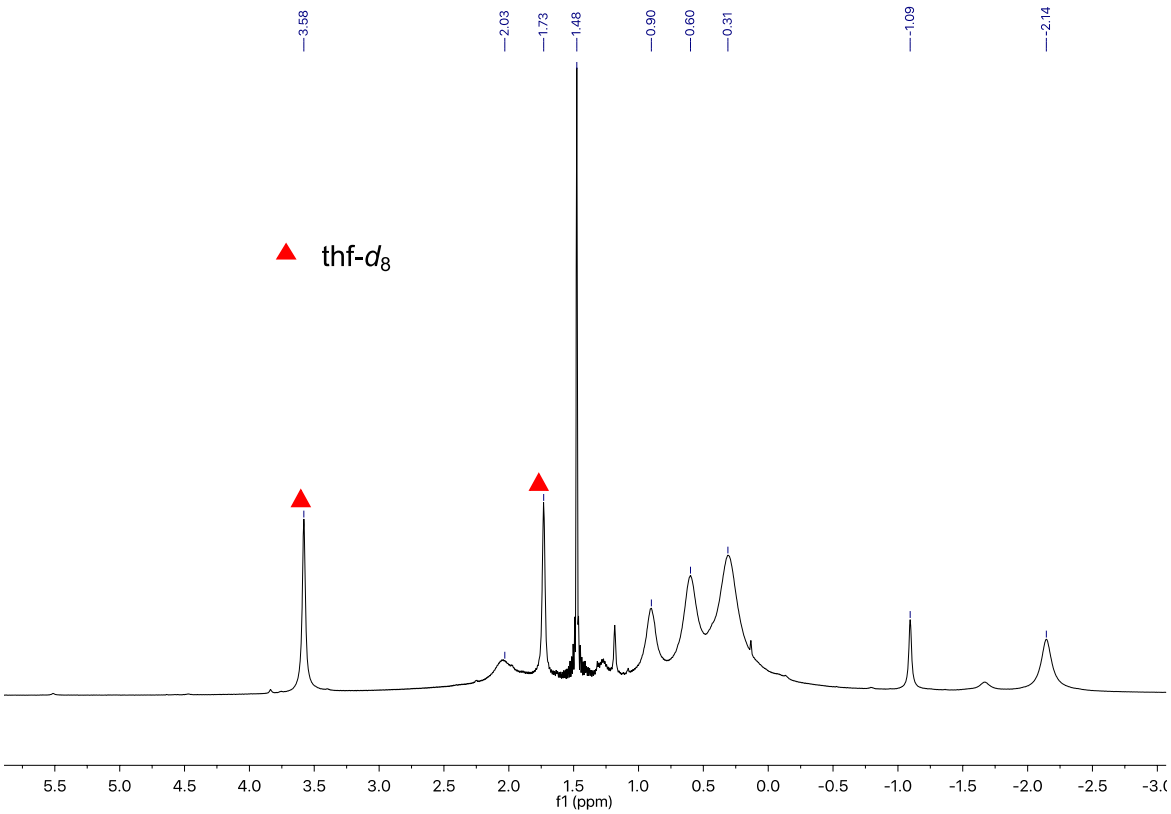

Figure S15. ^{1}H NMR spectrum (400 MHz, 23 °C, thf-d_8) of the reaction mixture after reaction of **[Cs]-1** with CO in thf-d_8

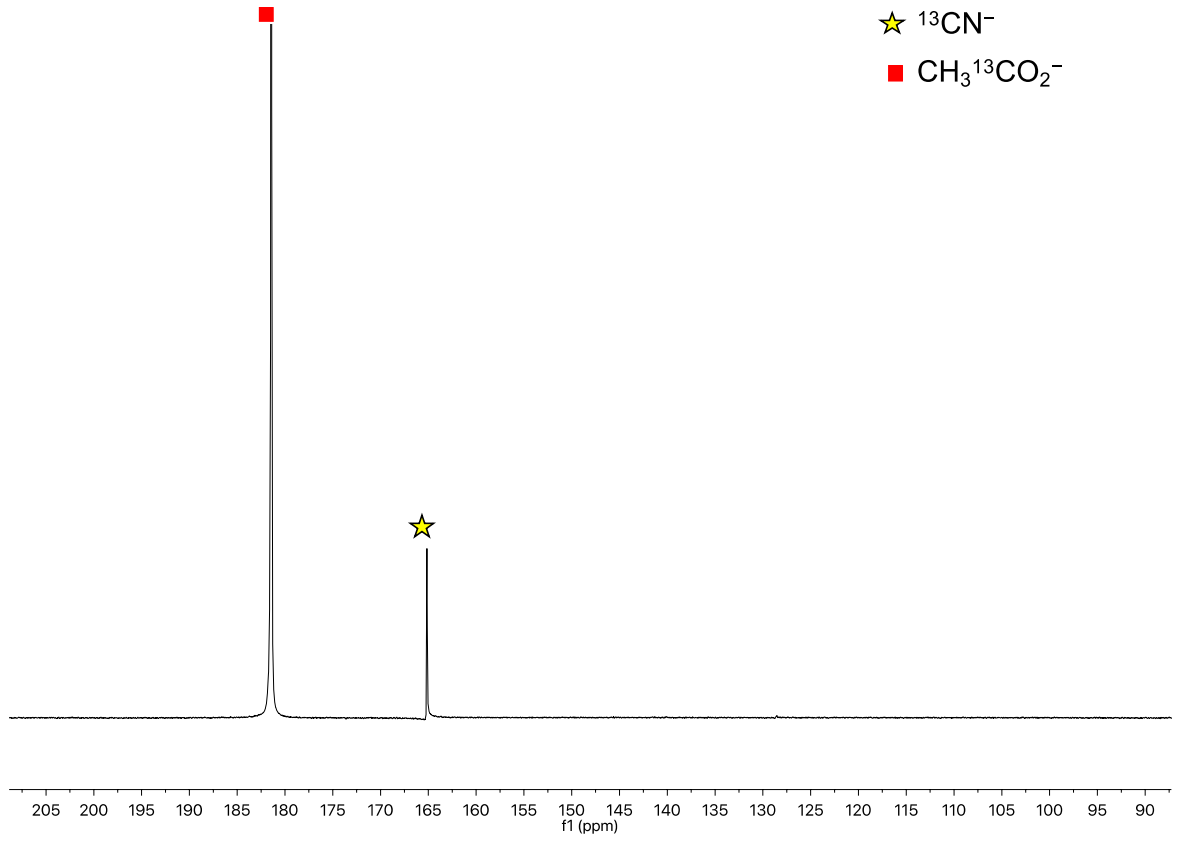

Figure S16. ^{13}C NMR spectrum (151 MHz, 23 °C, D_2O) after hydrolysis of the reaction mixture of **[Cs]-1** with ^{13}CO in thf-d_8 with a pD = 12 D_2O solution. $NaO_2{}^{13}CCH_3$ was added as an internal standard.

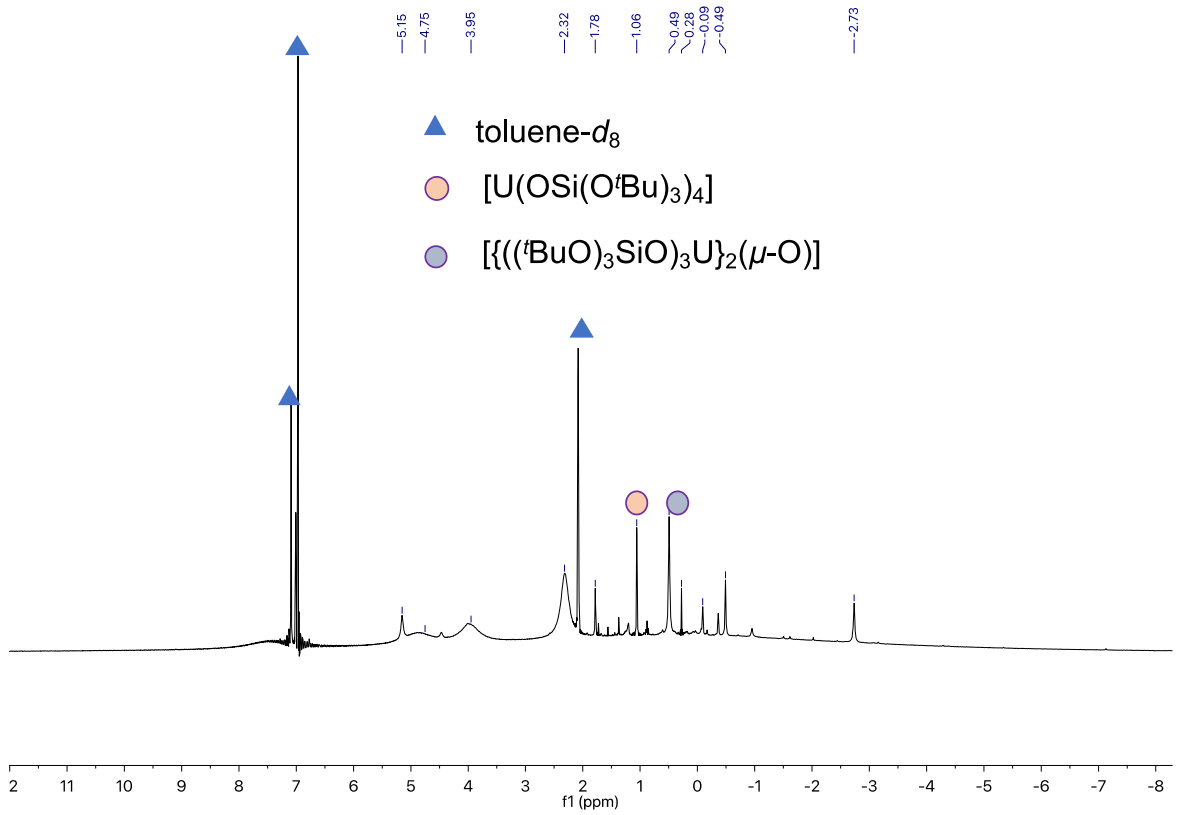

Figure S17. ^{1}H NMR spectrum (400 MHz, 23 °C, toluene-d_8) of the reaction of **[NBu$_4$]-1** with CO in toluene-d_8.

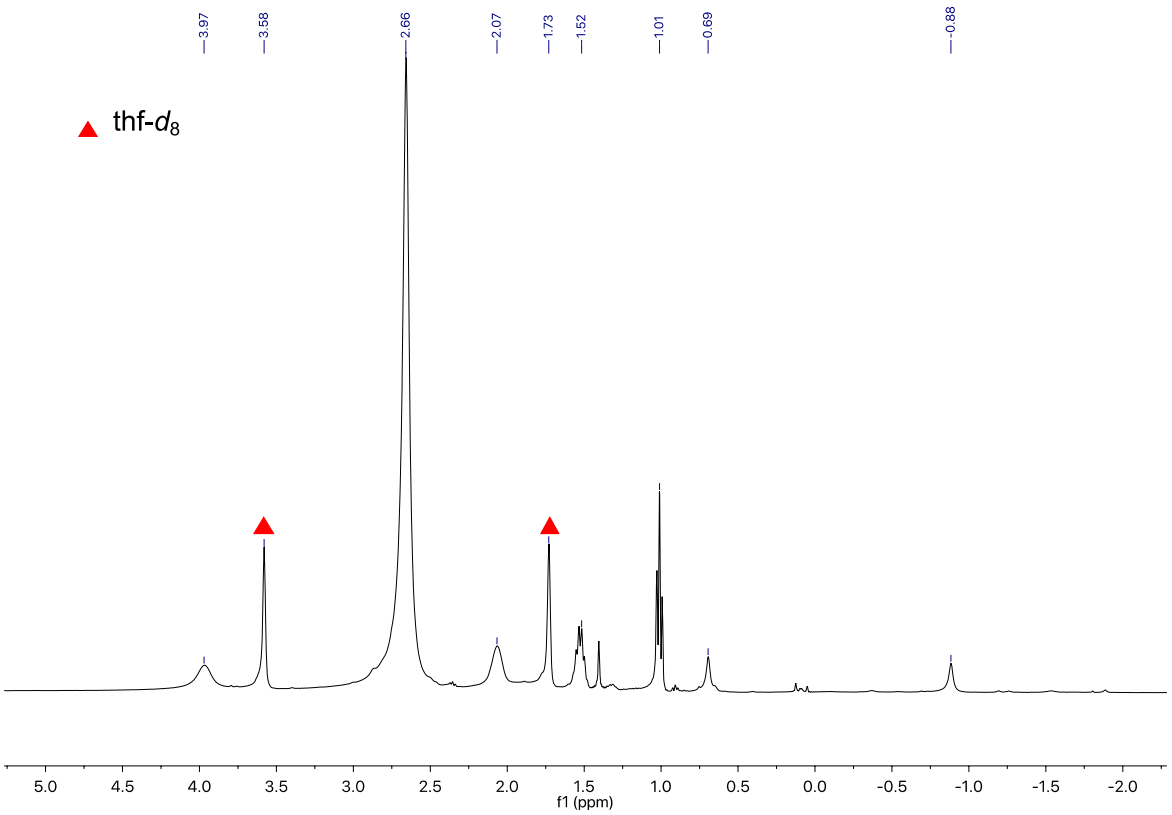

Figure S18. ^{1}H NMR spectrum (400 MHz, 23 °C, thf-d_8) of the reaction mixture of **[NBu$_4$]-1** with CO in thf-d_8.

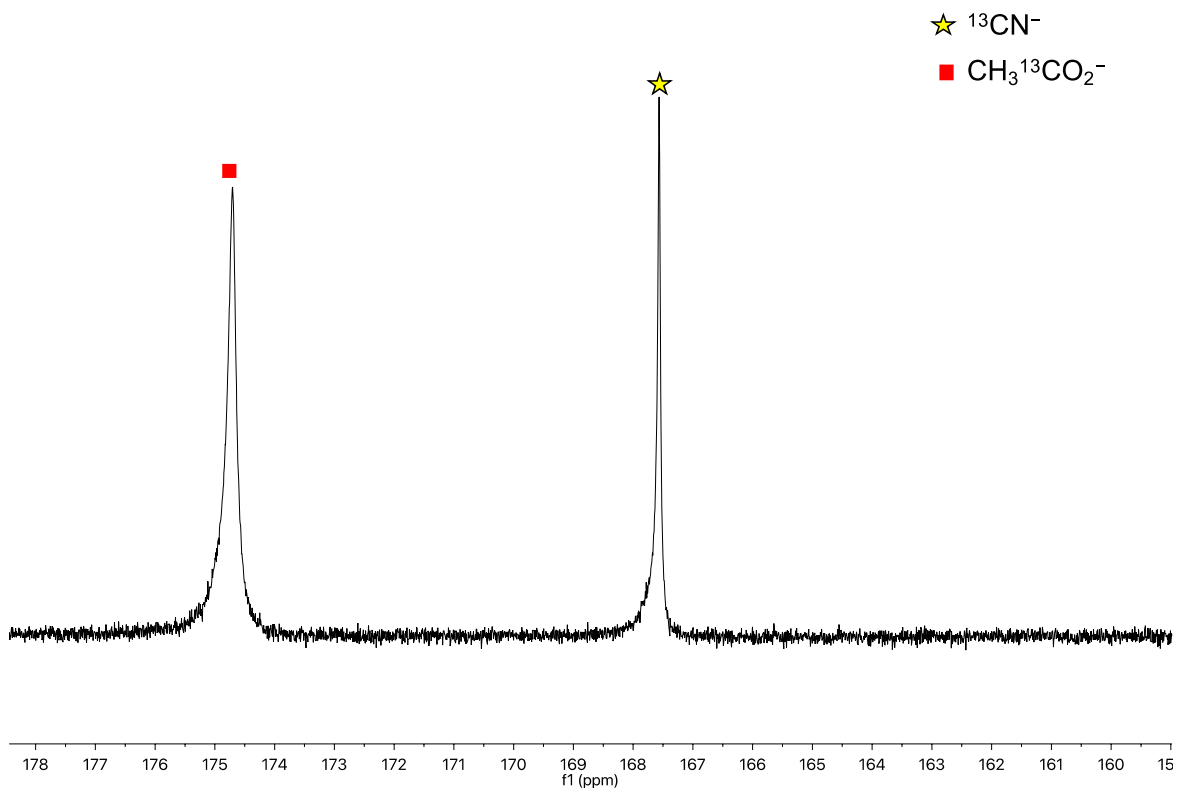

Figure S19. ^{13}C NMR spectrum (151 MHz, 23 °C, D_2O) after hydrolysis of the reaction mixture of **[NBu$_4$]-1** with ^{13}CO in thf-d_8 with a pD = 12 D_2O solution. $NaO_2{}^{13}CCH_3$ was added as an internal standard.

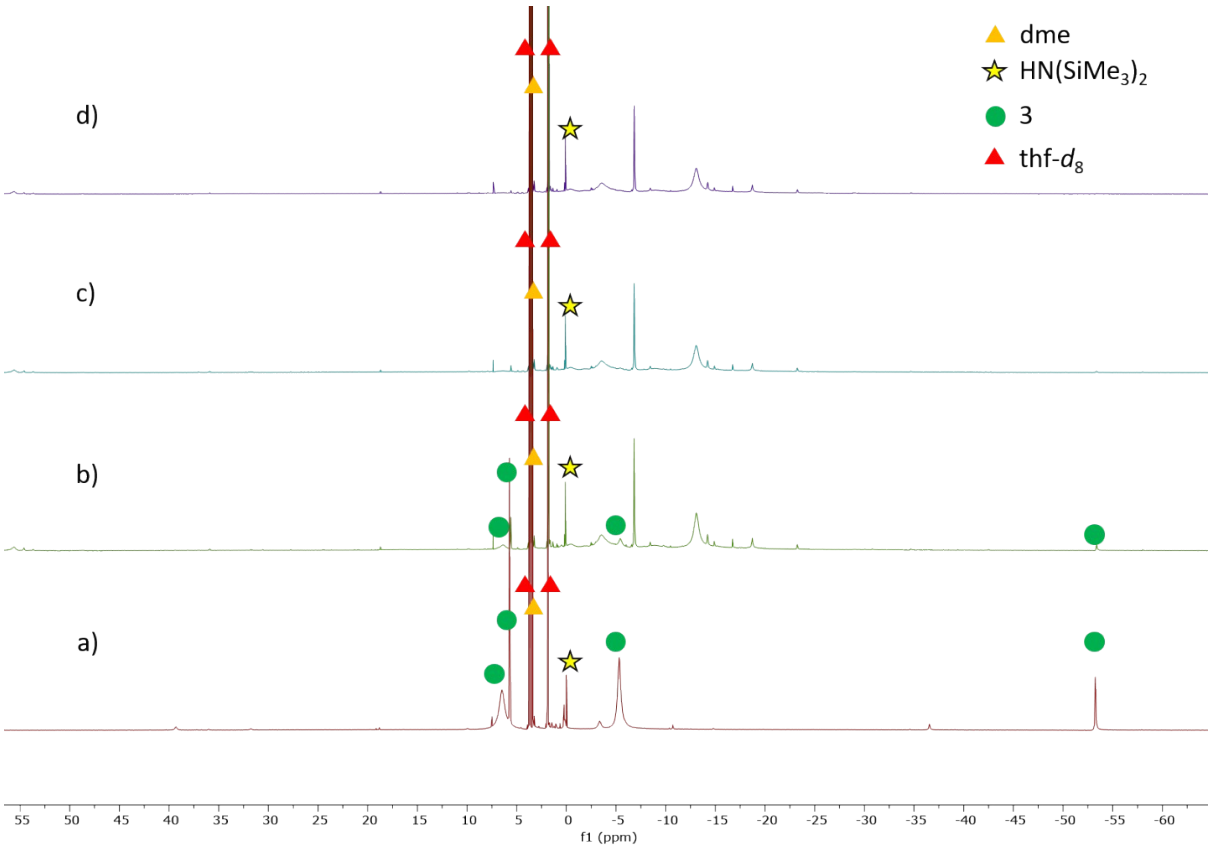

Figure S20. ^{1}H NMR spectra (400 MHz, thf-d_8) of the reaction mixture of **3** and excess CO (1 atm) (a) before the introduction of CO, (b) 17 min after CO introduction, (c) 45 min after CO introduction, and (d) 1 h 15 min after CO introduction.

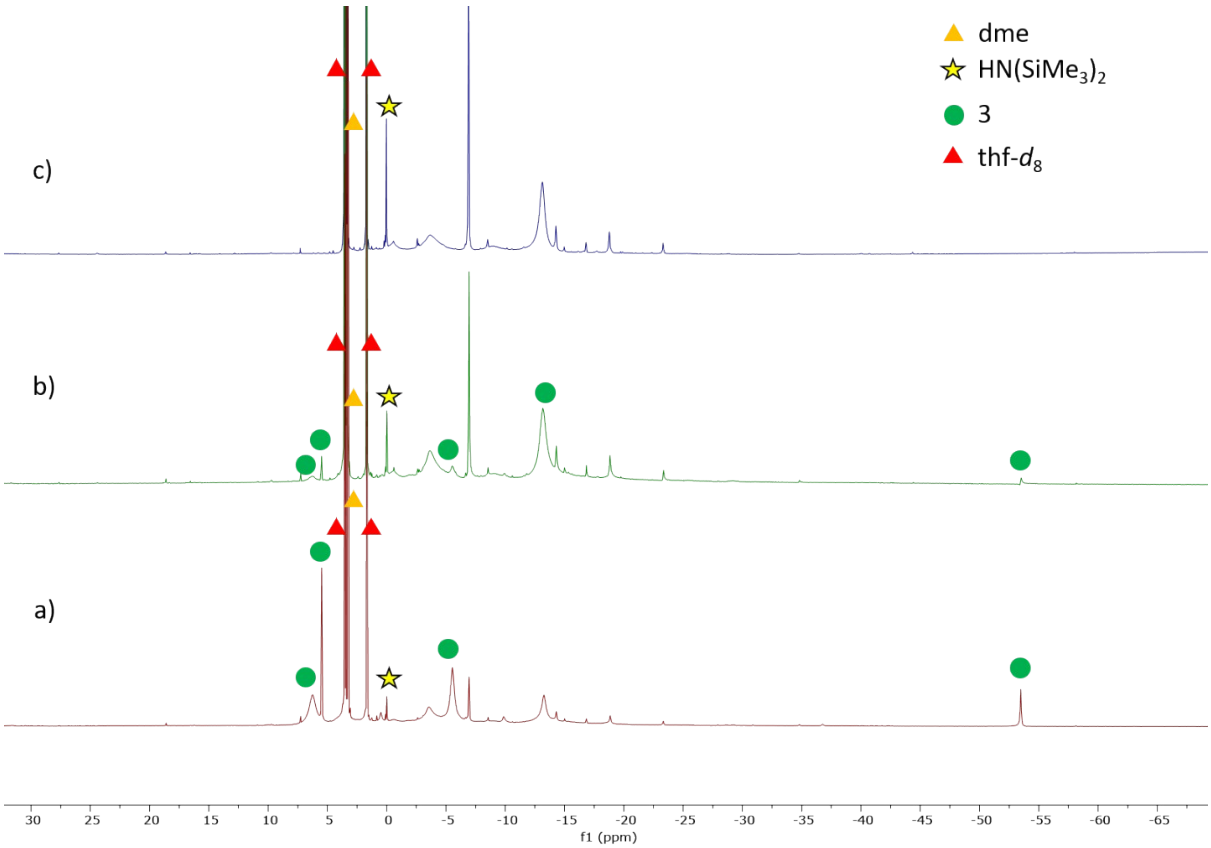

Figure S21. ^{1}H NMR spectra (400 MHz, 23 °C, thf-d_8) of the reaction mixture of **3** and ^{13}CO (1-2 equiv) after (a) 13 min, (b) 3 h 22 min, and (c) 70 h.

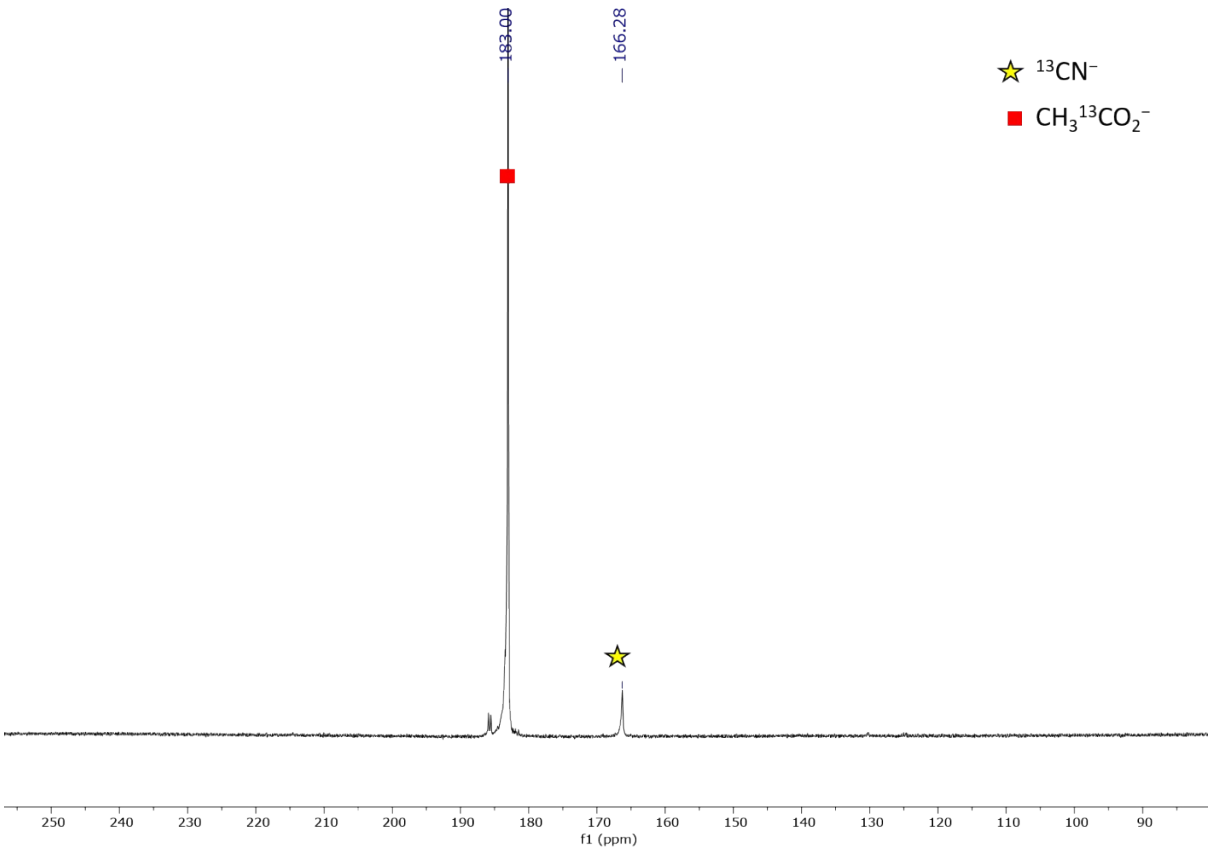

Figure S22. ^{13}C NMR spectrum (151 MHz, 23 °C, D_2O) after hydrolysis of the **3** / ^{13}CO reaction mixture with a pD = 12 D_2O solution. $NaO_2{}^{13}CCH_3$ was added as an internal standard.

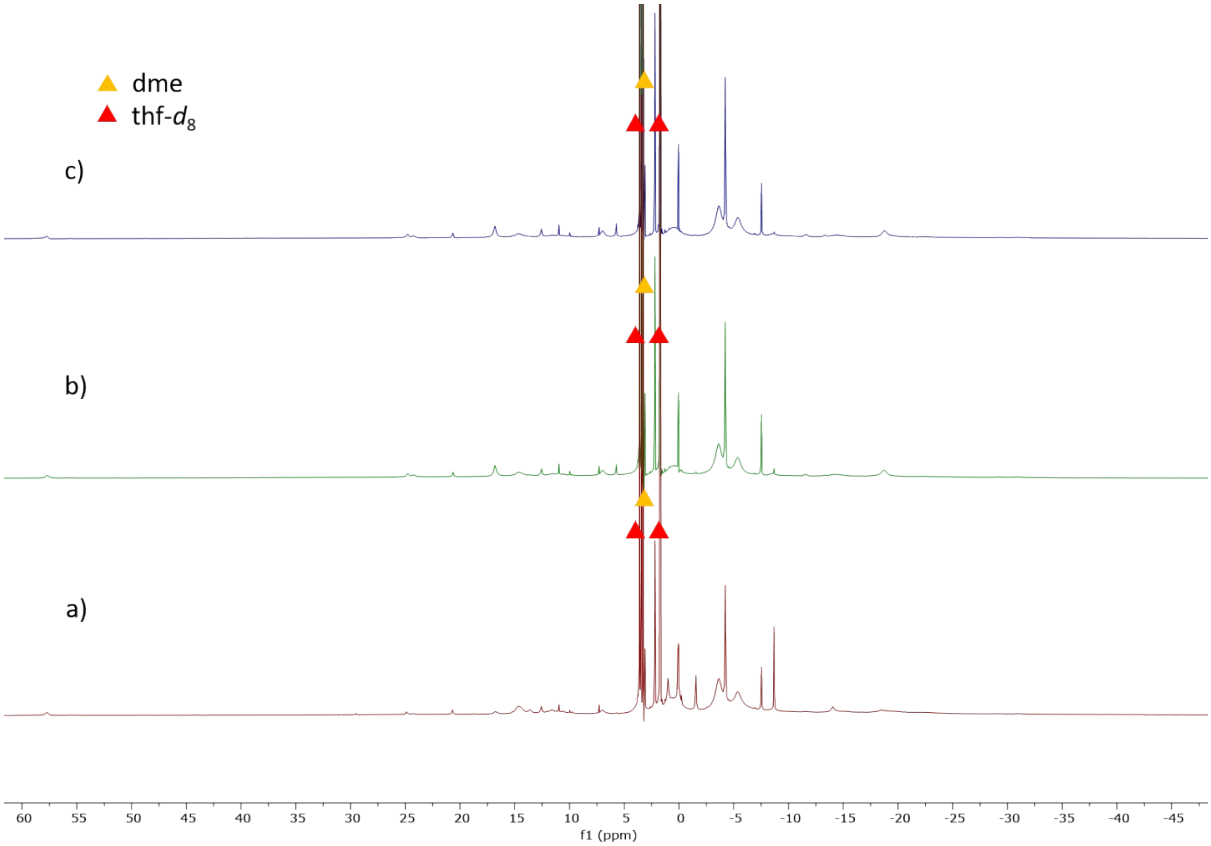

Figure S23. ^{1}H NMR spectra (400 MHz, 23 °C, thf-d_8) of the reaction mixture of **5** and excess CO (1 atm) after (a) 10 min, (b) 30 min, and (c) 90 min.

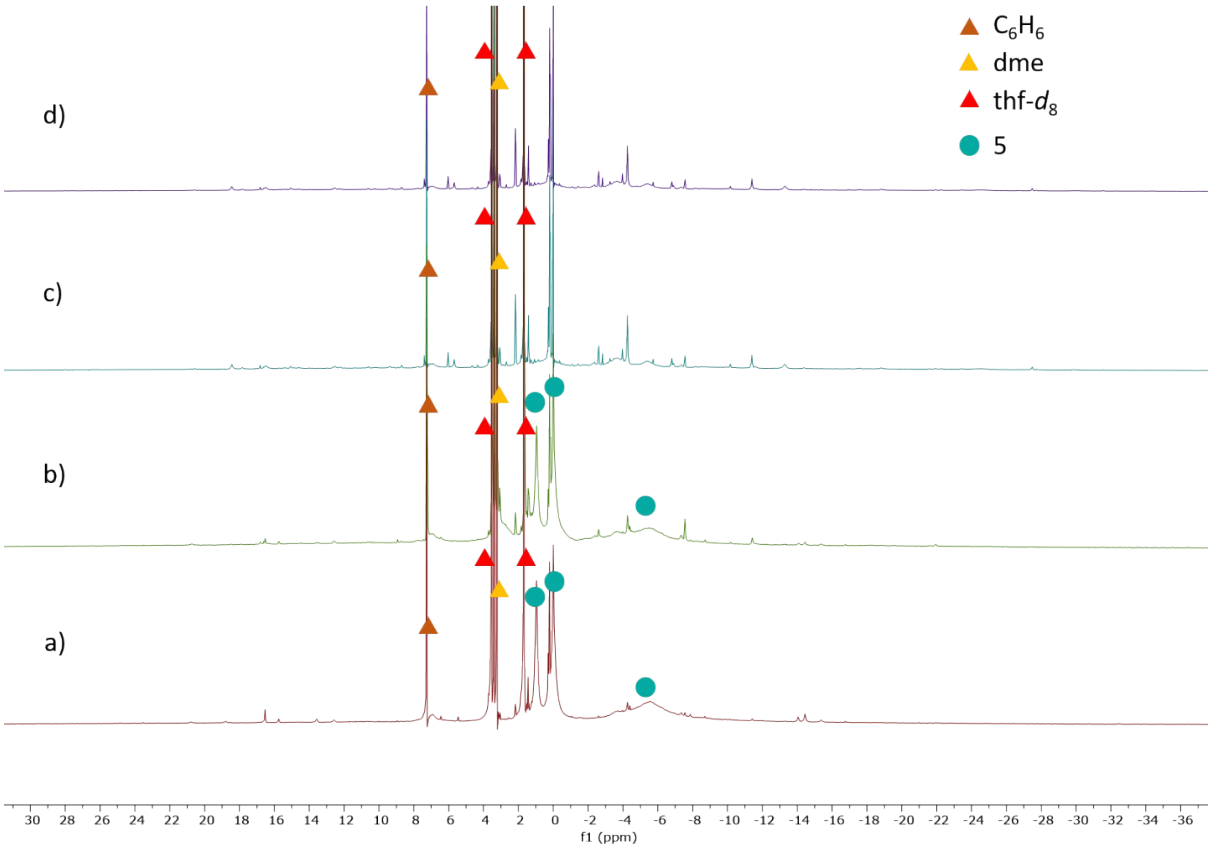

Figure S24. ^{1}H NMR spectra (400 MHz, 23 °C, thf-d_8) of the reaction mixture of **5** and ^{13}CO (1-2 equiv) after (a) 10 min, (b) 2 h, (c) 21 h, and (d) and 24 h.

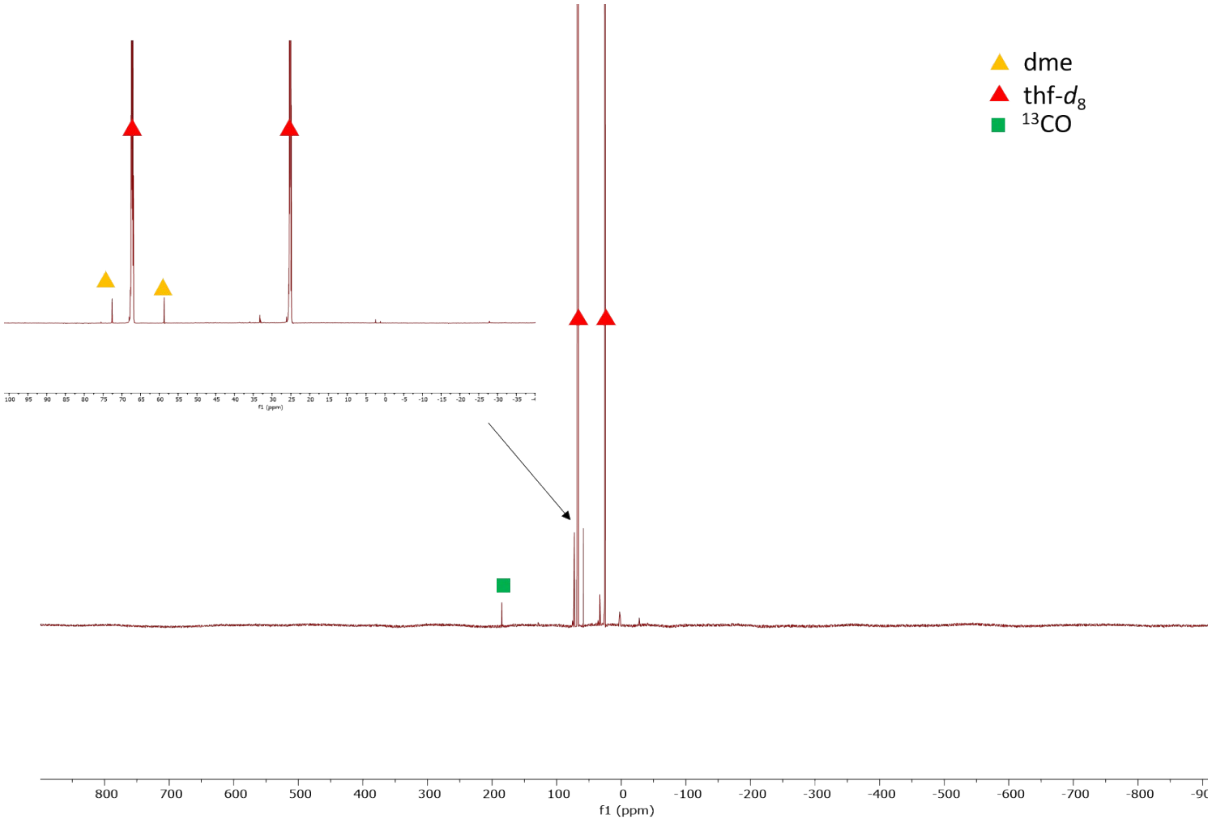

Figure S25. ^{13}C NMR spectrum (151 MHz, 23 °C, thf-d_8) of the reaction mixture of **5** and ^{13}CO (1-2 equiv).

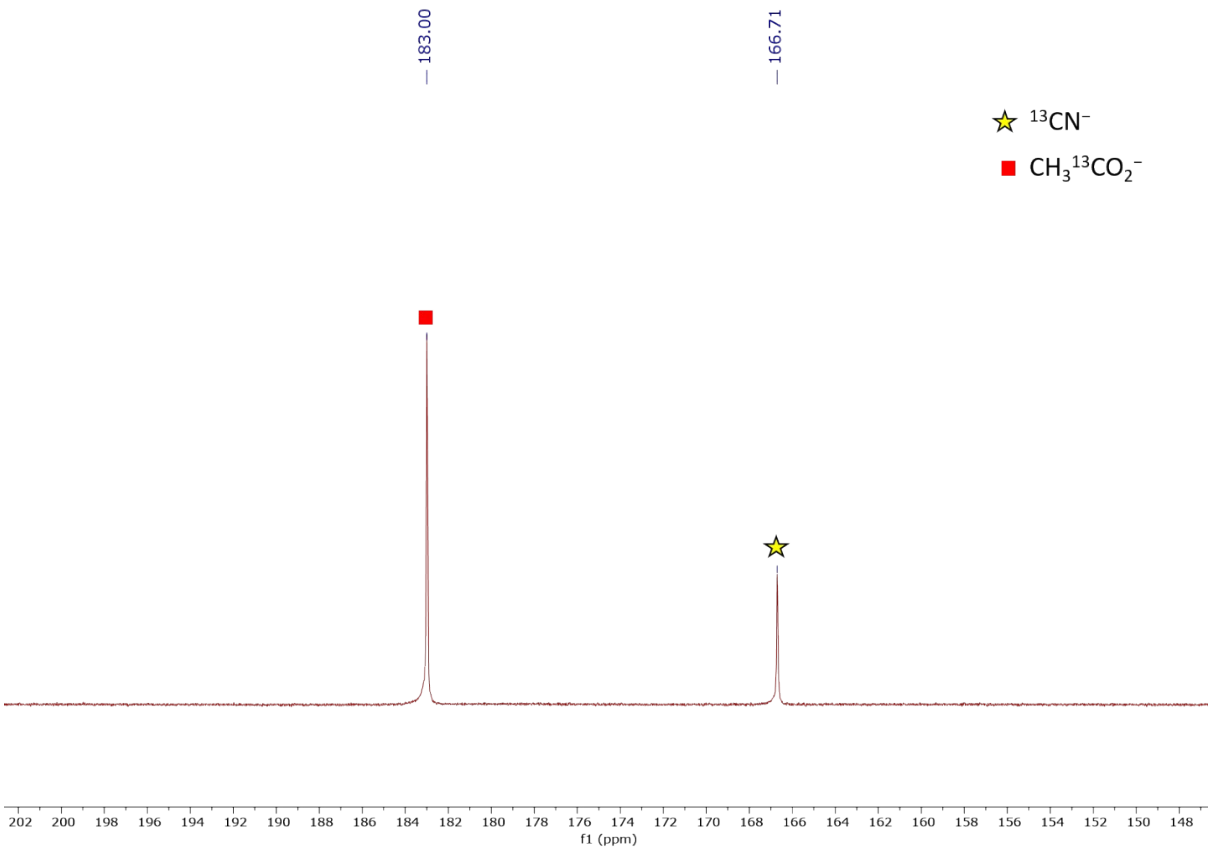

Figure S26. ^{13} NMR spectrum (151 MHz, 23 °C, D_2O) after hydrolysis of the reaction mixture of **5** and ^{13}CO (1-2 equiv) with pD = 12 D_2O.

CO_2 Reactivity

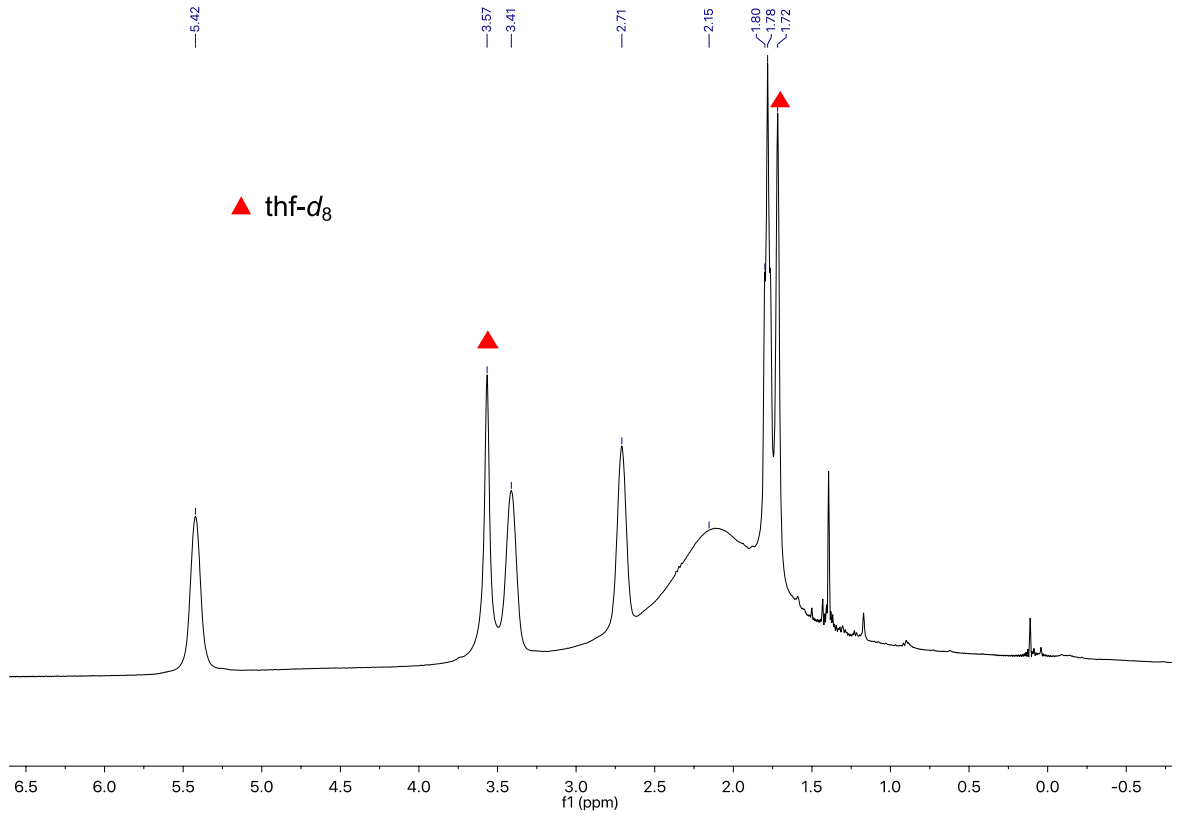

Figure S27. ^{1}H NMR spectrum (400 MHz, 23 °C, thf-d_8) of the reaction mixture of **[NBu$_4$]-1** and 6 equiv of $^{13}CO_2$.

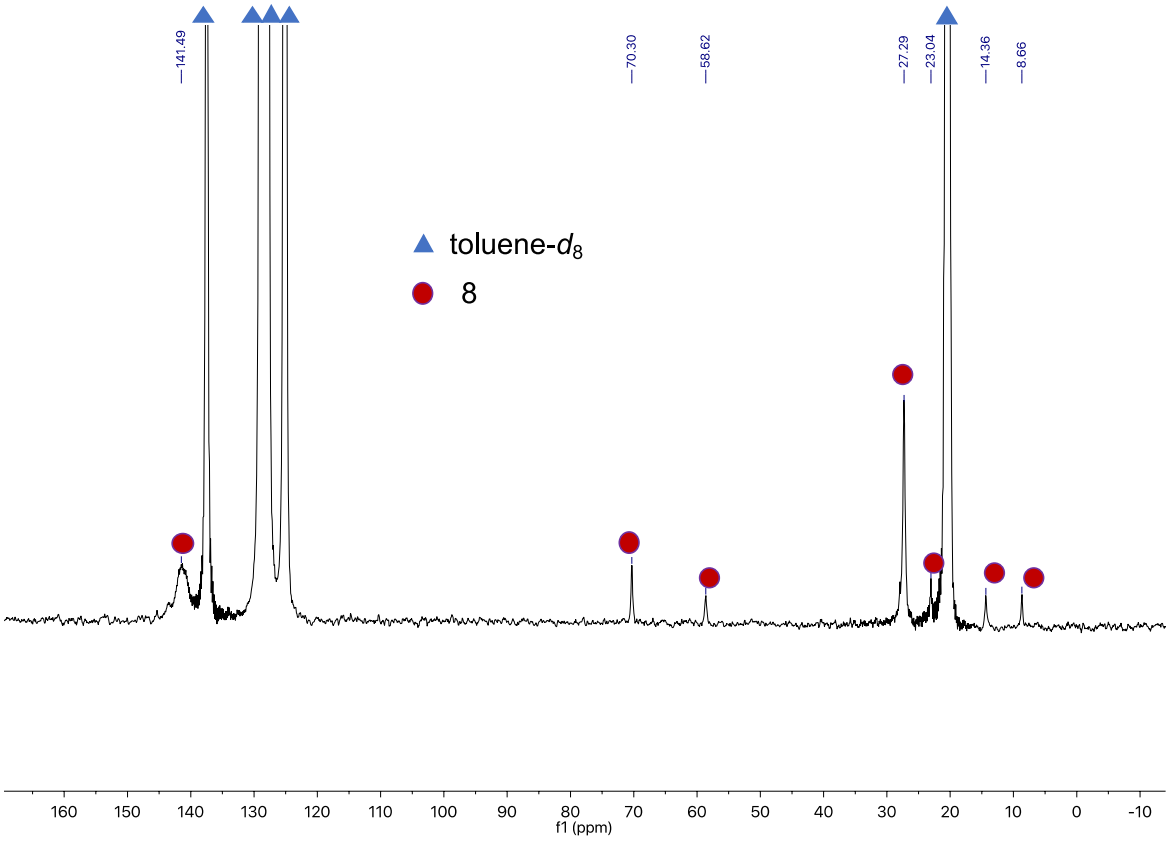

Figure S28. ^{13}C NMR spectrum (151 MHz, 23 °C, toluene-d_8) of the reaction mixture of **[NBu$_4$]-1** and $^{13}CO_2$.

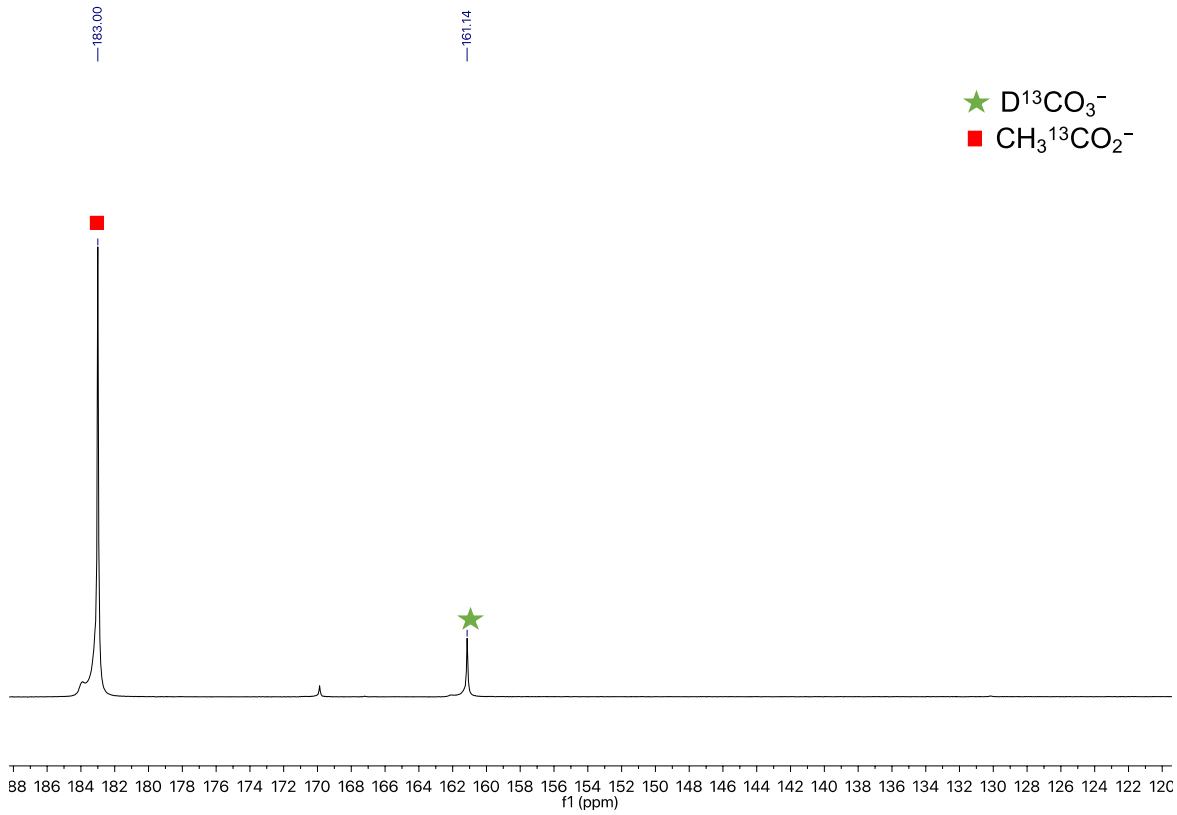

Figure S29. ^{13}C NMR spectrum (151 MHz, 23 °C, D_2O) after hydrolysis of the reaction mixture of **[NBu$_4$]-1** and 6 equiv of $^{13}CO_2$ with pD = 12 D_2O.

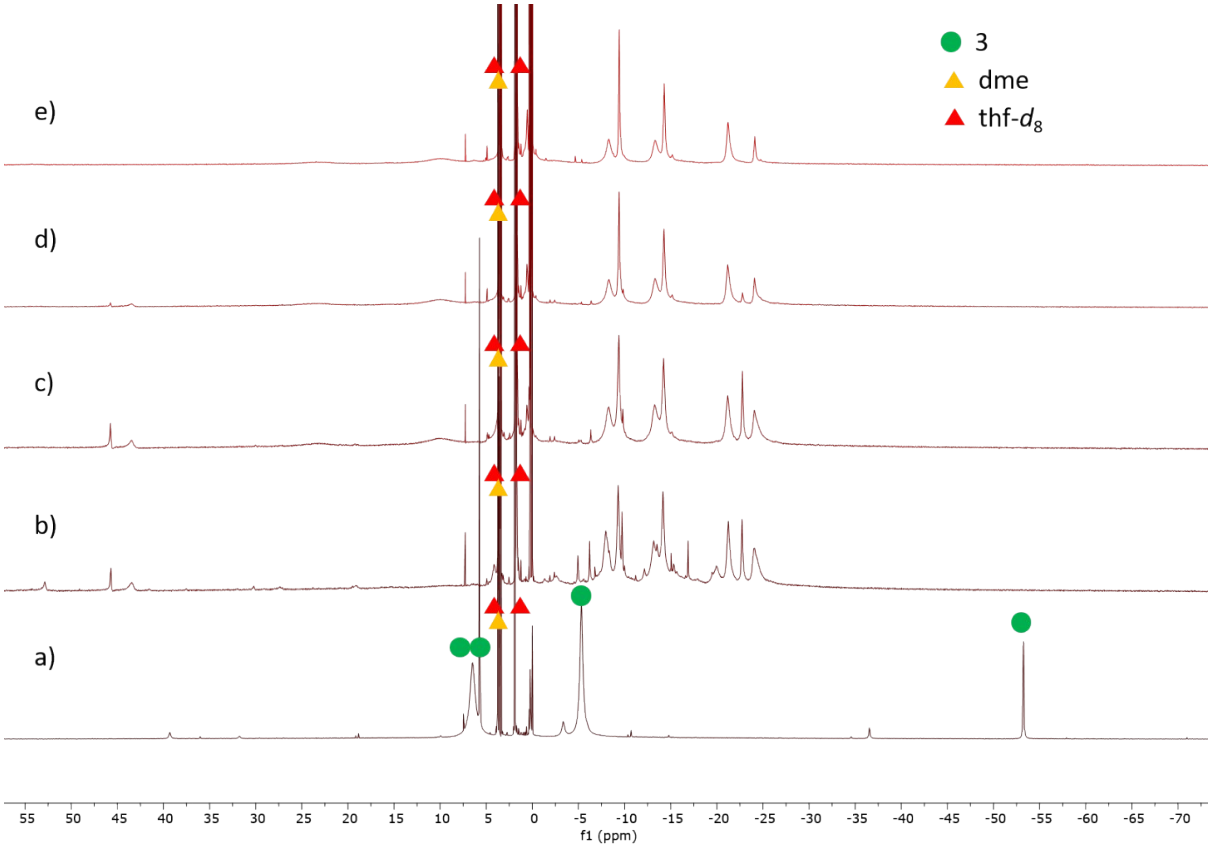

Figure S30. ^{1}H NMR spectra (400 MHz, 23 °C, thf-d_8) of the reaction mixture of **3** and excess CO_2 (1 atm) (a) before the CO_2 addition, (b) 30 min after CO_2, (c) 1 h after CO_2, (d) 1 h 30 min after CO_2, and (e) 7 h after CO_2.

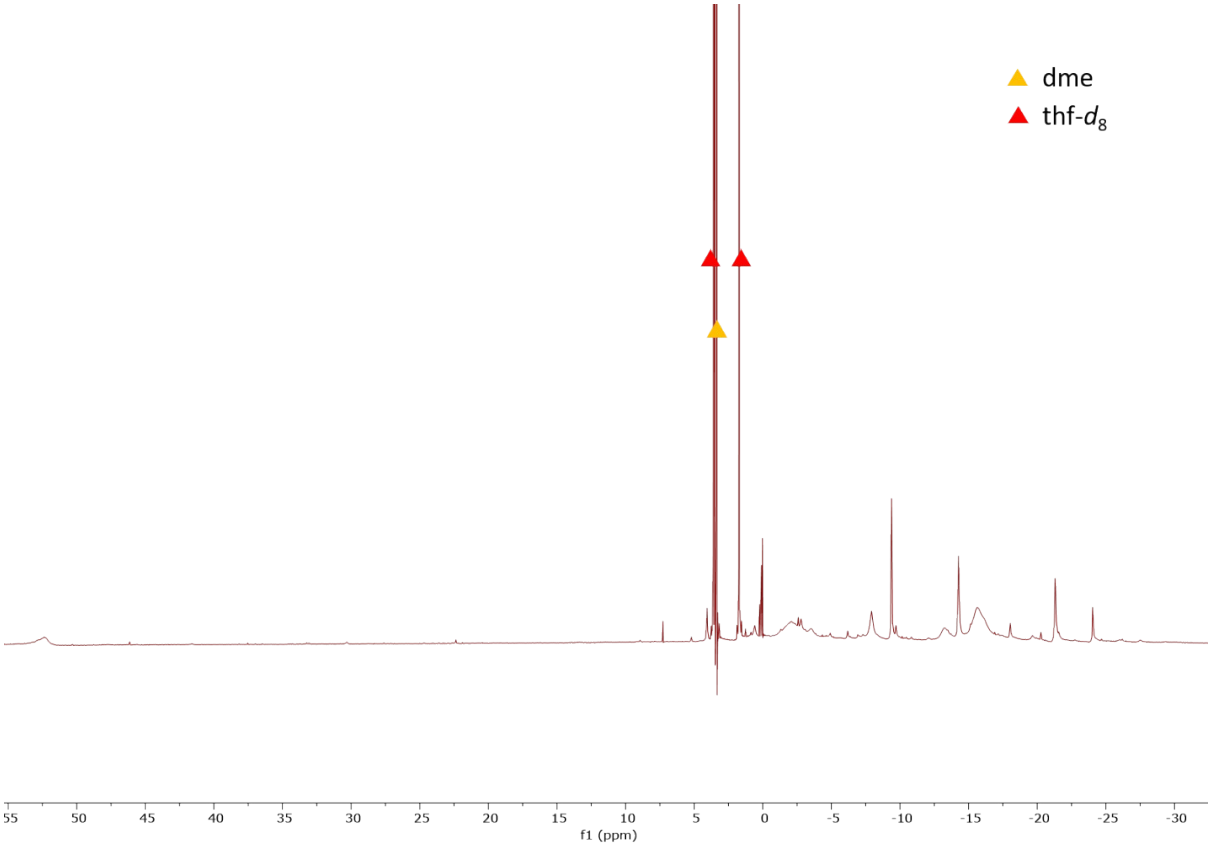

Figure S31. ^{1}H NMR spectrum (400 MHz, 23 °C, thf-d_8) of the reaction mixture of **3** and 2 equiv $^{13}CO_2$ after 1 h.

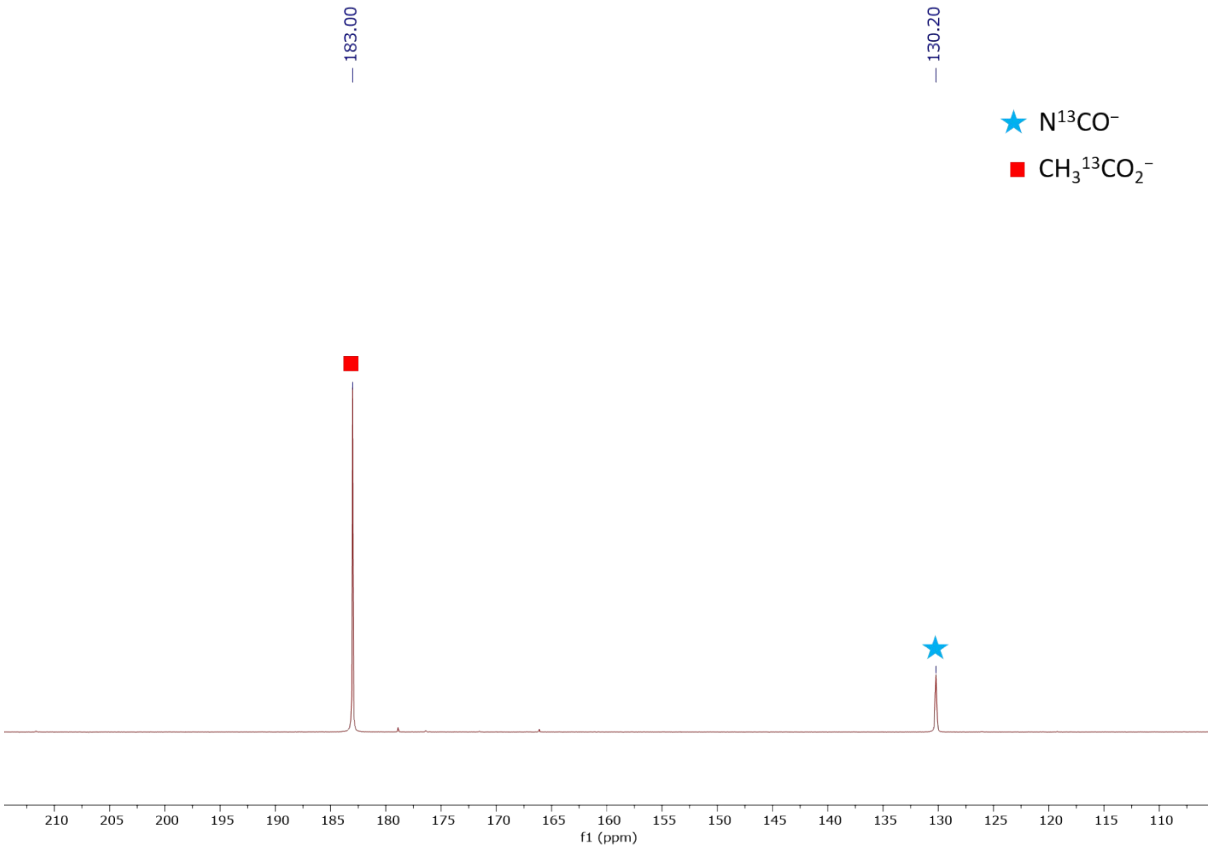

Figure S32. ^{13}C NMR spectrum (151 MHz, 23 °C, D_2O) after hydrolysis of the reaction mixture of **3** and 2 equiv of $^{13}CO_2$ with pD = 12 D_2O. $NaO_2{}^{13}CCH_3$ was added as an internal standard.

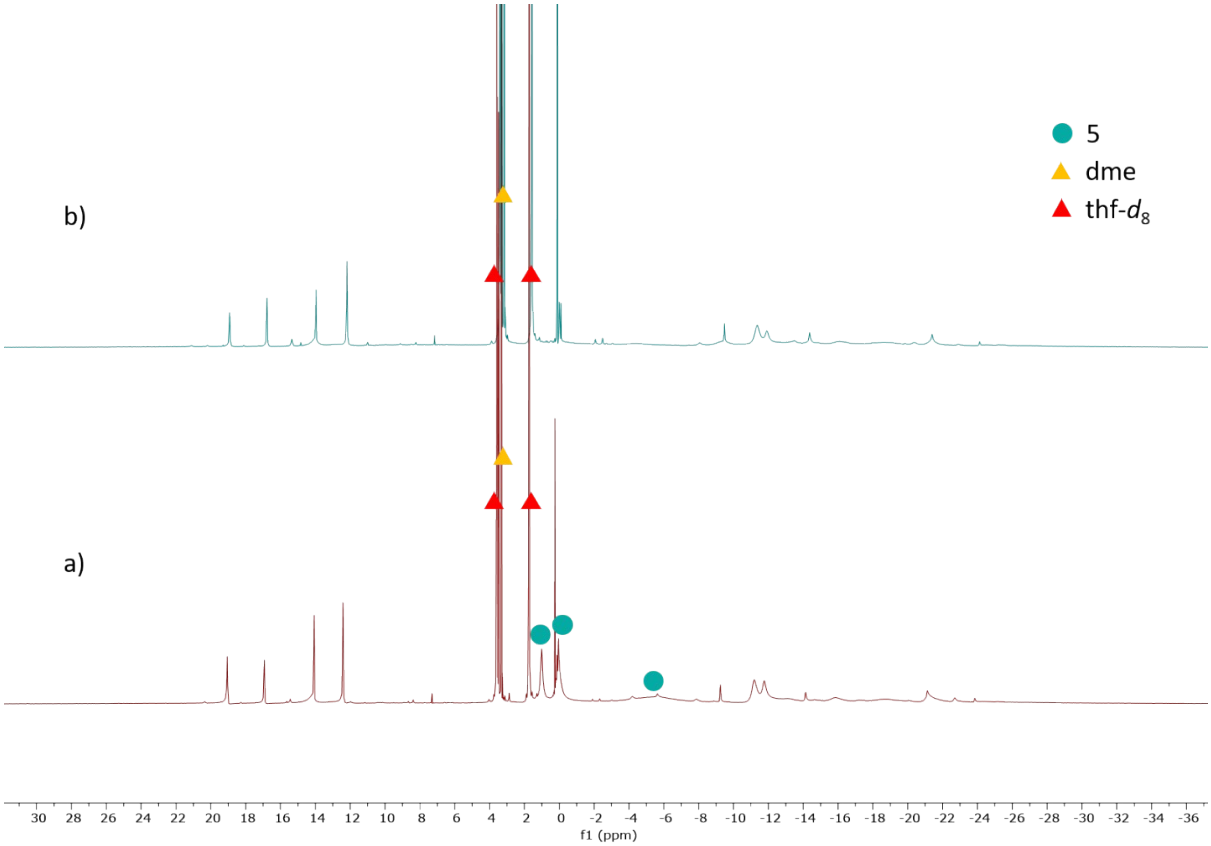

Figure S33. ^{1}H NMR spectrum (400 MHz, 23 °C, thf-d_8) of the reaction mixture of **5** and excess CO_2 (1 atm) (a) immediately after addition and (b) 1 h 10 min after addition.

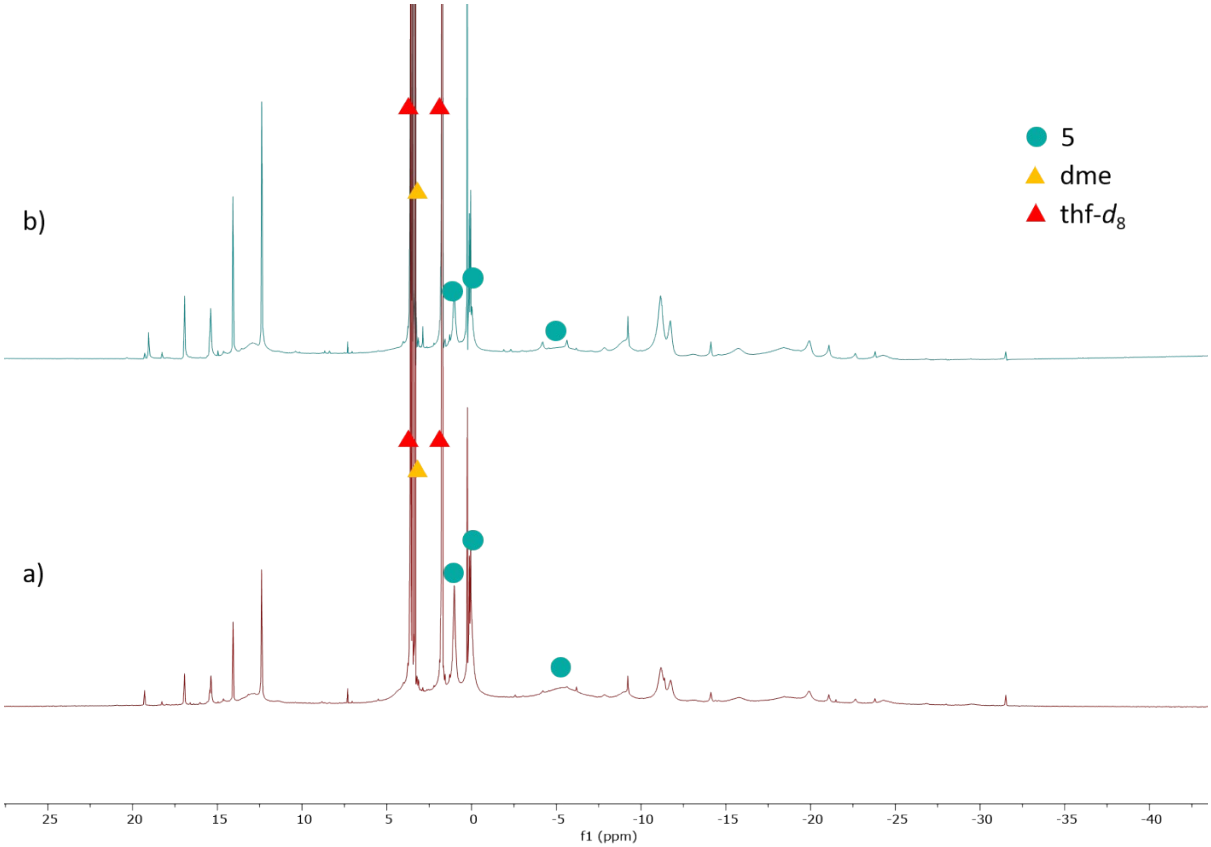

Figure S34. ^{1}H NMR spectra (400 MHz, thf-d_8) of the reaction mixture of **5** and (a) 2 equiv of $^{13}CO_2$, after 6 h 38 min and (b) after 7 h 50 min with 4 more equiv of $^{13}CO_2$ added, so 6 equiv $^{13}CO_2$ total.

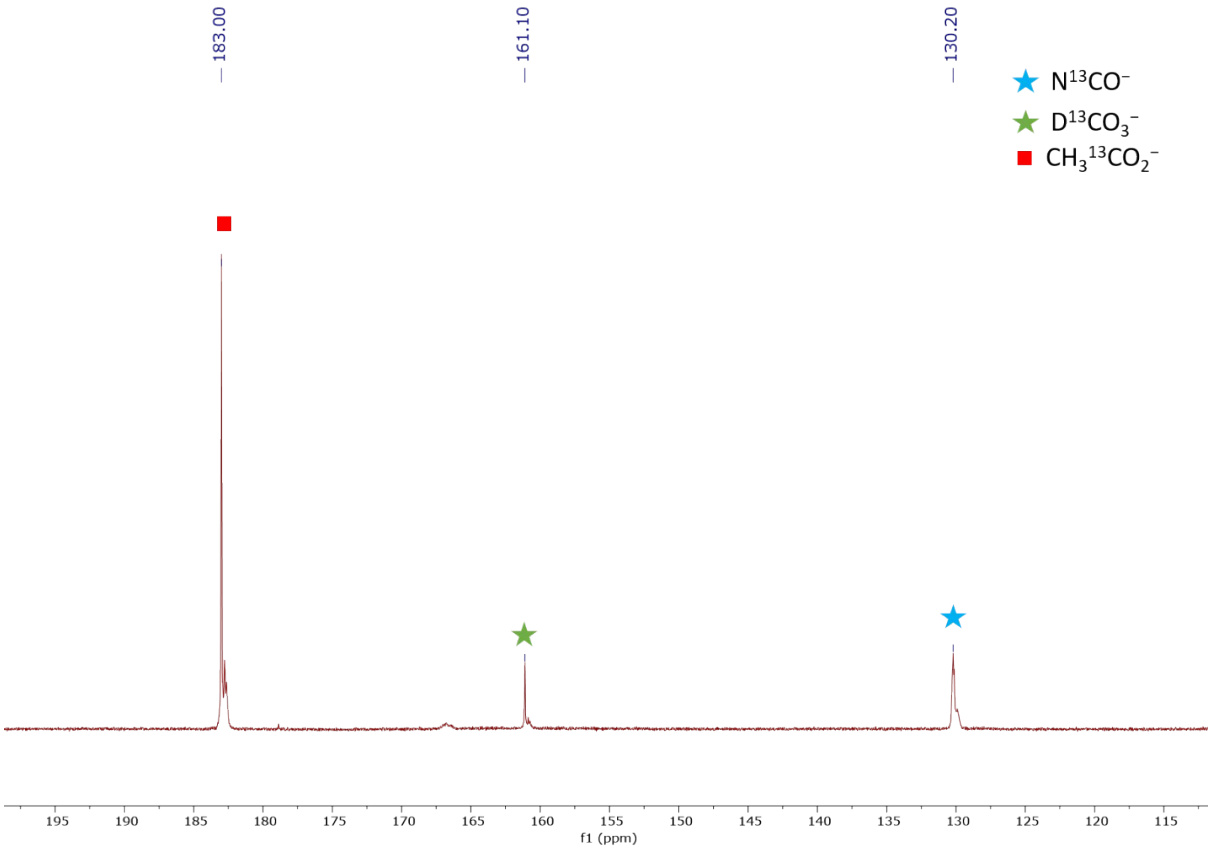

Figure S35. ^{13}C NMR spectrum (151 MHz, 23 °C, D_2O) of the hydrolyzed reaction mixture of **5** and 6 equiv of $^{13}CO_2$ with pD = 12 D_2O.

H_2 Reactivity

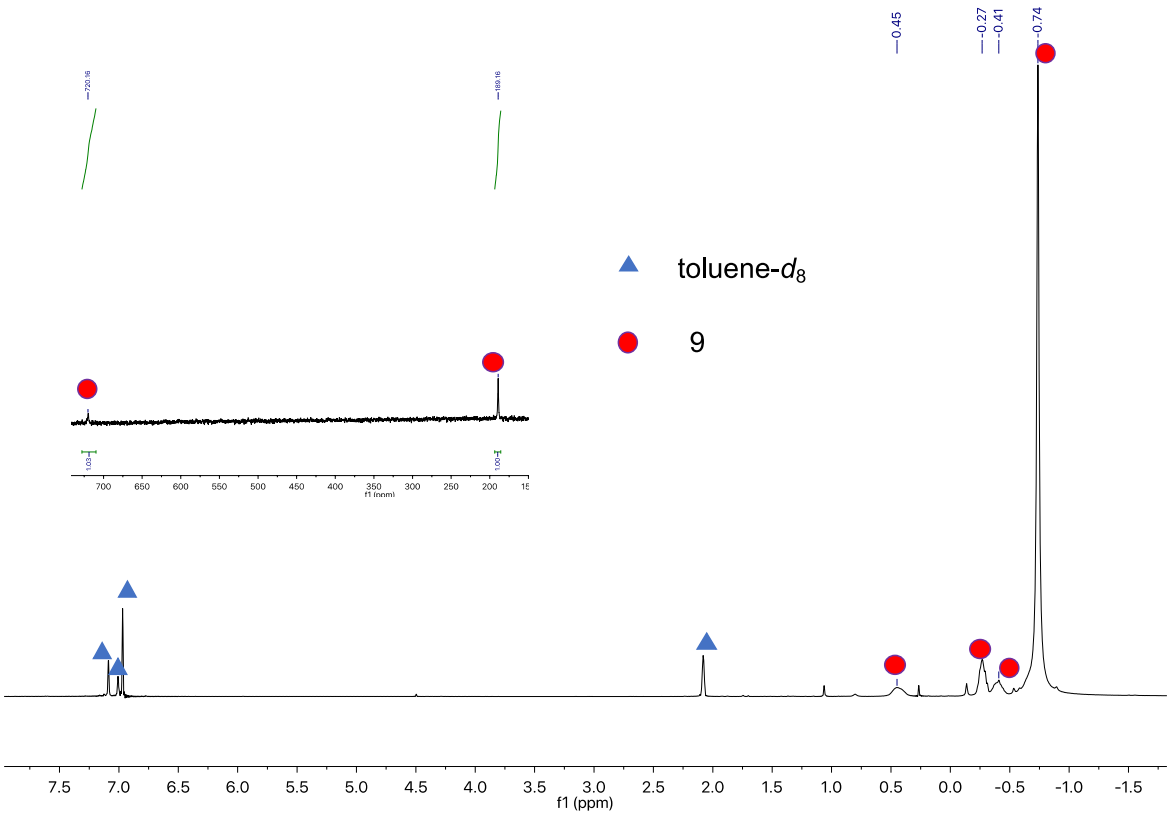

Figure S36. ^{1}H NMR spectrum (400 MHz, 23 °C, toluene-d_8,) of the reaction mixture of **[NBu$_4$]-1** and H_2. The left-side image shows the peaks for the NH and H protons.

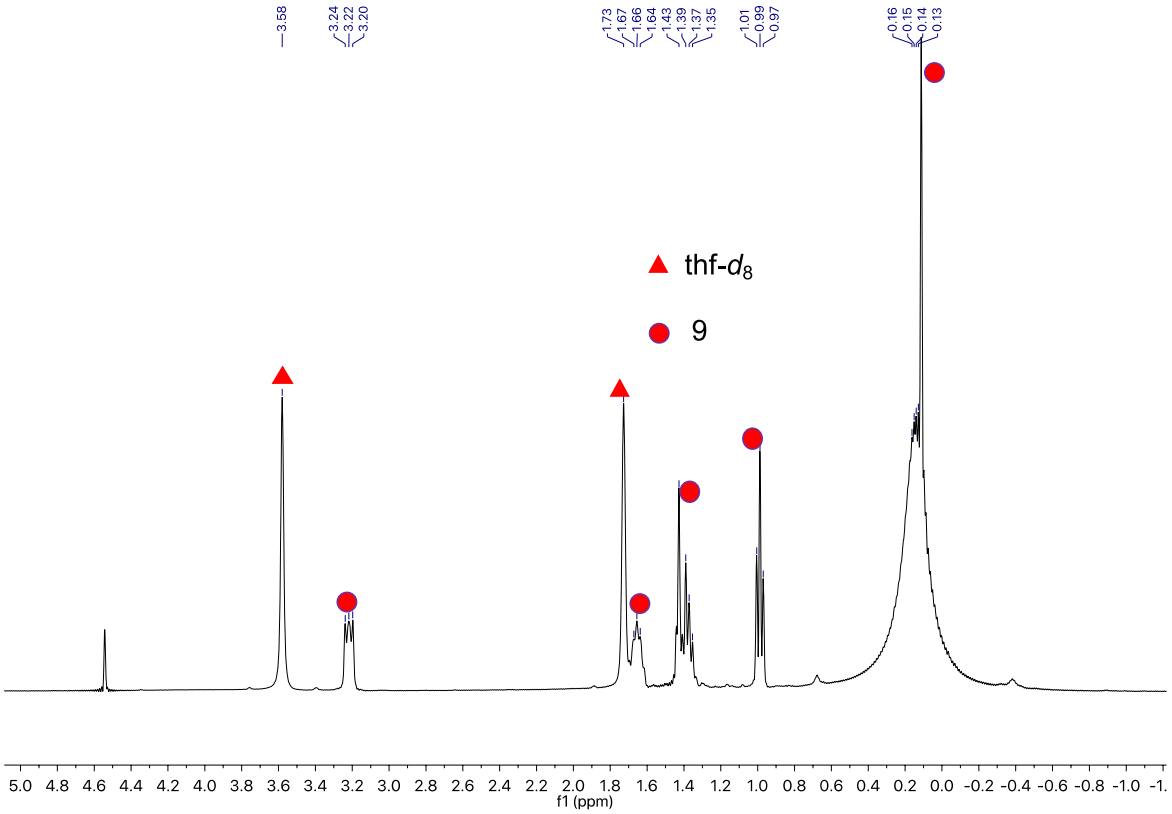

Figure S37. ^{1}H NMR spectrum (400 MHz, 23 °C, thf-d_8) of the reaction mixture of **[NBu$_4$]-1** and H_2.

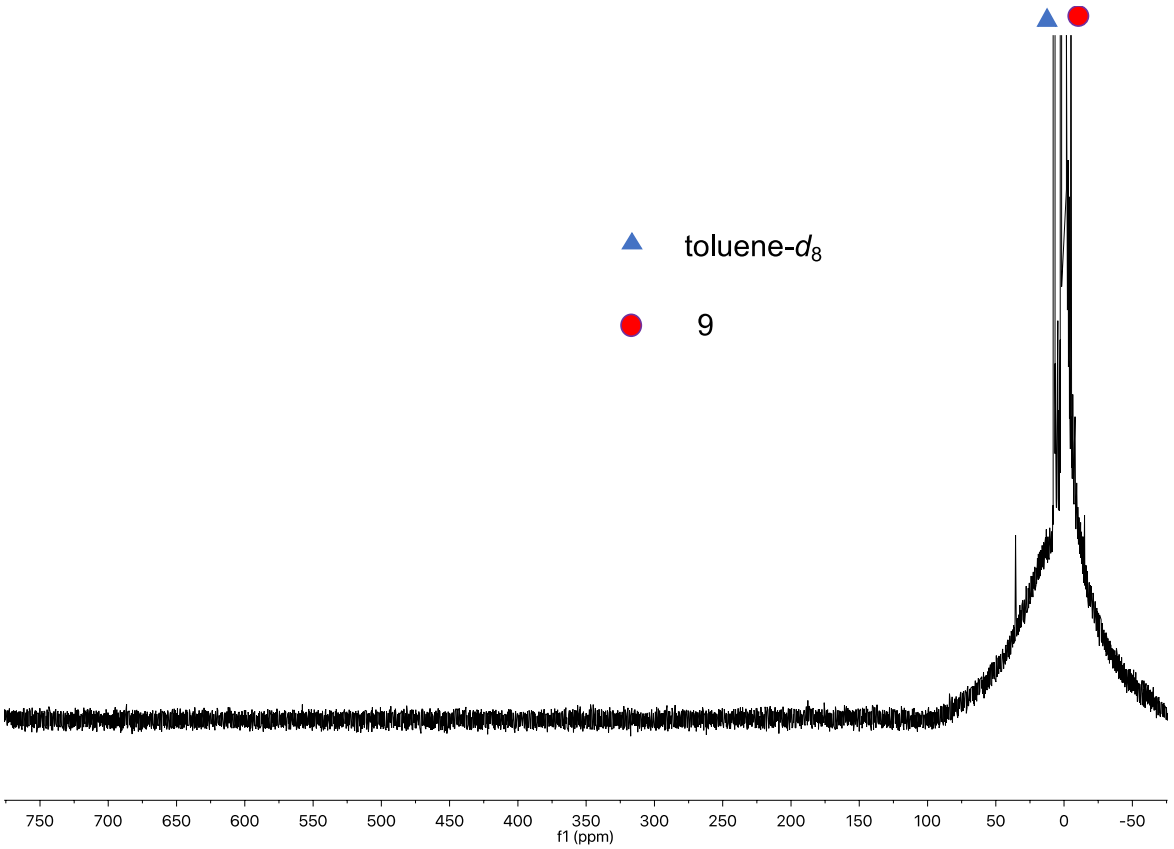

Figure S38. ^{1}H NMR spectrum (400 MHz, 23 °C, toluene-d_8) of the reaction mixture of **[NBu$_4$]-1** and D_2 on a large spectral window showing the disappearance of the peaks corresponding to NH and H protons.

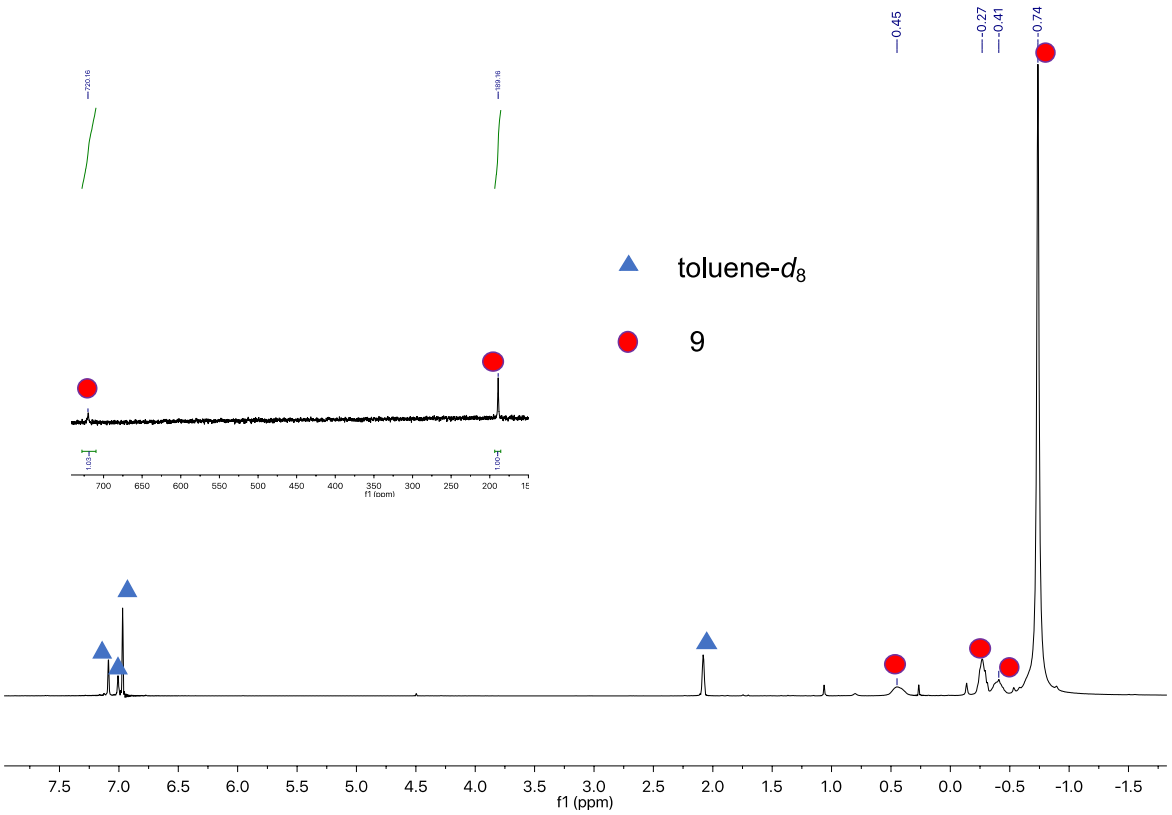

Figure S39. ^{1}H NMR spectrum (400 MHz, 23 °C) of isolated $[NBu_4][((^tBuO)_3SiO)_3U\}_2(\mu\text{-}NH)(\mu\text{-}H)]$, **9** in toluene-$d_8$

X-ray Crystallographic Details and Refinement Data

The diffraction data for all compounds were measured at low temperature [140 or 100 K] using Cu K_α or Mo K_α radiation on a Rigaku SuperNova dual system in combination with Atlas type CCD detector. The data reduction was carried out by *CrysAlis*^{Pro}.[9] The solutions and refinements were performed by *SHELXT*[10] and *SHELXL*,[11] respectively. The crystal structures were refined using full-matrix least-squares based on F^2 with all non-hydrogen atoms anisotropically defined. Hydrogen atoms were placed in calculated positions by means of the "riding" model. For compound **[NBu$_4$]-1**, the NBu_4 cation was very disordered and its geometry and geometry was corrected by means of restraints concerning atomic distances (DFIX and SADI cards). All light atoms (C, N, O) were anisotropically restrained (SIMU and RIGU cards). For compound **2**, some similarity restraints have been employed in the case of a disordered NBu_4 cation (DFIX and SIMU cards). In the case of compound **4**, restraints have been included to model a disordered toluene (FLAT, SADI, DFIX and SIMU cards).For compound **7**, some constraints have been employed for the refinement of some carbons, nitrogens and oxygens in order to get reasonable ellipsoids (EADP cards). In the case of compound **5**, some restraints were used for the refinement of a disordered DME belonging to the $[Na(DME)_3]^+$ cation (SADI and SIMU cards). For compound **9**, in order to adjust two disordered moieties (one *tert*-butyl and $NBu4^+$) some similarity restraints were employed (SADI and SIMU cards). In the case of compound **8**, one ligand displayed rotational disorder and it was treated by adjusting the atomic distances and their adp's (SADI, DFIX and SIMU cards). Pseudo merohedral twinning was found for compound **7** and treated directly by *CrysAlis*^{Pro} [9] obtaining this BASF factor: 0.37(1). CCDC numbers: **[NBu$_4$]-1**, 1913264, **2**, 1913257**; 4**, 1913258; **6**, 1913259; **7**, 1913260; **5** 1913261; **9**, 1913262; **8**, 1913263.

Table S1. Crystal data and structural refinement parameters for complexes $[NBu_4][\{((^tBu_3O)_3SiO)_3U\}_2(\mu\text{-}N)]$, **$[NBu_4]$-1**, $[NBu_4][\{((Me_3Si)_2N)_3U\}_2(\mu\text{-}N)]$, **2**, and $[\{((Me_3Si)_2N)_3U\}_2(\mu\text{-}N)]$, **4**.

	$[NBu_4]$-1	**2**	**4**
Formula	$C_{88}H_{198}N_2O_{24}Si_6U_2$	$C_{52}H_{144}N_8Si_{12}U_2$	$C_{50}H_{124}N_7Si_{12}U_2$
Crystal size (mm)	0.337x0.226x0.199	0.15×0.06×0.02	0.33×0.09×0.07
Crystal System	monoclinic	monoclinic	monoclinic
Space Group	*I*2	*I*2/*a*	$P2_1/n$
Volume (Å^3)	5810.2(3)	24839.8(11)	7609.56(13)
a (Å)	14.2946(4)	27.5312(6)	14.65806(12)
b (Å)	16.3627(3)	21.7757(6)	31.4333(2)
c (Å)	25.1526(6)	43.5129(11)	17.60034(19)
α (°)	90	90	90
β (°)	99.031(3)	107.785(3)	110.2211(11)
γ (°)	90	90	90
Z	2	12	4
Formula Weight	2313.07	1694.88	1636.69
Density (g cm^{-3})	1.322	1.360	1.429
μ (mm^{-1})	2.906	12.840	13.952
F(000)	2400	10368.0	3300.0
Temperature (K)	100(2)	140.00(10)	139.99(10)
Total Reflections	60518	87079	80831
Unique Reflections	17734	18125	14974
R_{int}	0.0345	0.0531	0.0397
R Indices [I > 2σ(I)]	R_1 = 0.0498	R_1 = 0.0377	R_1 = 0.0336
	wR_2 = 0.1173	wR_2 = 0.0829	wR_2 = 0.0810
Largest Diff. Peak and Hole (e.A^{-3})	1.661 and -1.000	1.463 and -2.401	1.654 and -1.962
GOF	1.061	0.986	1.163

F(000), structure factor evaluated in the zeroth-order case, h=k=l= 0; R(int) =∑|Fo2−Fo2(mean)| /∑[Fo2]; I, measured intensities; 'Largest diff. peak and hole', maximum and minimum electron density found in the final Fourier difference map; GOF, goodness of fit (= {∑ [w(Fo2−Fc2)2]/(n−p)}1/2, where n is the number of reflections and p is the total number of parameters refined).

Table S2. Crystal data and structural refinement parameters for complexes $[Na(dme)_3][((Me_3Si)_2N)_3U(\mu\text{-}N)U(N(SiMe_3)_2)_2(OSi(O^tBu)_3)]$, **5**, $[\{((Me_3Si)_2N)_2U(\mu\text{-}O)]_3$, **6**, and $[((Me_3Si)_2N)_2U(\mu\text{-}O)U(\mu\text{-}\kappa^2\text{-}O,N\text{-}OC(=C)SiMe_2NSiMe_3)U(N(SiMe_3)_2)_2]$, **7**.

	5	**6**	**7**
Formula	$C_{54}H_{147}N_6NaO_{10}Si_{11}U_2$	$C_{36}H_{108}N_6O_3Si_{12}U_3$	$C_{31}H_{89}N_5O_2Si_{10}U_2$
Crystal size (mm)	0.19×0.10×0.09	0.07×0.06×0.04	0.21×0.15×0.02
Crystal System	triclinic	triclinic	triclinic
Space Group	$P\bar{1}$	$P\bar{1}$	$P\bar{1}$
Volume (Å^3)	4440.8(2)	6960.3(4)	5671.5(4)
a (Å)	15.1641(4)	12.4529(4)	14.4014(6)
b (Å)	15.3150(4)	21.7100(6)	19.5701(8)
c (Å)	19.3228(6)	26.8860(7)	20.1516(9)
α (°)	88.488(2)	83.801(2)	91.085(4)
β (°)	87.105(2)	78.048(3)	92.236(4)
γ (°)	82.328(2)	78.888(3)	91.691(4)
Z	2	4	4
Formula Weight	1848.81	1724.45	1321.03
Density (g cm^{-3})	1.383	1.646	1.547
μ (mm^{-1})	12.018	21.660	5.944
F(000)	1884.0	3336.0	2600.0
Temperature (K)	140.00(10)	140.00(10)	139.99(11)
Total Reflections	32284	48673	22606
Unique Reflections	17171	24554	22606
R_{int}	0.0402	0.0500	-
R Indices [I > 2σ(I)]	R_1 = 0.0390 wR_2 = 0.1007	R_1 = 0.0408 wR_2 = 0.0844	R_1 = 0.0855 wR_2 = 0.2150
Largest Diff. Peak and Hole (e.A^{-3})	1.917 and -1.097	3.294 and -2.279	6.993 and -2.057
GOF	1.052	0.994	1.068

F(000), structure factor evaluated in the zeroth-order case, h=k=l= 0; R(int) =∑|Fo2−Fo2(mean)| /∑[Fo2]; I, measured intensities; 'Largest diff. peak and hole', maximum and minimum electron density found in the final Fourier difference map; GOF, goodness of fit (= {∑ [w(Fo2−Fc2)2]/(n−p)}1/2, where n is the number of reflections and p is the total number of parameters refined).

Table S3. Crystal data and structural refinement parameters for complexes $[NBu_4][\{((^tBuO)_3SiO)_3U\}_2(\mu\text{-}NC_2O_4)]$, **8**, and $[NBu_4][\{((^tBuO)_3SiO)_3U\}_2(\mu\text{-}NH)(\mu\text{-}H)]$, **9**.

	8	**9**
Formula	$C_{90}H_{198}N_2O_{28}Si_6U_2$	$C_{95}H_{208}N_2O_{24}Si_6U_2$
Crystal size (mm)	0.29×0.24×0.20	0.26×0.04×0.01
Crystal System	monoclinic	monoclinic
Space Group	$P2_1/n$	$P2_1/c$
Volume (Å^3)	12124.9(3)	12127.7(2)
a (Å)	16.9403(2)	13.74703(14)
b (Å)	40.0672(5)	32.4889(3)
c (Å)	17.9903(2)	27.4987(3)
α (°)	90	90
β (°)	96.8053(12)	99.0810(10)
γ (°)	90	90
Z	4	4
Formula Weight	2401.09	2407.22
Density (g cm^{-3})	1.315	1.318
μ (mm^{-1})	8.541	8.514
F(000)	4976	5008
Temperature (K)	140.00(10)	100.01(10)
Total Reflections	24134	24736
Unique Reflections	22290	21791
R_{int}	0.0501	0.0384
R Indices [I > 2σ(I)]	R_1 = 0.0730 wR_2 = 0.1878	R_1 = 0.0288 wR_2 = 0.0664
Largest Diff. Peak and Hole (e.A^{-3})	6.335 and -6.619	1.877 and -2.482
GOF	1.061	1.018

F(000), structure factor evaluated in the zeroth-order case, h=k=l= 0; R(int) =∑|Fo2−Fo2(mean)| /∑[Fo2]; I, measured intensities; 'Largest diff. peak and hole', maximum and minimum electron density found in the final Fourier difference map; GOF, goodness of fit (= {∑ [w(Fo2−Fc2)2]/(n−p)}1/2, where n is the number of reflections and p is the total number of parameters refined).

Structural Discussion of $[\{((Me_3Si)_2N)_3U\}_2(\mu\text{-}N)]$, 4.

Complex **4** crystallizes in the $P2_1/n$ space group with one molecule per asymmetric unit and four molecules per unit cell. For every molecule of **4**, there are two disordered toluene molecules in the lattice. **4** can be described as a bimetallic U^{4+}-U^{5+} complex with two $[((Me_3Si)_2N)_3U]^{n+}$ (n = 1, 2) tetrahedrons bridged by a nitride ligand; the 179.4(3)° U–N–U angle is nearly linear. The U=N=U bonding scheme of **4** appears less symmetric than **2** with U–

$N_{nitride}$ bond distances 2.080(5) Å and 2.150(5) Å. Consistent with an increase in oxidation state, the 2.274(5) Å U–$(N_{amide})_{avg}$ is ca. 0.08 Å shorter than the analogous 2.35(1) Å distance of **2** and the change in oxidation state appears to have influenced the U–N_{amide} distances of each uranium ion equally. The U–$(N_{nitride})_{avg}$ distance becomes longer, however, and the change in twist angle reflects a reorientation in the ligands from staggered to gauche; in **4**, the U–$(N_{nitride})_{avg}$ bond distance is 2.12(4) Å, whereas it is 2.078(4) Å in **2**, and the 18(1)° twist angle of **4** is larger than the 1.7(4)° angle of **2**. The shortening of the U–$(N_{amide})_{avg}$ bond distances by ca. 0.08 Å between the U^{4+}-U^{4+} and U^{4+}-U^{5+} structures and the nearly linear U–N–U angle also occur in the similar complexes, $[NBu_4][\{(C_6H_3Me_2\text{-}3,5)(^tBu)N)_3U\}_2(\mu\text{-}N)]$ and $[\{(C_6H_3Me_2\text{-}3,5)(^tBu)N)_3U\}_2(\mu\text{-}N)]$. However, for other metrical parameters, the trend is reversed; the U^{4+}-U^{5+} $[\{(C_6H_3Me_2\text{-}3,5)(^tBu)N)_3U\}_2(\mu\text{-}N)]$ has the shorter U–$(N_{nitride})_{avg}$ bond distance, 2.0625 Å, than its U^{4+}-U^{4+} analogue, 2.079(2) Å. Further, 25.3° and 0° twist angles of $[NBu_4][\{(C_6H_3Me_2\text{-}3,5)(^tBu)N)_3U\}_2(\mu\text{-}N)]$ and $[\{(C_6H_3Me_2\text{-}3,5)(^tBu)N)_3U\}_2(\mu\text{-}N)]$, respectively, indicate the U^{4+}-U^{4+} displays the gauche arrangement of amide ligands whereas those of the U^{4+}-U^{5+} complex are staggered. Lastly, $[\{(C_6H_3Me_2\text{-}3,5)(^tBu)N)_3U\}_2(\mu\text{-}N)]$ retains a symmetric U=N=U bonding scheme upon oxidation. These results depict the complicated nature of bonding in molecular uranium complexes.

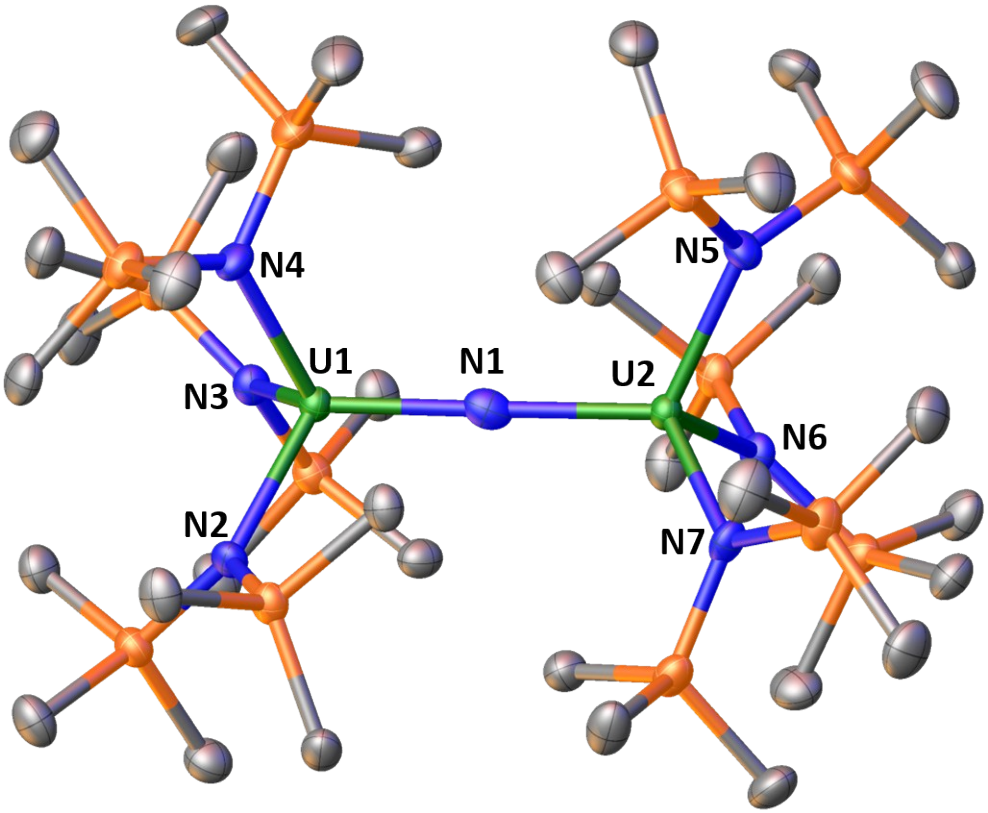

Figure S40. Molecular structure of [{((Me$_3$Si)$_2$N)$_3$U}$_2$(μ-N)], **4**, with thermal ellipsoids drawn at the 50% probability level. Hydrogen atoms and two molecules of toluene have been omitted for clarity.

Table S4. Comparison of bond lengths (Å) and angles (°) of $[NBu_4][\{((Me_3Si)_2N)_3U\}_2(\mu\text{-}N)]$, **2**, $[\{((Me_3Si)_2N)_3U\}_2(\mu\text{-}N)]$, **4**, $[NBu_4][\{(C_6H_3Me_2\text{-}3,5)(^tBu)N)_3U\}_2(\mu\text{-}N)]$, and $[\{(C_6H_3Me_2\text{-}3,5)(^tBu)N)_3U\}_2(\mu\text{-}N)]$.

Complex	**2** [a]	**4**	**$[NBu_4][\{(C_6H_3Me_2\text{-}3,5)(^tBu)N)_3U\}_2(\mu\text{-}N)]$**	**$[\{(C_6H_3Me_2\text{-}3,5)(^tBu)N)_3U\}_2(\mu\text{-}N)]$**
$U\text{–}N_{nitride}$	2.076(5), 2.083(5), 2.075(2)	2.080(5), 2.150(5)	2.077(4), 2.080(4)	2.0625(3), 2.0625(3)
$U\text{–}(N_{nitride})_{avg}$	2,078(4)	2.12(4)	2.079(2)	2.0625
$U\text{–}N_{amide}$	2.338(5), 2.340(5), 2.342(4), 2.347(4), 2.350(5), 2.354(4), 2.364(5), 2.365(5), 2.366(5)	2.268(4), 2.271(4), 2.272(4), 2.274(4), 2.277(4), 2.283(4)	2.276, 2.285, 2.294, 2.302, 2.377, 2.414	2.235, 2.235, 2.241, 2.241, 2.253, 2.253
$U\text{–}(N_{amide})_{avg}$	2.35(1)	2.274(5)	2.32(5)	2.243(7)
U–N–U	178.7(2), 180.0	179.4(3)	175.1(2)	180
Twist Angle [b]	1.7(4)	18(1)	25.3	0

[a.] Taken as an average of 1.5 molecules in the unit cell of **2**. [b.] Defined as the average angle between the two closest adjacent planes defined by $N_{nitride,}$ U, and N_{amide} atoms.

Structural Characterization of Oxo Products 6 and 7.

The trimeric μ-oxo complex **6** crystallizes in the $P\bar{1}$ space group with two molecules per asymmetric unit. The U(IV) ions are four-coordinate and bound in a pseudo tetrahedral fashion by two $N(SiMe_3)_2$ and two μ_2-oxo ligands. The $N(SiMe_3)_2$ ligands are oriented perpendicular to the 6-membered ring defined by the U_3O_3 core. The 2.28(1) Å $U–(N_{amide})_{avg}$ bond distance is typical of U(IV) / $N(SiMe_3)_2$ complexes. The 2.10(2) Å $U–(O_{oxo})_{avg}$ bond distance is in the range of U–O bond distances (2.05(1) Å-2.166(4) Å) distance found in similar structures.[12] The average U–O–U angle (144(1)°) is also similar, 133(1)).[12] The structure of **7** shows the presence of a dinuclear complex with two four-coordinate U(IV) ions bridged by a μ-oxo ligand and a dianionic κ^2-*O*,*N*-OC(=C)$SiMe_2NSiMe_3$ ligand formed by insertion of CO into the uranium–methylene bond of **3**. The $U1–(N_{amide})_{avg}$, = 2.27(4) Å and $U2–(N_{amide})_{avg}$ = 2.26(1) Å bond lengths are typical of U(IV) and are equivalent within error. The uranium–oxo bond distances are close but inequivalent, U1–O1 = 2.082(15) Å vs U2–O1 = 2.130(15) Å. The dianionic κ^2-*O*,*N*-OC(=C)$SiMe_2NSiMe_3$ ligand binds to the U1–O1–U2 fragment to afford a 7-membered ring. The 1.32(3) Å C–C bond is consistent with a double bond.

Magnetic Data

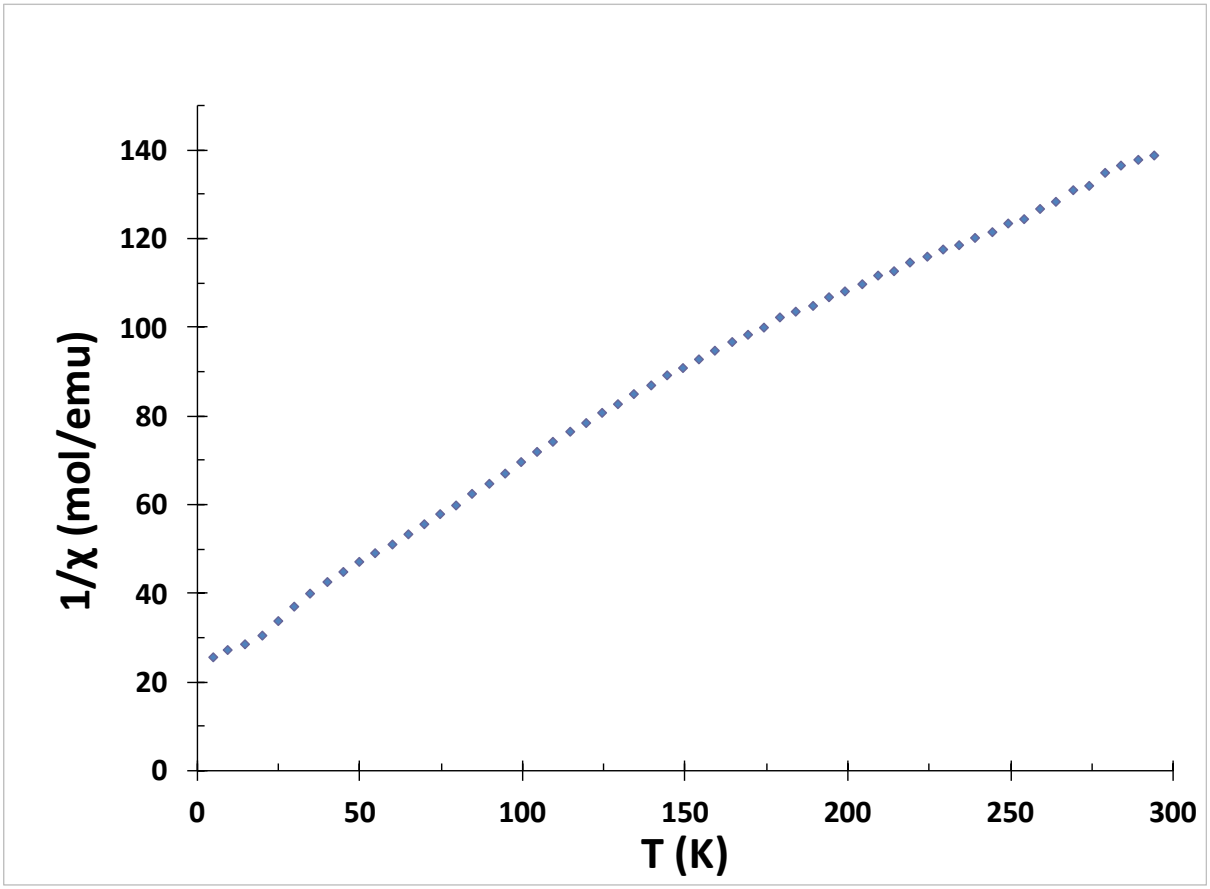

Figure S41. 1/χ vs T plot of complex **[NBu$_4$]-1**

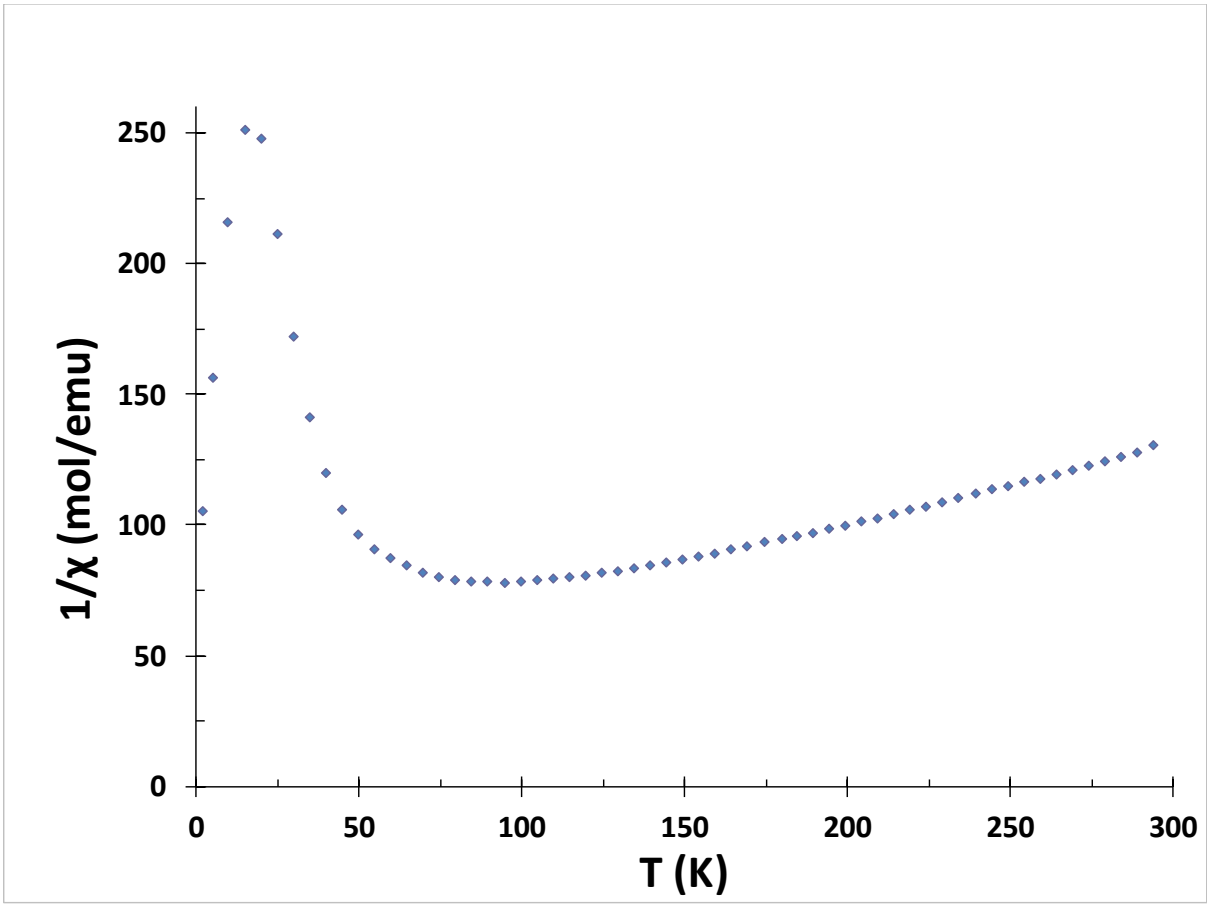

Figure S42. 1/χ vs T plot of complex **2**

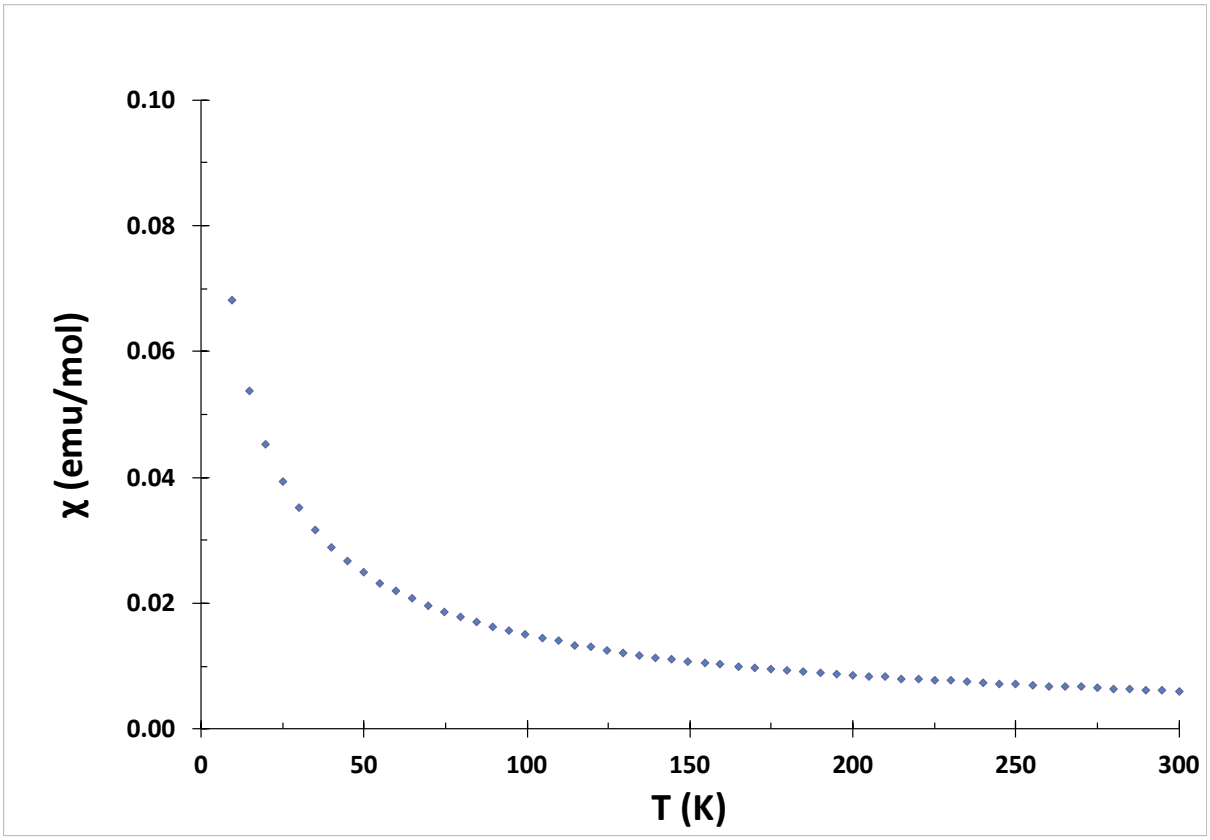

Figure S43. χ vs T plot of complex **4**

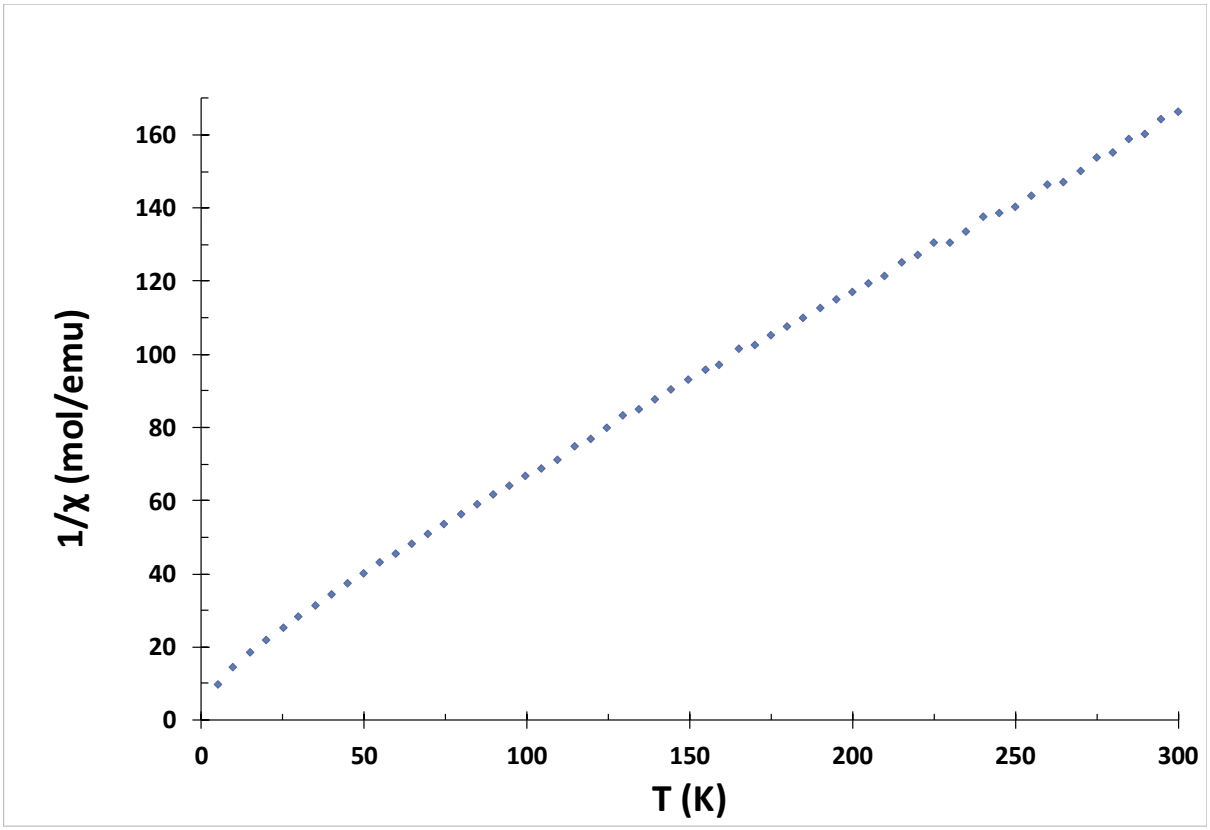

Figure S44. 1/χ vs T plot of complex **4**

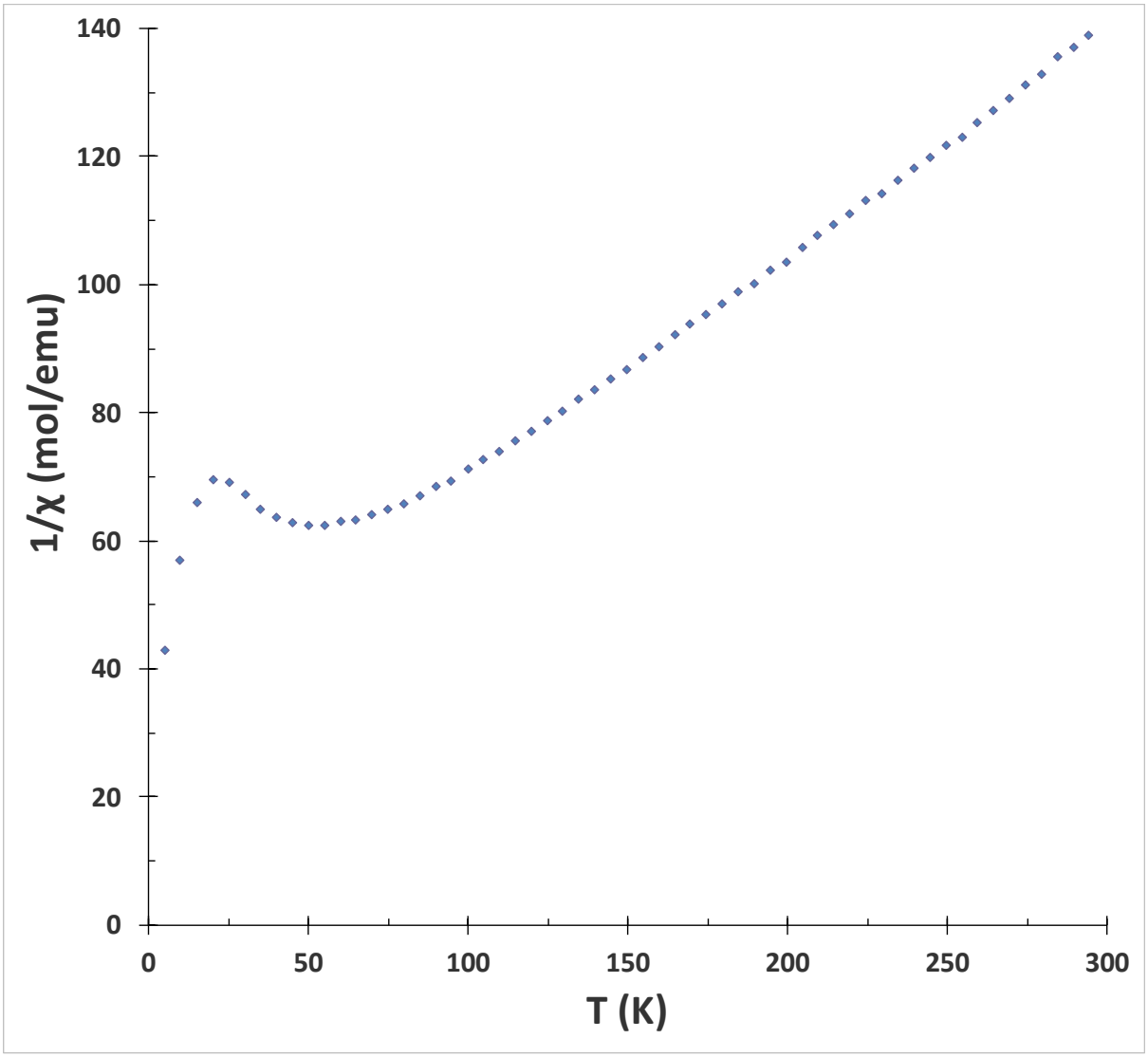

Figure S45. 1/χ vs T plot of complex **5**

IR Spectra

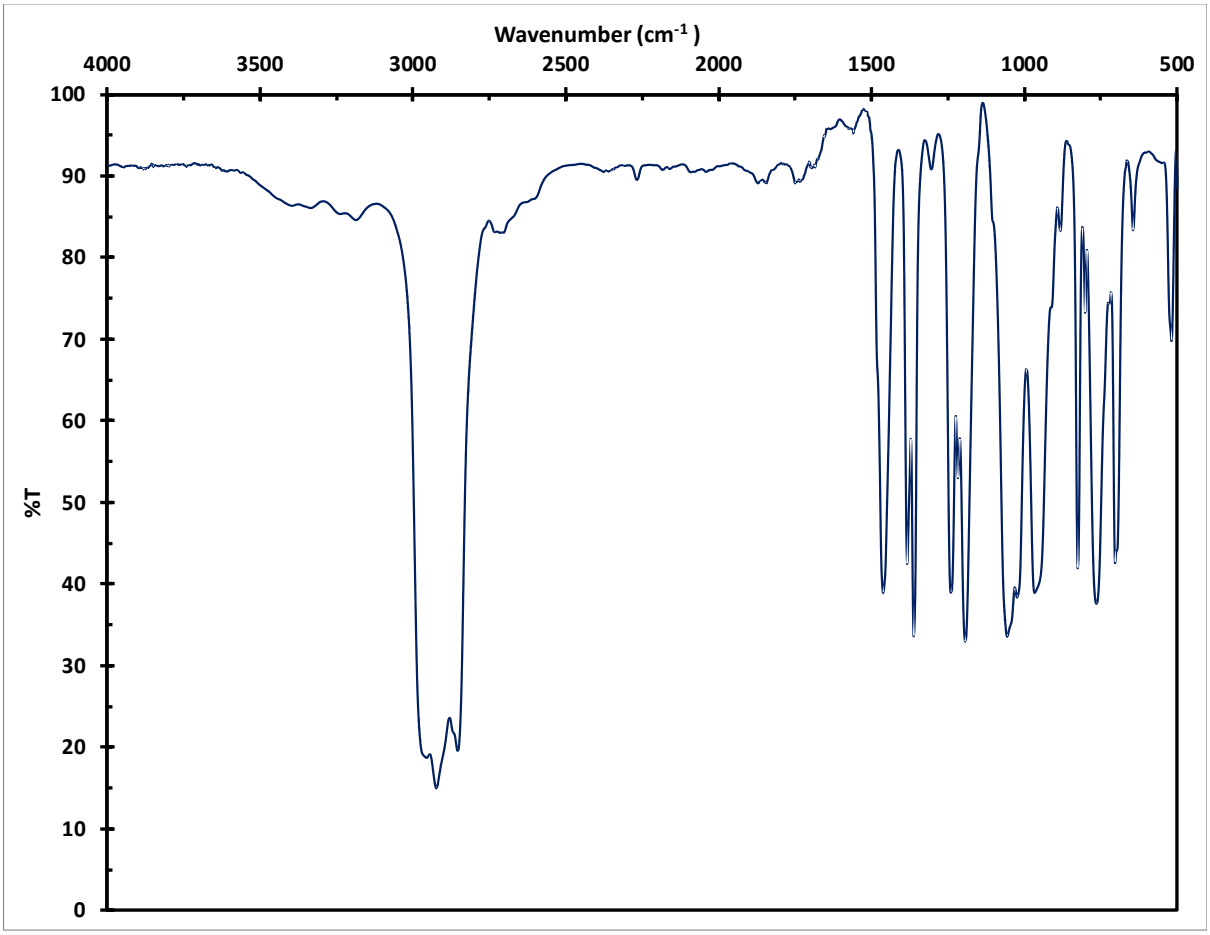

Figure S46: IR spectrum of isolated complex **[NBu$_4$-1]** in Nujol.

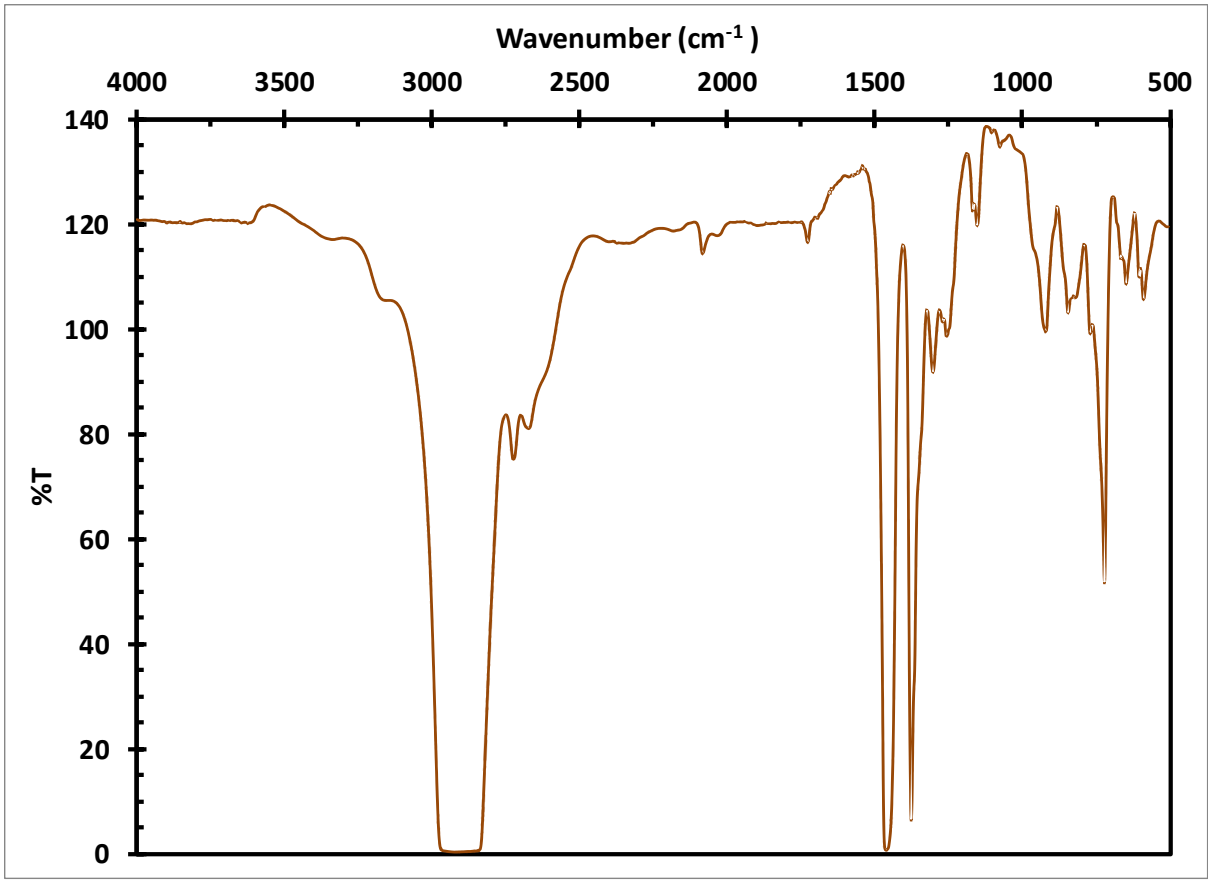

Figure S47: IR spectrum of isolated complex **2** in Nujol.

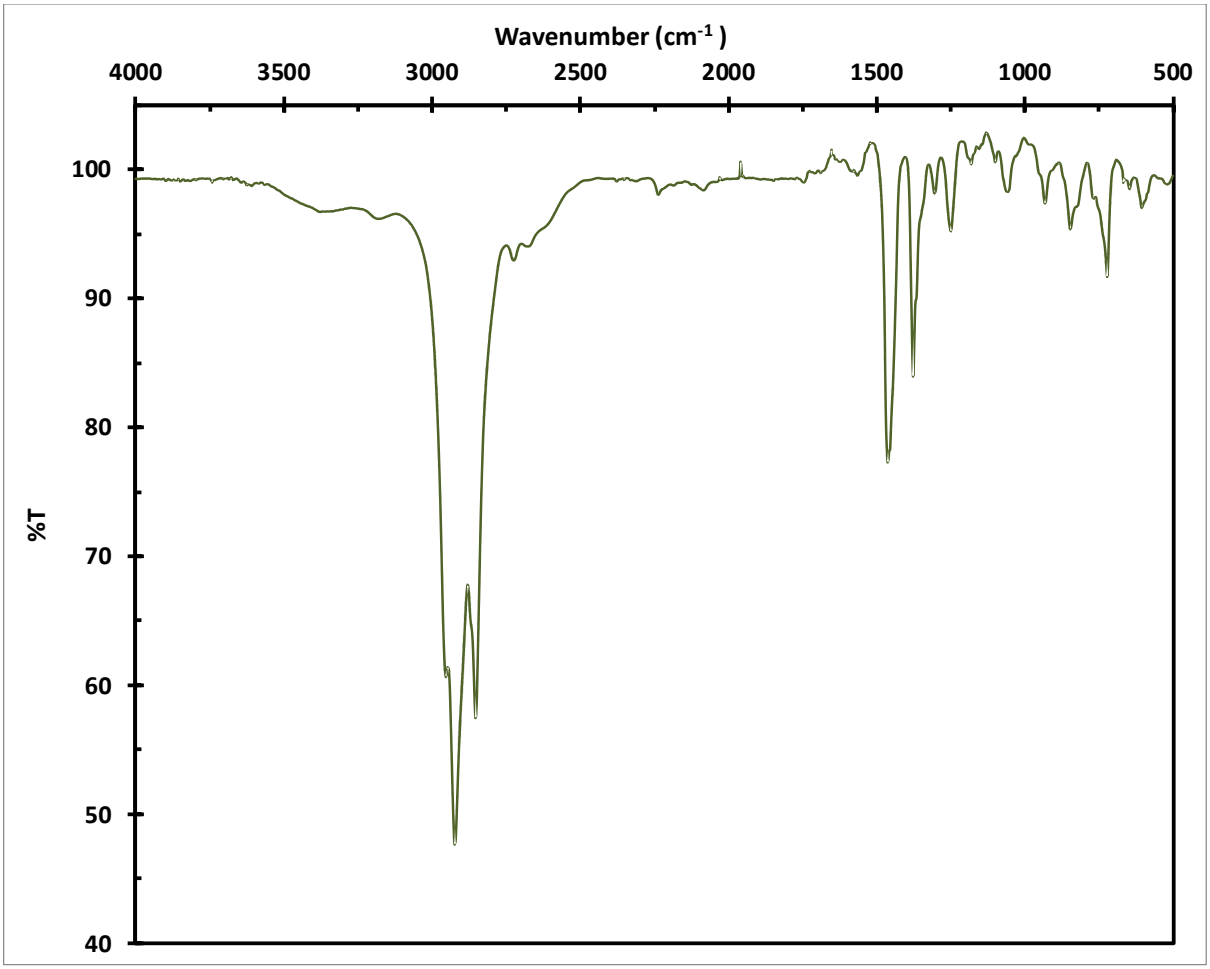

Figure S48: IR spectrum of isolated complex **5** in Nujol.

UV-Vis-NIR Spectra

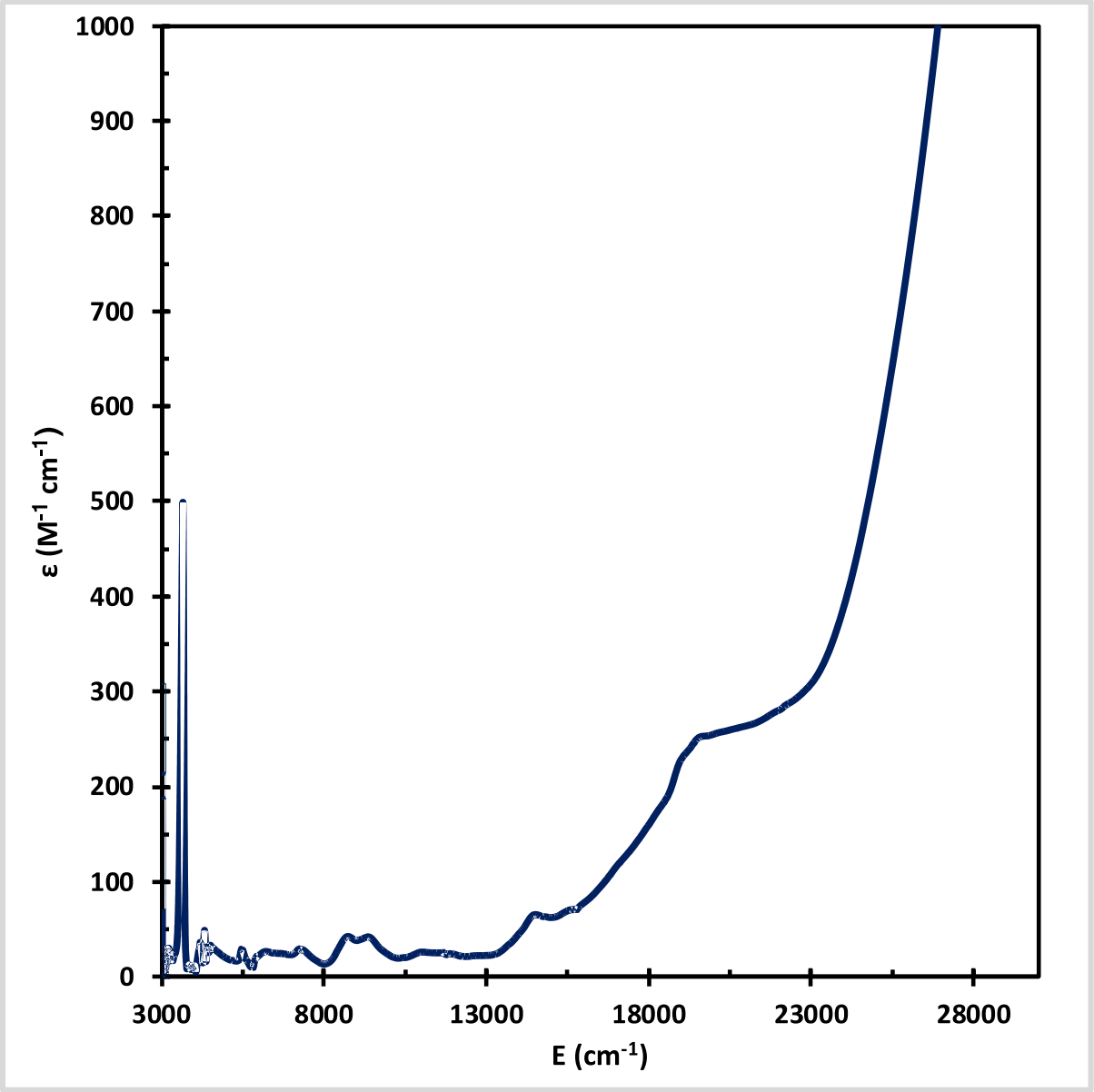

Figure S49: UV-Vis-NIR spectrum of a 6.5mM THF solution of complex **[NBu$_4$-1]**.

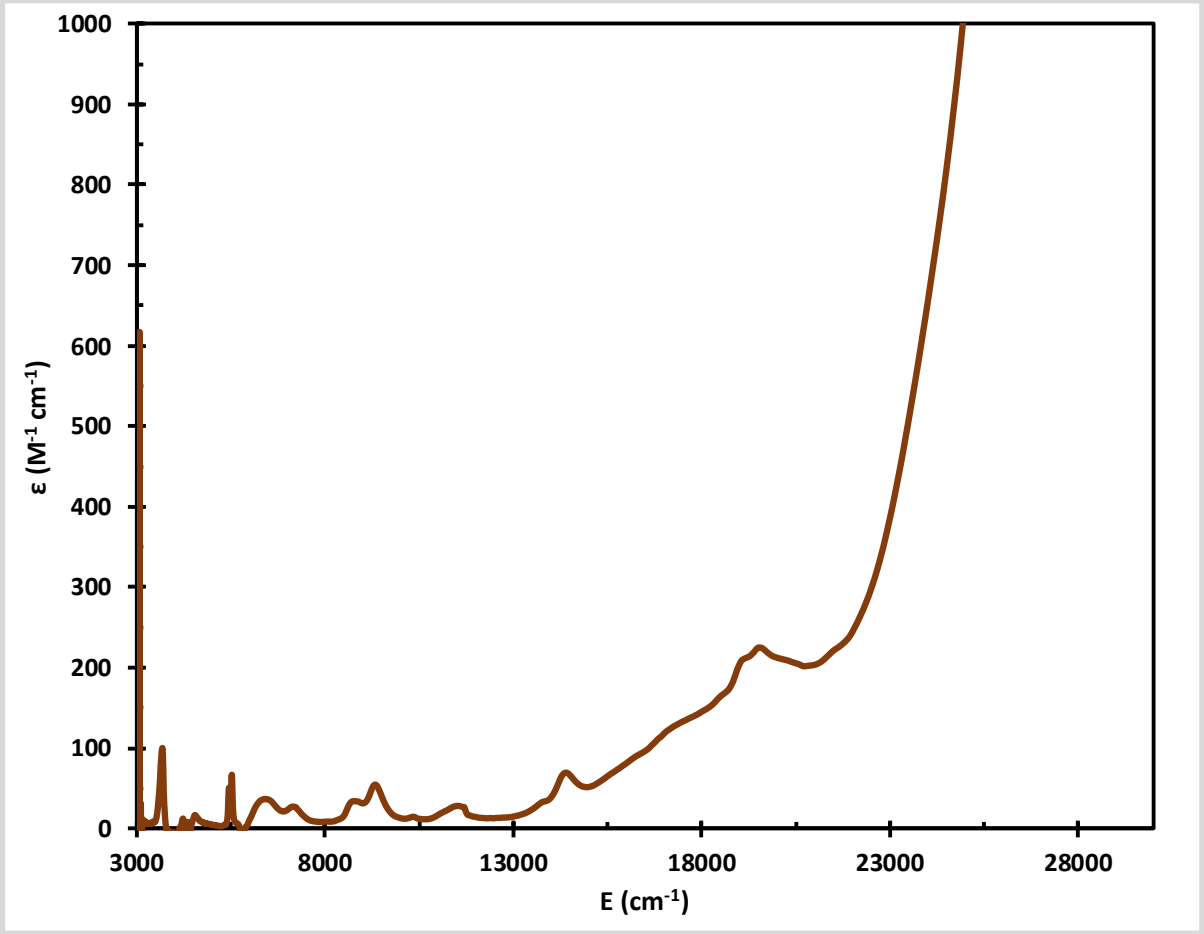

Figure S50: UV-Vis-NIR spectrum of a 10mM THF solution of complex **2**.

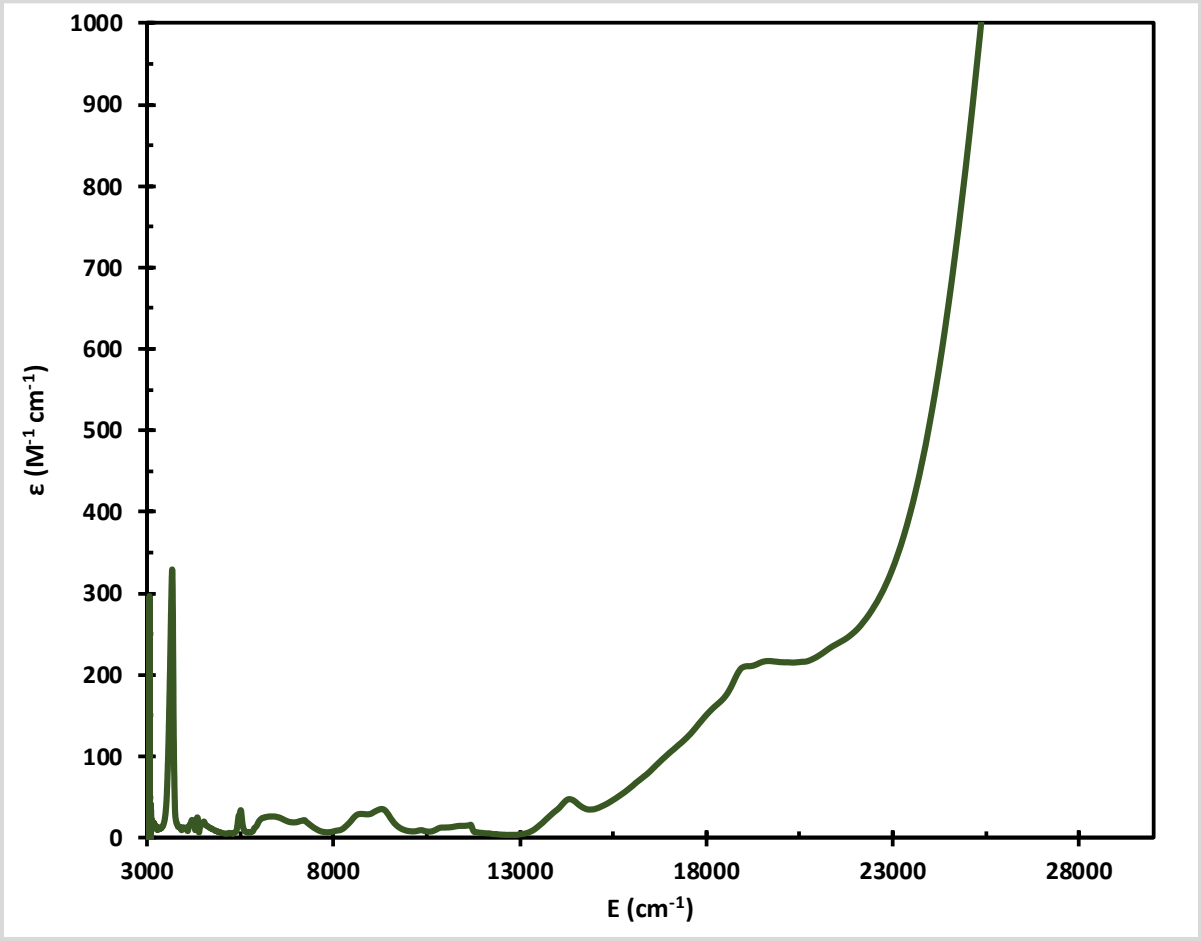

Figure S51: UV-Vis-NIR spectrum of a 10mM THF solution of complex **5**.

Computational Details

Density functional theory (DFT) computations on the experimentally synthesized complexes were performed with B3LYP[13][14] and M06L[15][14] in combination with the def2-SVP[16] basis for all the light elements, while the def-SD basis set and the corresponding Stuttgart–Dresden (SDD)[17] effective core potentials were chosen for U (60 core electrons). The structural parameters of the complexes were fixed according to X-ray data for all heavy atoms, while hydrogen positions were relaxed at M06L-D3. Singlet open-shell and triplet states were computed within the broken-symmetry formalism, starting from the converged quintet ansatz. Scalar relativistic effects for U were included through the SD-ECP. All computations were performed in ORCA 4.0.[18]

Table S5. B3LYP/def2-SVP/def-SDD: Energy difference in meV between the different possible spin-states of the complexes. Data are reported relative to the most stable spin-state.

	O	**N**	**NO**
Open-Shell Singlet	35.57	**0**	**0**
Triplet	518.11	364.84	391.65
Quintet	**0**	7.42	4.65

Table S6. M06L/def2-SVP/def-SDD: Energy difference in meV between the different possible spin-states of the complexes. Data are reported relative to the most stable spin-state.

	O	**N**	**NO**
Open-Shell Singlet	923.11	**0**	956.42
Triplet	461.57	520.55	602.61
Quintet	**0**	24.84	**0**

While the most stable spin state for the all-siloxide and the all-amide complex does not change with M06L compared to B3LYP, the situation for the mixed complex is more delicate (Tables S5 and S6). In fact, while semi-local functionals such as M06L have the advantage of mimicking the effects of static correlation, they also over-delocalize electron density and struggle to describe correctly the distribution of charges in asymmetric ligand environments, such as in the mixed ligand complex. For instance, the two uranium centers in the mixed ligand complex are not symmetrically equal, since their environments differ; therefore, their bond order should reflect the asymmetric nature of the compound. As shown in Figure S52, B3LYP is able to capture this asymmetry, while in M06L is not observed. Nevertheless, despite the fundamental difference between the functionals, the computed Mayer bond order trend is the same both in M06L and B3LYP (Figure S52).

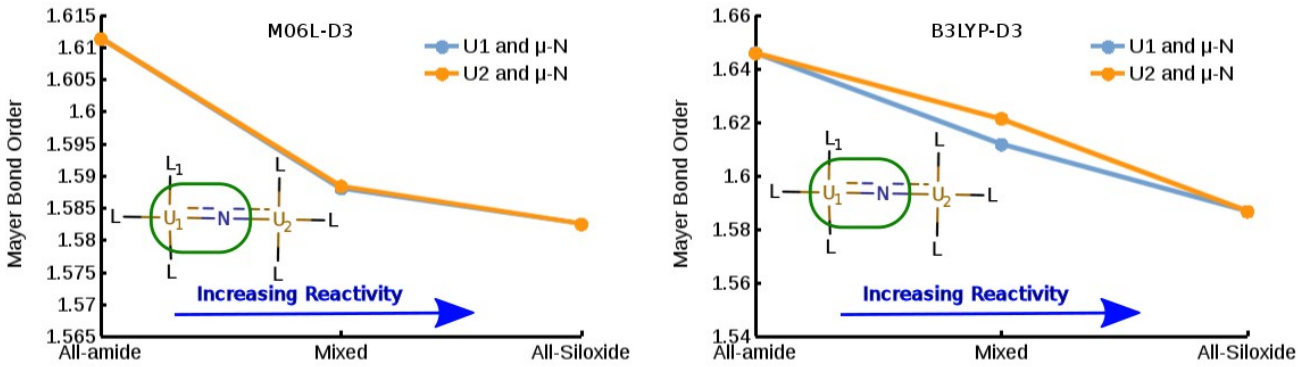

Figure S52. Mayer Bond Order for U-N bond in function of the complexes ordered per increasing reactivity (*left*) M06L/def2-SVP/def-SDD. (*right*) B3LYP-D3/def2-SVP/def-SDD.

References

1) Andersen, R. A. *Inorg. Chem.* **1979**, *18*, 1507-1509.

2) Camp, C.; Pécaut, J.; Mazzanti, M. *J. Am. Chem. Soc.* **2013**, *135*, 12101-12111.

3) Fortier, S.; Wu, G.; Hayton, T. W. *J. Am. Chem. Soc.* **2010**, *132*, 6888-6889.

4) Mougel, V.; Camp, C.; Pécaut, J; Copéret, C.; Maron, L.; Kefalidis, C. E.; Mazzanti M. *Angew. Chem. Int. Ed.* **2012**, *51*, 12280-12284.

5) Jordan, R. F.; Bajgur, C. S.; Dasher, W. E.; Rheingold, A. L. *Organometallics* **1987**, *6*, 1041-1051.

6) Bain, G. A.; Berry, J. F.; *J. Chem. Educ.* **2008**, *85*, 532-536.

7) Bénaud, O.; Berthet, J. -C.; Thuéry, P.; Ephritikhine, M. *Inorg. Chem.* **2010**, *49*, 8117-8130.

8) Cooper, O.; Camp, C.; Pécaut, J.; Kefalidis, C. E.; Maron, L.; Gambarelli, S.; Mazzanti, M.; *J. Am. Chem. Soc.* **2014**, *136*, 6716-6723.

9) *CrysAlis*^{Pro}, Rigaku Oxford Diffraction, release 1.171.39.46, 2018.

10) *SHELXT* - Integrated space-group and crystal-structure determination¸ G. M. Sheldrick**,** *Acta Crystallogr.*, *Sect. A* **2015**, *71*, 3-8.

11) *SHELXL* - Crystal structure refinement, G. M. Sheldrick**,** *Acta Crystallogr.*, *Sect. C* **2015**, *71*, 3-8.

12) Berthet, J. -C.; Ephritikhine, M.; Lance, M.; Nierlich, M.; Vigner, J. *J. Organomet. Chem.* **1993**, *460*, 47-53.

13) (a) Lee, C.; Yang, W.; Parr, R. G. Development of the Colle-Salvetti Correlation-Energy Formula into a Functional of the Electron Density. *Phys. Rev. B* **1988**, *37* (2), 785–789.; (b) Stephens, P. J.; Devlin, F. J.; Chabalowski, C. F.; Frisch, M. J. Ab Initio Calculation of Vibrational Absorption and Circular Dichroism Spectra Using Density Functional Force Fields. *J. Chem. Phys.* **1994**, *98*, 11623–11627; (c) Becke, A. D. Density-Functional Thermochemistry. III. The Role of Exact Exchange. *J. Chem. Phys.* **1993**, *98* (7), 5648.

14) S. Grimme, J. Antony, S. Ehrlich and H. Krieg, *J. Chem. Phys.*, 2010, **132**, 154104.

15) Y. Zhao and D. G. Truhlar, *J. Chem. Phys.*, 2006, **125**, 194101.

16) F. Weigend and R. Ahlrichs, *Phys. Chem. Chem. Phys.*, 2005, **7**, 3297–305.

17) W. Küchle, M. Dolg, H. Stoll and H. Preuss, *J. Chem. Phys.*, 1994, **100**, 7535–7542.

18) F. Neese, *Wiley Interdiscip. Rev. Comput. Mol. Sci*, **2012**, *2*, 73–78.